OBSERVATIONS OF ATMOSPHERIC RIVERS WITH CLOUDSAT CPR AND AQUA AMSR-E

Jason B. Dodson

Thomas H. Vonder Haar

CIRA Cooperative Institute for Research in the Atmosphere

Colorado
State
University

THESIS

OBSERVATIONS OF ATMOSPHERIC RIVERS WITH CLOUDSAT CPR AND

AQUA AMSR-E

Submitted by

Jason B. Dodson

Department of Atmospheric Science

In partial fulfillment of the requirements

For the Degree of Master of Science

Colorado State University

Fort Collins, Colorado

Spring 2008

ABSTRACT OF THESIS

OBSERVATIONS OF ATMOSPHERIC RIVERS WITH CLOUDSAT CPR AND

AQUA AMSR-E

"Atmospheric rivers" are filamentary water vapor structures, occurring primarily over

oceans, thousands of kilometers long that form along the leading edge of cold fronts.

These "rivers" are an important link between weather and climate by transporting large

amounts of moisture (on the order of $10^8 kgs^{-1}$) through the middle latitude regions and

causing heavy precipitation events along coastal regions. The CloudSat satellite, launched

28 April 2006, is designed to measure vertical cloud structure and fill a long-existing gap

in satellite observations. CloudSat and Aqua observed 22 river events (with multiple

overpasses for each river) over a period from November 2006 to April 2007. In this

project, CloudSat CPR observations of cloud location and cloud type are used along with

moisture observations from Aqua AMSR-E to create a preliminary average profile of

vertical cloud structure within atmospheric rivers.

The CloudSat observations (using Aqua moisture and precipitation measurements as

references) are first presented for case studies of four river events out of the total 22

events. The observations show deep convective (vertical extent more than 7km) and

nimbostratus cloud (vertical extent more than 4km) bands more than 100km in horizontal

width occurring in three of the four cases, and shallow convection (vertical extent less

than 4km) occurring in the fourth case. Deep layer clouds occur most frequently during the river's early and middle stages, and these deep clouds usually erode into low and (sometimes) high cloud bands in the river's later life.

The CloudSat measurements are then combined into composite frequency plots to show the typical cloud locations within and near the river with respect to the river's water vapor structure. Frequency plots are presented for all 92 overpasses along with categories of overpasses based on time of occurrence within the rivers' life spans to give a preliminary time evolution of cloud structure. Then, scatter plots comparing moisture structure properties with cloud structure properties are displayed to show any possible relationship between moisture and clouds. Finally, some statistics about the frequency of occurrence of different cloud types within the rivers are presented.

Jason B. Dodson
Department of Atmospheric Science
Colorado State University
Fort Collins, Colorado 80523
Spring 2008

ACKNOWLEDGEMENTS

TABLE OF CONTENTS

1. INTRODUCTION

Understanding the complexities of the atmospheric component of the water vapor cycle continues to be an important topic in atmospheric research. In particular, water vapor transport within the middle latitudes occurs largely through complicated and turbulent processes, as opposed to the more broad-scale flow found in the tropics and subtropics. One prominent mode of transport occurs over the oceans along the leading edge of a polar cold front. Large quantities of water vapor converge along frontal boundaries and are carried polewards by pre-frontal low level jets. These bands of water vapor are typically only a few hundred kilometers across, but can stretch over thousands of kilometers across the ocean and can transport as much water instantaneously as major terrestrial rivers (Newell 1992). These properties have led to the name "atmospheric river" being given to these meteorological features (Fig 1.1).

Atmospheric rivers are significant components of water vapor transport in midlatitude ocean regions, serving as a link between weather and climate. As weather features, atmospheric rivers can trigger linear convective storms over the oceans and heavy orographically-forced rain events when making landfall (White 2003). Rivers also influence weather by transporting large amounts of latent heat into extratropical cyclones' cores, which can lead to rapid intensification (Zhu 1994). As part of global circulation, much of the water vapor transport occurring within a baroclinic wave's warm advection region (the "warm conveyor belt") occurs along frontal boundaries, at low

levels. With much of the middle latitude's water vapor transport occurring in atmospheric rivers, pre-frontal meteorological processes become important in affecting other parts of the water vapor cycle, such as precipitation and vertical transport.

1.1 Previous Studies of Atmospheric Rivers

1.1.1 Polar Fronts

Atmospheric rivers are primarily pre-frontal meteorological features, and so the first research directly related to atmospheric rivers concerned the characteristics and climatology of polar fronts. There is abundant literature written about polar frontal features, and covering them in detail is beyond the scope of this review. However, it is useful to note one paper in particular, Browning 1973, which describes the characteristics of low level jets occurring in advance of extratropical cyclones. The low level jet is a very important feature of atmospheric rivers, so this paper serves as a basis for future observations and research on river characteristics.

1.1.2 Identification of Atmospheric Rivers

Several types of water vapor structures occur over the ocean. The first of these structures were identified in the 1960s using large amounts of surface observations and data from recently-launched meteorological satellites. Many studies and observations of these structures have been made since then. The atmospheric river is one of these water vapor structures, but it was understood as a distinct and separate entity only more recently. The atmospheric river, originally called the "tropospheric river", was first

identified by Newell et al in 1992. The identification of these rivers came from a study of midlatitude transport of trace gases (e.g. carbon monoxide). Analysis of ECMWF meteorological output over October 1984 depicted long narrow bands of large water vapor transport in the south Atlantic and Indian Oceans. Further work revealed a pattern of four or five of these rivers occurring simultaneously in the Northern and Southern hemispheres, with each tropospheric river transporting an amount of water vapor on the order of $10^8 kgs^{-1}$, close to the output of the Amazon River (hence the name "atmospheric river"). They also distinguished between atmospheric rivers and the "moisture bursts" or "moisture plumes" identified previously (e.g. McGuirk 1987) by noting the low-level nature of the rivers as opposed to more elevated moisture plumes. This pilot study identified the potential necessity of including these features as a major part of midlatitude water vapor transport.

1.1.3 Studies of River Characteristics

The atmospheric river was noted in 1992 as being a low level pre-frontal feature, as opposed to the tropical moisture plumes identified earlier. The role of the pre-frontal low level jet in producing orographic precipitation had been identified long before 1992 (Ralph 2005), but Newell et al were the first to link the filamentary water vapor structures and associated water vapor transport with the low level jets. Much more information about the local structure of the rivers was learned by examining the data collected from two field experiments. The California Land-falling Jets Experiment (CALJET) conducted over winter 1997/1998 and the Pacific Land-falling Jets Experiment (PACJET) conducted over winter 2000/2001 collected data from airplane-released dropsondes in

3

and around atmospheric rivers. These dropsondes were combined with satellite observations to create a comprehensive set of measurements characterizing rivers. These measurements were used to develop an understanding of many meteorological variables within atmospheric rivers, such as moisture distribution, wind and jets, temperature and instability, and deep-layer cloud properties (e.g. integrated cloud liquid water).

1.1.4 Studies of River Effects on Weather and Climate

There has been much research on the atmospheric rivers' influences on both weather and climate. Rivers are sufficiently frequent and intense to bridge a gap between these two fields of study.

The effects of polar fronts and low level jets on weather were heavily researched before atmospheric rivers were first identified. In 1994 Zhu and Newell identified an important link between atmospheric rivers and rapidly-intensifying midlatitude cyclones (sometimes termed a "bomb"). Rivers carry large amounts of water vapor into the pre-frontal convergence zone, resulting in large latent heat release which enhances the cyclone's strength (Zhu 1994). A few years later data from CALJET project was used to investigate the link between atmospheric rivers and orographic rainfall along the North American western coastline. It has been long known that heavy rainfall along the west coast is often linked to strong upslope flow and low level jets, so CALJET (and later PACJET) provided an opportunity to study river-influenced orographic rainfall in detail. Along these lines of research, a recent paper demonstrated a strong relationship between atmospheric river landfalls and flooding within the Russian River basin in California (Ralph 2006).

In 1997 Zhu and Newell made an estimate of the rivers' role in global climate, and found the rivers to have a large role in midlatitude water vapor transport, with more than 90% of water vapor transport occurring along less than 10% of the Earth's zonal length (Zhu 1998). Further research in this area later on determined that moisture transported in rivers often comes from the subtropics rather than from the tropics, and discovered a possible link between river moisture sources and ENSO (Bao 2006).

1.2 Motivation for Research

At the present, there is much research about the meteorological structure and its variability within atmospheric rivers. Most of that research focuses on water vapor and wind found within the rivers, which comprise the majority of the water transport occurring within rivers (Ralph 2004). However, much less is known about the cloud structure within rivers. There is knowledge of integrated and top layer cloud properties as measured by passive microwave and infrared satellite sensors, and limited measurements of vertical cloud structure from a few field experiments, but there is almost no knowledge of the variety of cloud structures occurring within many rivers.

Knowledge of the atmospheric river's cloud structure is necessary for developing a better model for the processes occurring within the river. Many atmospheric processes are difficult to measure directly or remotely, such as rising motion and latent heat release. This is particularly true over ocean regions where surface measurements are sparse and atmospheric soundings only occur on islands and during field experiments. Observing

5

atmospheric rivers suffers in this regard as rivers are primarily ocean-based features which are heavily affected by terrain once the river makes landfall. Over the oceans, clouds can serve as tell-tale signals of the meteorological processes occurring in low-measurement situations. If the typical cloud structure within an atmospheric river is known, then it is possible to infer what meteorological processes must be producing those clouds. This may be useful in operational meteorology for forecasting the intensity of landfalling rivers and associated extratropical cyclones. This information could also be used by theorists and modelers to compare theoretical predictions of cloud features within rivers with observations.

The main purpose of this project is to develop a preliminary understanding of vertical cloud structure within atmospheric rivers. This consists of both the location of the clouds relative to other meteorological features within the river (e.g. total column precipitable water) and the types of clouds commonly occurring within rivers. This task is completed using measurements of river events occurring during the 2006-2007 winter months taken by NASA's CloudSat and Aqua satellites (Fig 1.2). The rivers' moisture structures are observed using the Aqua satellite's AMSR-E sensor, and the vertical cloud structure is detected using CloudSat's Cloud Profiling Radar. The radar is a new research tool that provides previously unavailable information about vertical cloud structure within the complex meteorological features it observes. This new ability to peer though cloud tops is needed to fill a current gap in knowledge about the clouds found within and around atmospheric rivers.
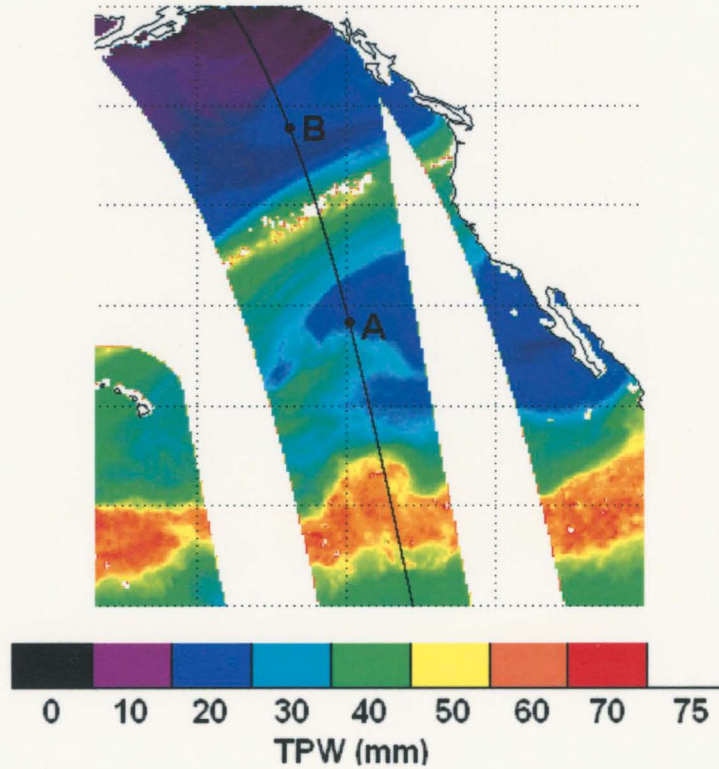
Figure 1.1: Total Column Precipitable Water (TPW) map depicting a strong river making landfall on the North American west coast on the afternoon of Nov 6th 2006. Note the filamentary structure of the river's central moisture axis. The black line represents CloudSat's orbit.
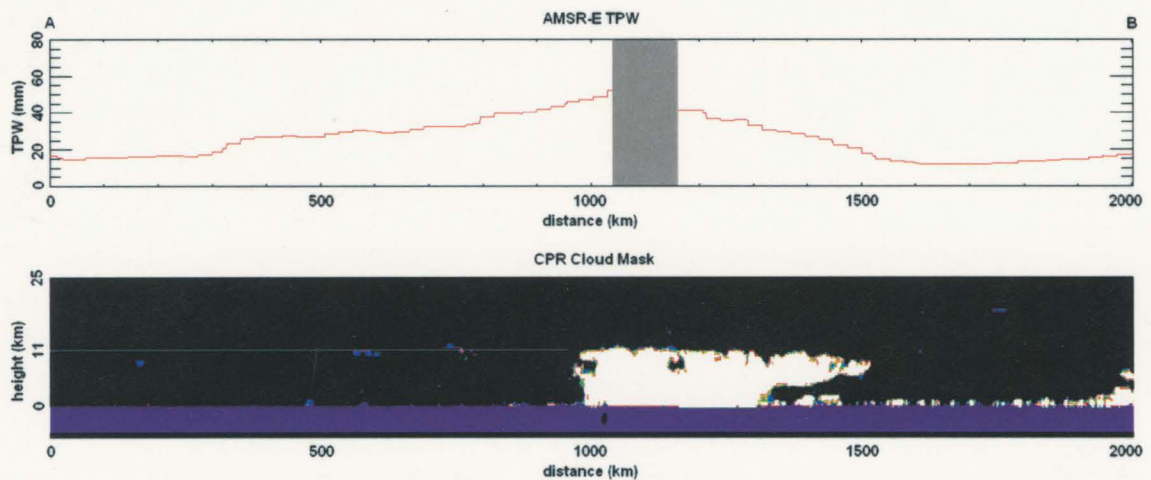
Figure 1.2: Observations taken by AMSR-E and CloudSat of the river event show in Fig. 1.1. The upper panel shows the TPW occurring along CloudSat's orbit, and the lower panel shows the vertical structure of clouds detected by Cloudsat . The layout of these plots will be discussed in more detail in the methodologies and results sections.

2. CLIMATOLOGY AND METEOROLOGICAL PROPERTIES OF ATMOSPHERIC RIVERS

2.1 Climatology of Atmospheric Rivers

Atmospheric rivers are pre-frontal meteorological features, so the frequency and potency of rivers are related to the frequency and potency of polar fronts. Atmospheric rivers can occur at any time of the year in all ocean basins for both hemispheres (Fig. 2.1). In the northern hemisphere, the strongest rivers occur from late fall to early spring coinciding with the period of strong midlatitude cyclone activity. During this active time period there can be up to four or five rivers occurring simultaneously in the northern hemisphere, corresponding with the number of baroclinic waves at the time (Zhu 1997).

Unlike their moisture plume counterparts (see 2.4), there has not been a great deal of research on the seasonal variability of atmospheric rivers as specific meteorological features. The closest thing to a climatological study currently available is Zhu et al 1997, which examined global average river moisture transport for January and July. It appears that global average moisture transport has little seasonal dependence. In the Northern Hemisphere, river transport in the midlatitudes was not considerably greater in January than July, though rivers are more common in January (Fig. 2.2). If the data are sufficient to draw conclusions about river climatology, then this suggests that summer rivers, being future in nature, may transport more moisture per river than winter rivers. This could be

possible because summer rivers generally have higher TPW values than winter rivers, simply because there is much more ambient moisture in the summer ocean atmosphere (Randel 1996).

2.2 Meteorological Structure of Atmospheric Rivers

2.2.1 Moisture Structure within Atmospheric Rivers

The filamentary structure of moisture is a signature characteristic for atmospheric rivers. As mentioned before, the majority of the moisture associated with atmospheric rivers is contained within corridors a few hundred kilometers wide and several thousand kilometers long, and seldom extending more than three or four kilometers above the surface.

The horizontal filamentary structure of river moisture is apparent in a planer TPW map, as Fig. 2.3 demonstrates. Typical maximum TPW values within rivers lie between 30mm and 40mm, and extreme events can contain values more than 60mm in small portions of the river's length. Fig. 2.4 shows TPW representations of different rivers occurring in the 2006-2007 winter season. In addition to variation in width and length, it should be noted that rivers are not always symmetric entities. A single river can change in width and intensity considerably along its length, and sometimes will curve and bend as outside meteorological features disrupt the river's internal processes. There is also variability in how far south the beginning of the TPW band extends. Some rivers are directly attached to tropical moisture, possibly transporting moisture from the deep tropics directly into the midlatitudes. Other rivers begin in the subtropics, feeding on

subtropical moisture converging along the frontal boundary. This variation in moisture sources can affect the rivers' roles in global moisture circulation, and itself is possibly affected by other features in global circulation like ENSO (Bao 2006).

A typical vertical cross-section of river moisture measured during CALJET via dropsondes is shown in Fig. 2.5. The majority of moisture within the river is confined to a width of two to three hundred kilometers just ahead of the frontal boundary at all levels below about 600mb. There is a sharp moisture gradient occurring right along the polar frontal boundary at most levels (particularly above 800mb), which leads to the moisture maxima at higher levels occur above or behind the polar frontal zones at lower levels. These measurements indicate that the atmospheric river is sloped, following the slope of the frontal boundary (as warm conveyor belt features are known to do). Measurements of other rivers show a similar moisture structure (Fig 2.7).

2.2.2 Wind Structure within Atmospheric Rivers

A common occurrence within an atmospheric river is the formation of a low level jet immediately in advance of the polar front. Low level jets are not synonymous with atmospheric rivers, but the large wind speeds found in low level jets are largely responsible for transporting the large quantities of moisture within rivers rapidly for thousands of kilometers across oceans. Understanding of low level jets predates the discovery of atmospheric rivers, and so the wind component and structure of rivers is fairly well understood.

Browning et al (1973) provides a useful summary of the pre-frontal low level jet. It is important to note that this low level jet is different from other common low level jets,

such as the Great Plains jet, which are connected to topographical causes. The pre-frontal low level jet is driven by the strong pressure gradient occurring along a frontal boundary. Early observations of low level jets found that wind speed within jets are close to the speeds predicted by geostrophy. These jets are seldom wider than 200km, and are vertically confined to only 1km to 2km above the surface (Fig 2.8). Surface friction prevents jets from forming very near the surface, and sets up a very intense shear zone in the lowest kilometer of the troposphere. This frictional convergence at the surface results in rising motion within the jet and sinking motion around the jet. These secondary circulations limit the vertical height of the low level jet. The sinking branches of the circulations erode the frontal temperature gradient through adiabatic heating, decreasing the pressure gradient and thus the geostrophic wind. This jet is typically only a couple hundred kilometers in width, and is present in the majority of the length of the river. It should be noted that pre-frontal jets can also occur along warm frontal boundaries, but these jets are less common than the cold frontal variants. Occasionally multiple jet maxima can form, typically when the polar front has multiple frontal surface boundaries.

Fig. 2.5 shows a vertical cross section of wind for a river occurring during the CALJET project. This river possesses two jet maxima occurring along the two frontal boundaries, about 900mb-850mb above the surface. The jets occur in the same regions of the frontal boundary as the high moisture values are found, allowing the jets to transport moisture rapidly along the polar front. Measurements of other rivers show that these low level jets are common to atmospheric rivers (Fig 2.7).

2.2.3 Moisture Transport within Atmospheric Rivers

Large moisture transport requires both significant quantities of moisture and a high enough wind speed to transport the moisture. Atmospheric rivers contain both moisture convergence and low level jets, and thus moisture transport is large within rivers. Fig 2.6 shows the vertical cross-section of moisture transport in the river measured by CALJET. The highest values of moisture transport occurs within a few hundred kilometers of the frontal boundary.

2.3 Influences on Weather and Climate by Atmospheric Rivers

2.3.1 Influences on Weather

Atmospheric rivers can greatly affect weather along the North American west coast, through both directly forcing moisture over the coastal terrain and by enhancing the strength of the midlatitude cyclones linked with the polar fronts.

Orographic lifting has long been known to be a major cause of precipitation in mountainous terrain. There is also a well-established link between rainfall intensity along the west coast and landfalling pre-frontal low level jets. Atmospheric rivers provide both the high moisture and the low level jet necessary for major coastal flooding events. A study specifically regarding atmospheric rivers suggests that although not all atmospheric rivers cause floods upon landfall, many if not most major floods near the west coast occur in the presence of atmospheric rivers (Figure 2.9). The chances of a river producing a flood is related to topography in the affected areas, the amount of moisture available for condensing, and the strength of the low level jet responsible for moisture transport. The

river event on November 5-7, 2006 was the cause of severe flooding across regions of Washington and Oregon, particularly in the Mt. Rainer area (Taylor 2006).

Atmospheric rivers can also strengthen midlatitude cyclones, leading to enhanced precipitation and other significant weather events in areas not directly within the river itself. A strong midlatitude cyclone requires a positive feedback loop between the upper-level baroclinic wave and the low level meteorological feature, such as frontal boundaries. Low level features can help enhance rising motion within a cyclone through latent heat transport. An atmospheric river contributes large amounts of latent heat release through both convection within the river itself and by moisture transported into the cyclone's core (Zhu 1994). It should be noted that strengthening the midlatitude cyclone can also enhance the polar front and associated atmospheric river, which affects the river's own meteorological significance.

2.3.2 Influences on Climate

Atmospheric rivers play large roles in the water vapor cycle, primarily in transporting water vapor from the subtropics to the polar regions. On a global circulation scale, the mean wind pattern in the midlatitudes alone cannot account for the majority of the water vapor transport northward within the midlatitudes. Transient midlatitude cyclones have been identified as the primary mechanism responsible for this transport, and atmospheric rivers are the primary form of water vapor transport over the ocean regions. Zhu and Newell (1997) estimated that about 90% of the water vapor transport within the midlatitudes occurs along atmospheric rivers, covering about 10% of the total zonal average area.

13

Atmospheric rivers also contribute much of the precipitation received along the North American west coast, as noted above. Even though the majority of rivers do not cause severe flooding events upon making landfall, these rivers are a necessary component of coastal climate.

2.4 Atmospheric Rivers and Moisture Plumes

In the Pacific, water vapor often takes a wide variety of structures beyond simple amorphous moisture pools. Bands and tongues of moisture are common occurrences in the tropics and subtropics, and are often referred to as "moisture plumes" or "moisture bursts" or "tropical plumes". Associated with moisture plumes are upper level cloud bands which have their own set of names and literature (Fig. 2.10). While these features may appear similar in name and appearance in meteorological maps, they do not usually share the same sets of features and the same formation mechanisms. Some are the results of tropical wave activity and momentum transfer from convective activity (Mecikalski 1998). These moisture plumes have slightly different structures as well, being more of a deep layer or high level feature than an atmospheric river (Davey 2000). For this reason, most of the samples used in this project are taken from the midlatitudes, minimizing the chances of a moisture plume contaminating the results.

Moisture plumes and atmospheric rivers are not always completely independent of each other. Moisture plumes often extend into the subtropics, where the moisture within the plume can be entrained into a passing extratropical cyclone and associated river (Fig. 2.11). This results in water vapor being transported directly from the tropics into the high

latitudes. However, rivers do not always form directly from moisture plumes (Fig. 2.12).

Much of the moisture within rivers comes from water evaporated from the subtropics and middle latitudes. Recent research suggests that the frequency of tropical-midlatitude connections depends on the current ENSO phase, with the highest frequency occurring during the neutral ENSO phase, and the lowest frequency occurring during strong El Nino events (Bao 2006). It appears that during strong El Nino events, the subtropics and middle latitudes serve as the most important moisture sources. Researching the details of tropical-midlatitude interaction is currently an active field of study. In terms of clouds within rivers, the interaction between rivers and plumes may cause high clouds to appear within the river when a "pure" river would not produce high clouds. For now, there is little that can be done to quantify this, but future studies may want to research the interactions between moisture plumes and atmospheric rivers in terms of cloud properties.
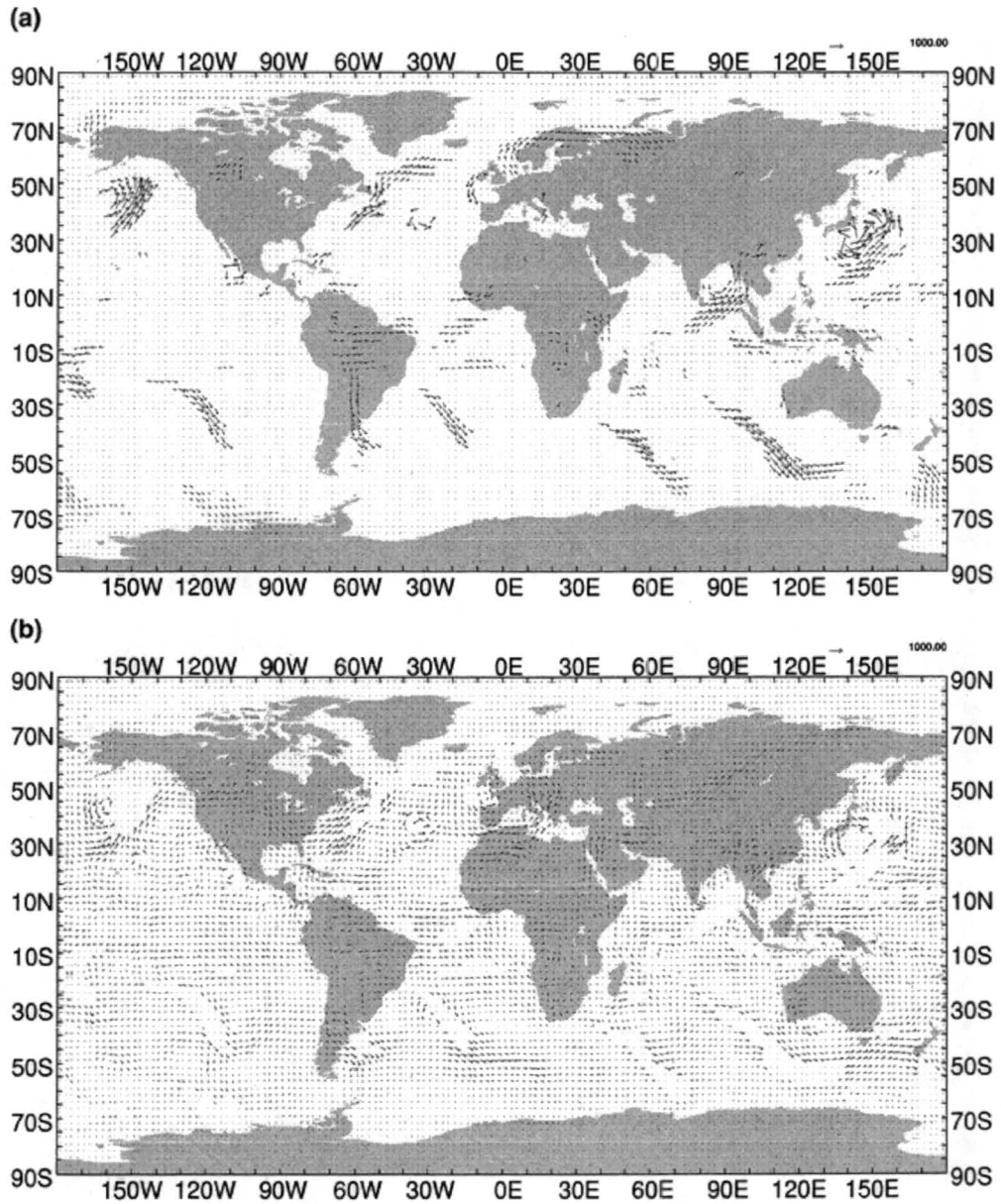
Figure 2.1) Moisture transport vectors within rivers (a) and outside rivers (b) on 12 October 1991, as calculated by Zhu et al 1997. There were three well-defined rivers in the Northern Hemisphere and five or six rivers in the Southern Hemisphere (taken from by Zhu et al 1997).
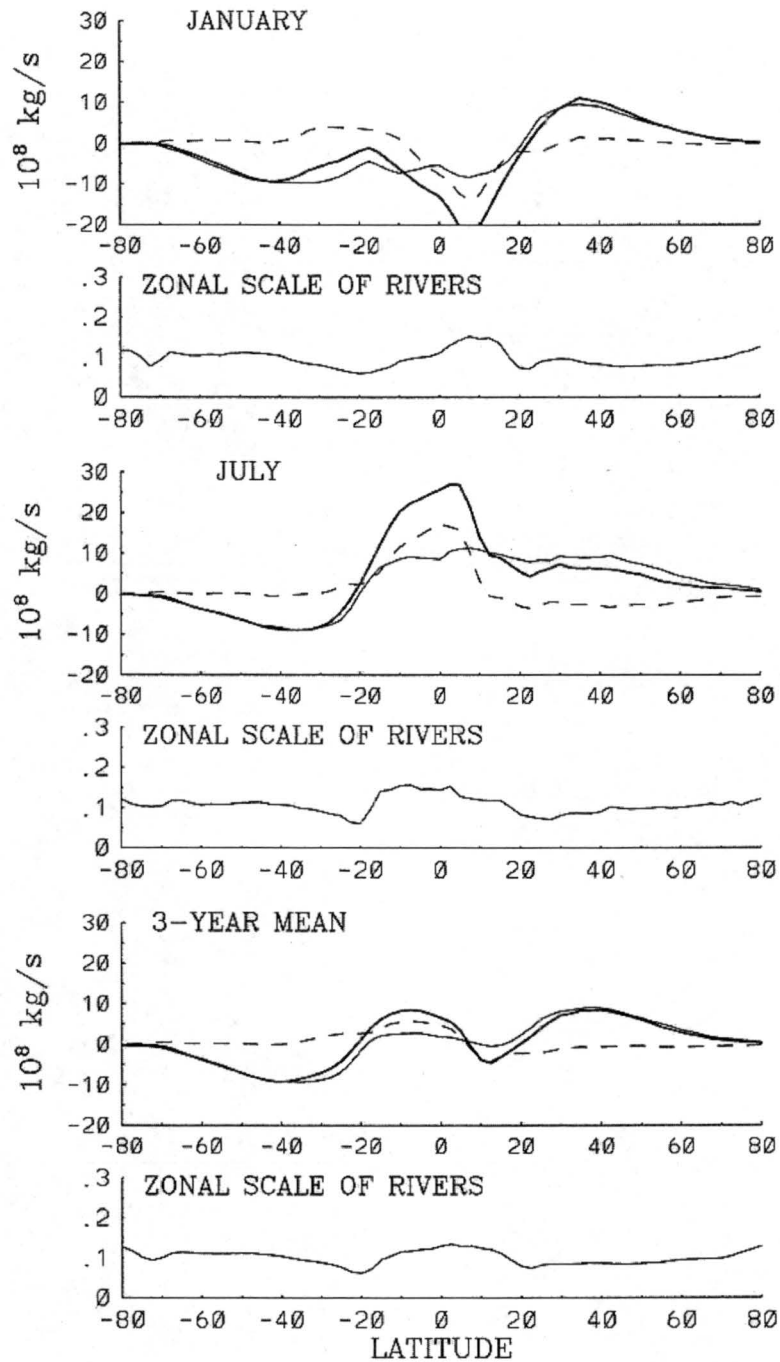
Figure 2.2) Zonal average northward moisture transport from atmospheric rivers and moisture plumes (thin solid line), broad-scale fluxes (dashed line), and the total transport (thick solid line) (from Zhu 1997).
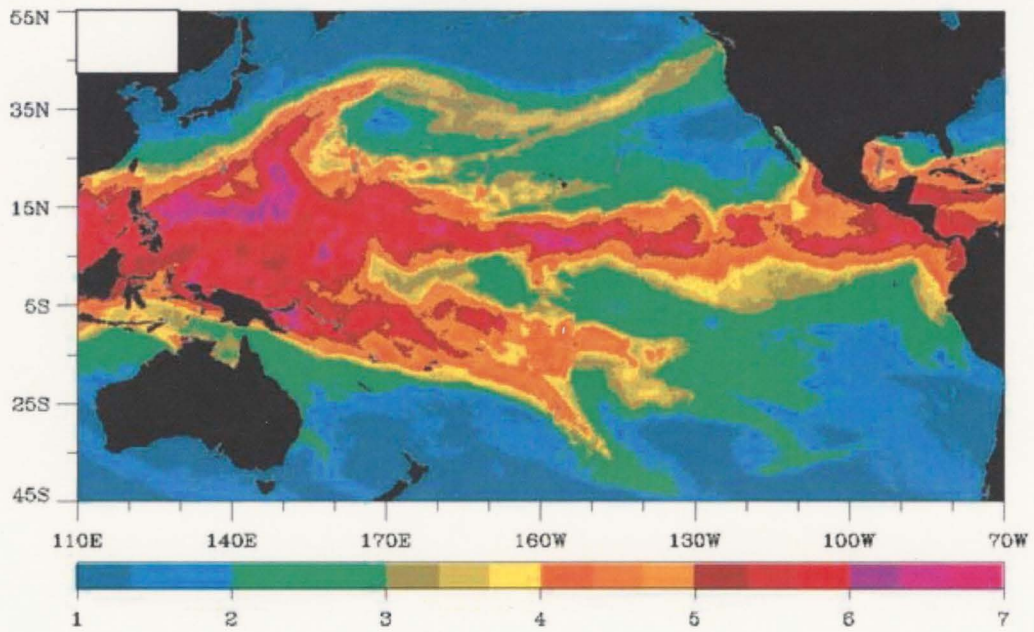
Figure 2.3) TPW map of an atmospheric river extending much of the Pacific's width (from Bao et al 2006).
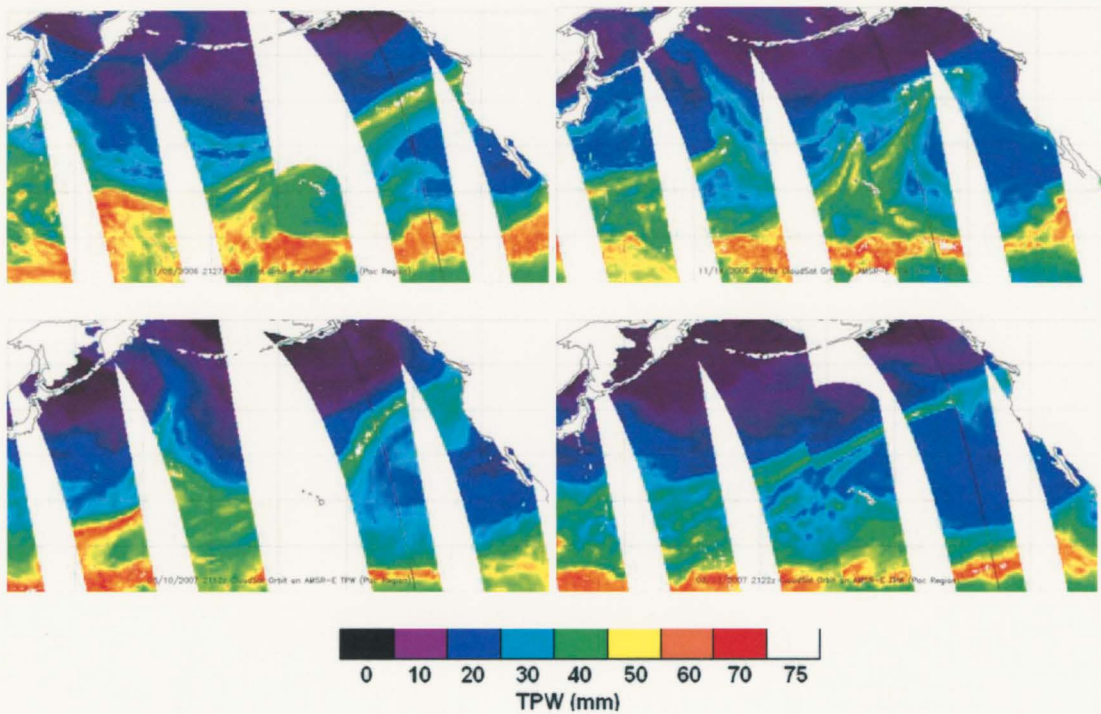
Figure 2.4) TPW observations of four river events occurring during the 2006-2007 winter seasons (these cases are discussed in the Results section).
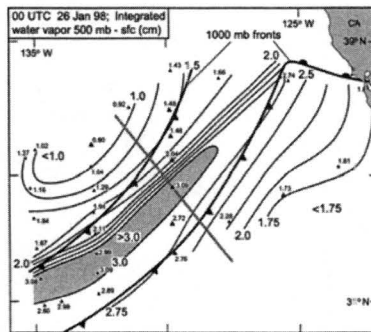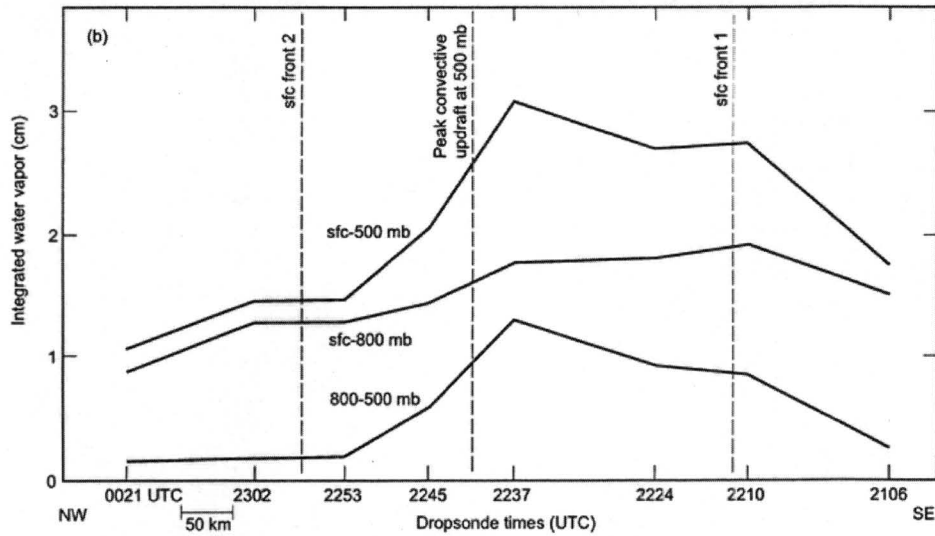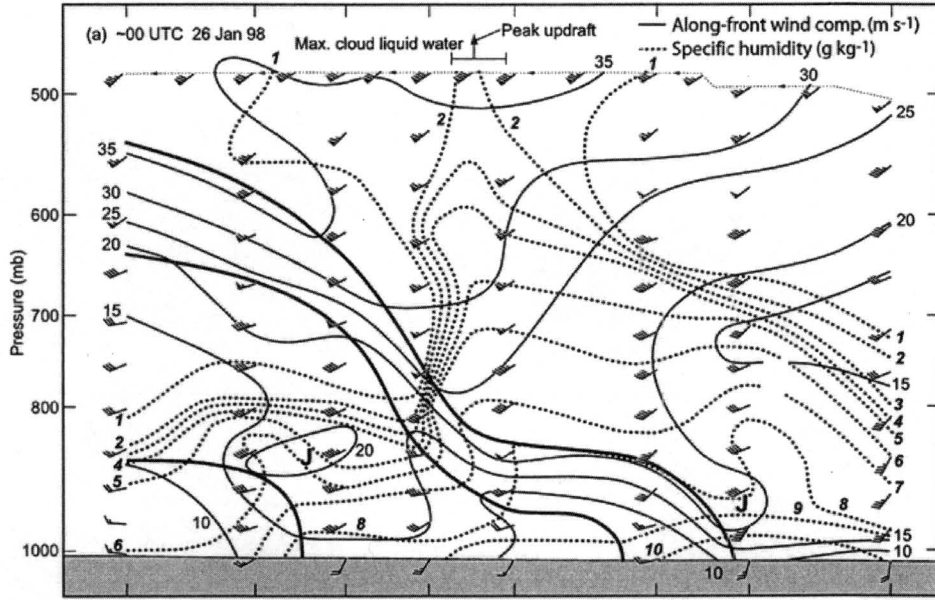
Figure 2.5) Vertical cross-section of a river observing during the CALJET project, showing wind and moisture relative to the frontal boundaries (from Ralph 2004). The bottom image shows the cross-sectional orientation.

19
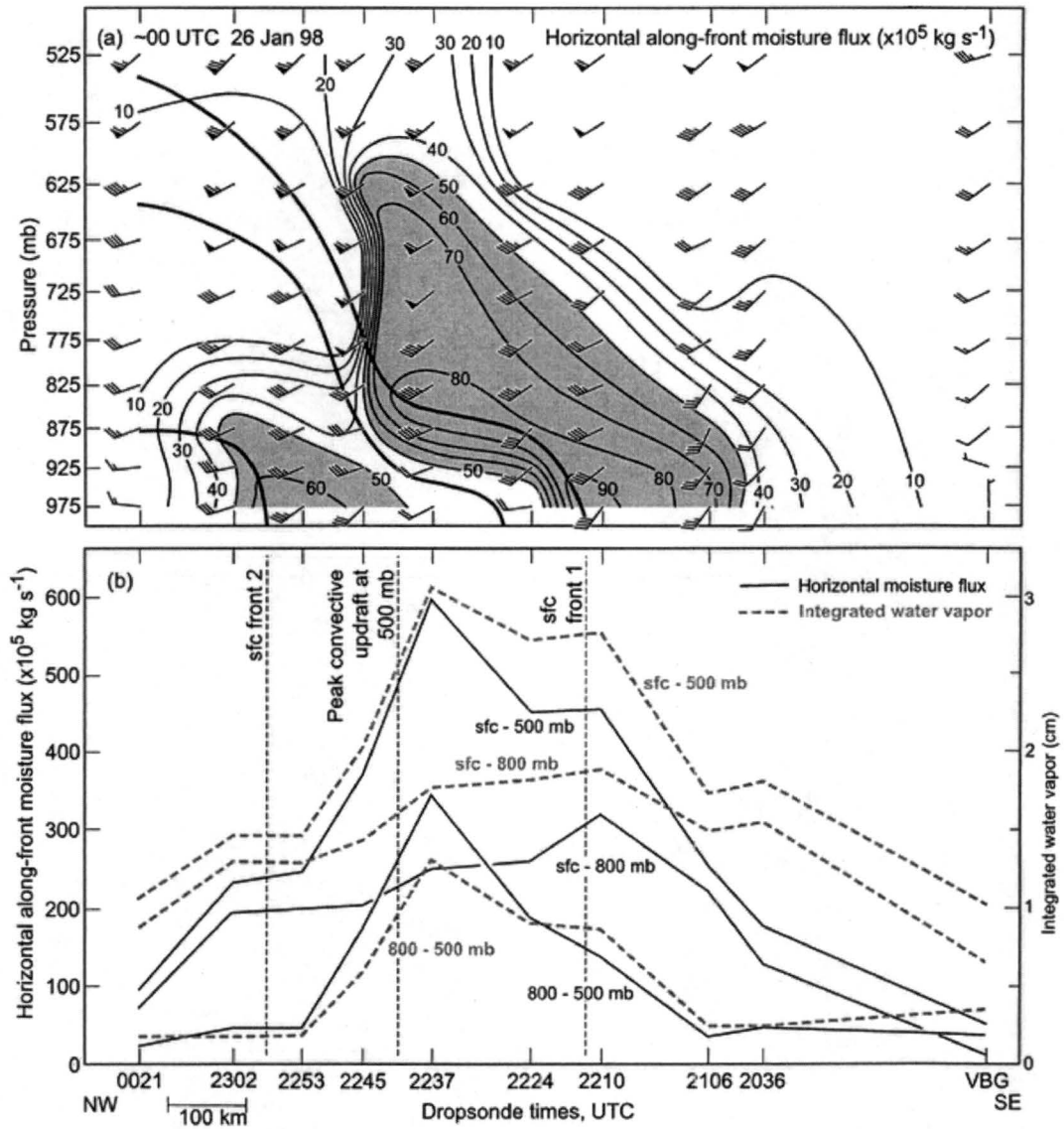
Figure 2.6) Vertical cross-section of a river observing during the CALJET project, showing moisture transport relative to the frontal boundaries (from Ralph 2004)
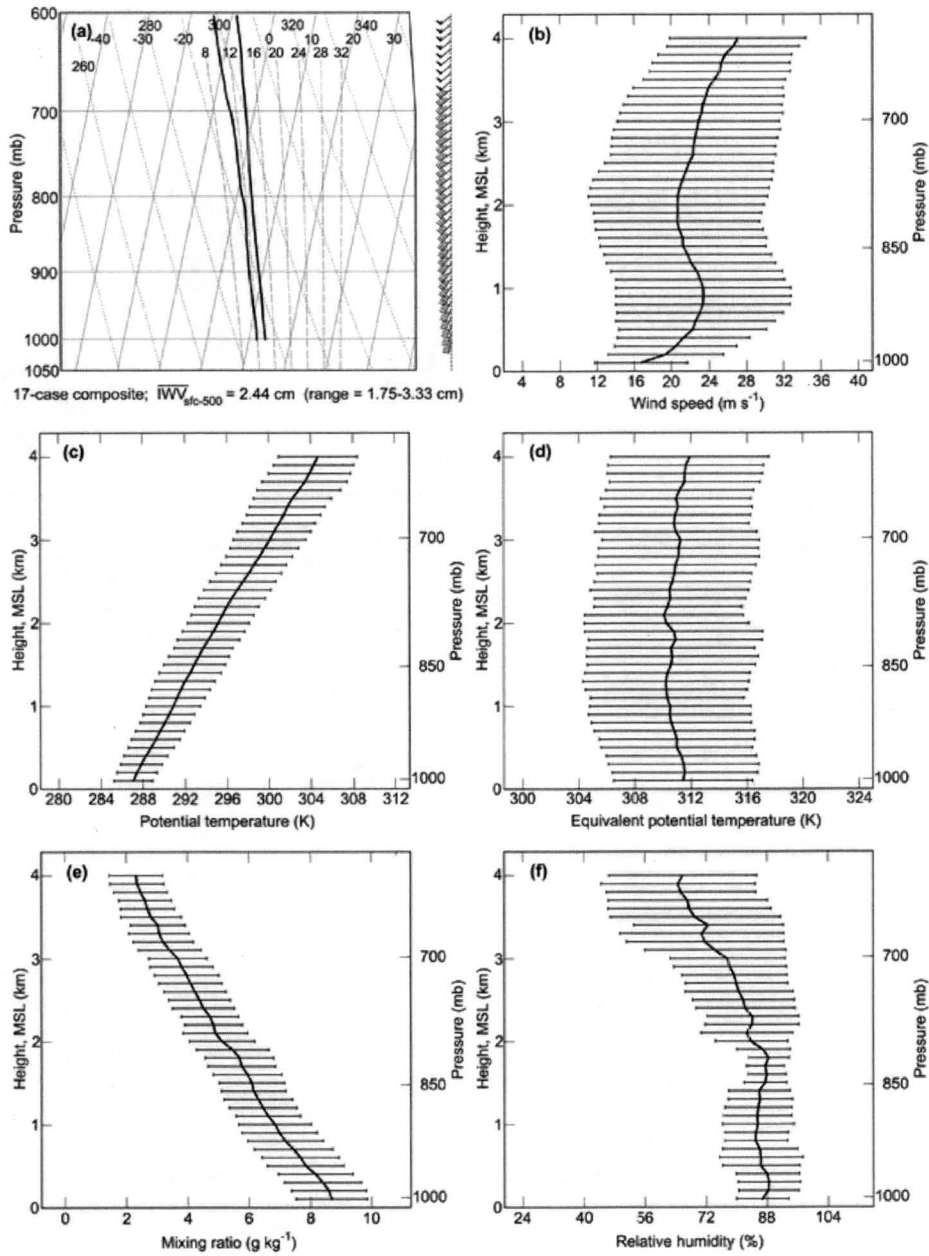
Figure 2.7) Average dropsonde profiles within atmospheric rivers from the CALJET and PACJET projects (from Ralph et al 2005).
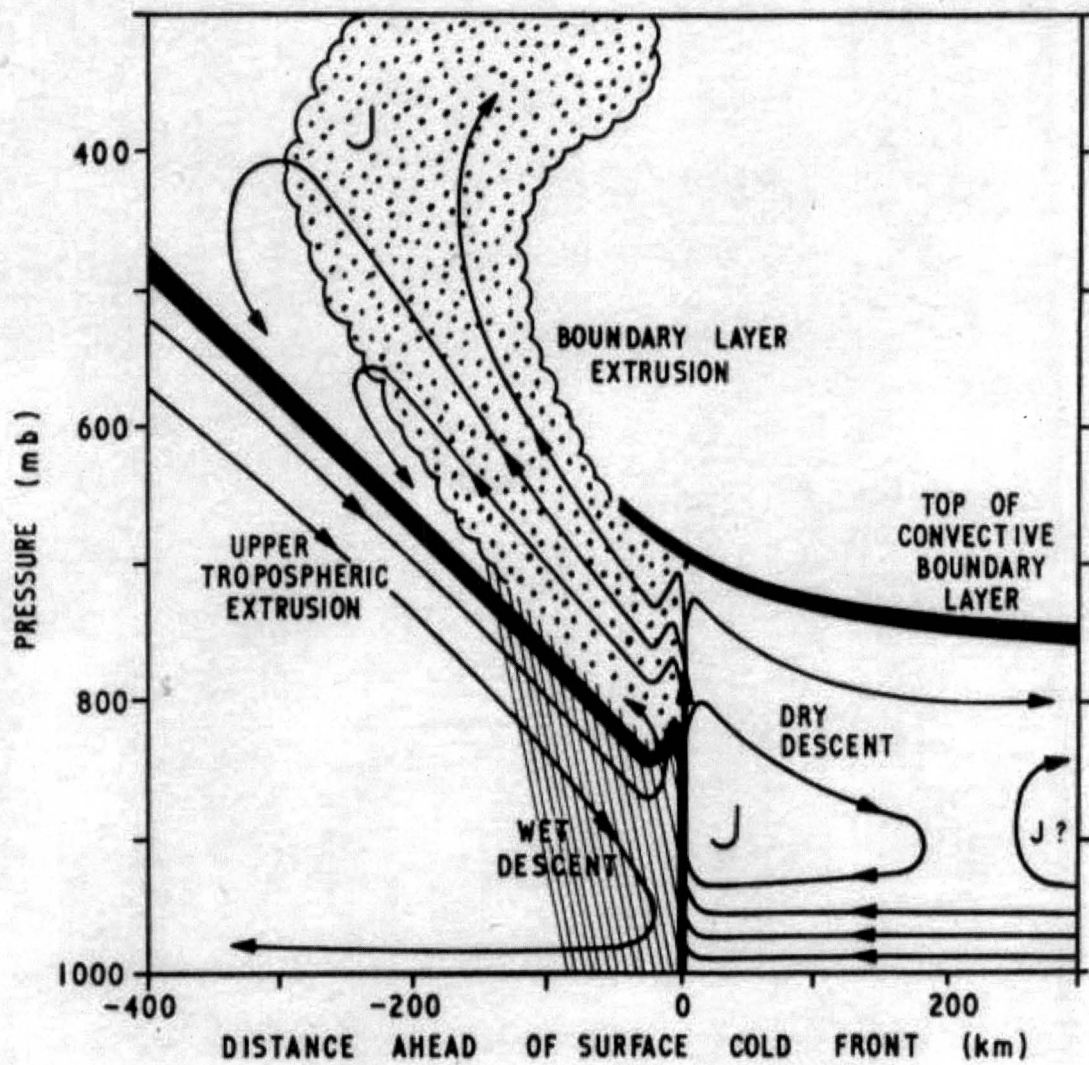
Figure 2.8) Conceptual vertical cross-section of a pre-frontal low level jet (from Browning 1973)
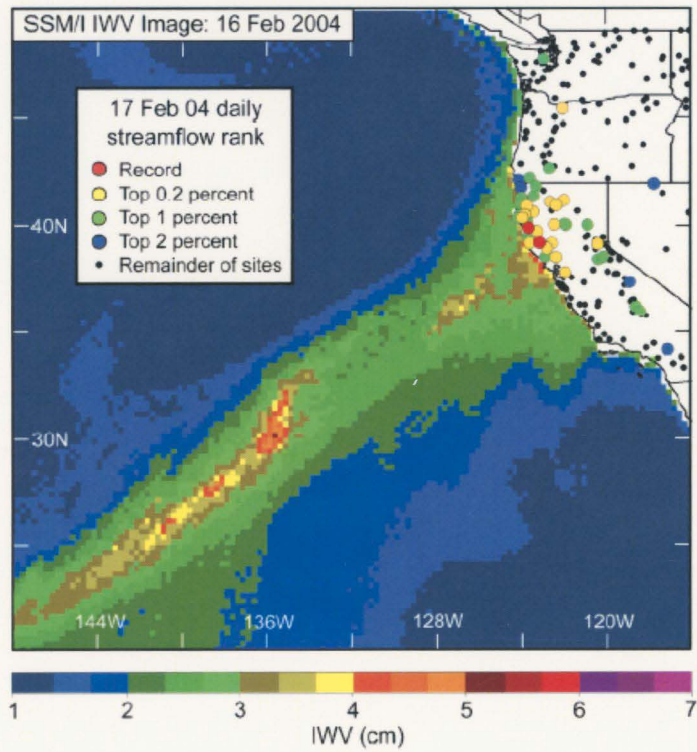
Figure 2.9) Atmospheric river event and related rainfall measured on the California coastline (from Ralph et al2006)

Figure 2.10) An example of a "moisture plume" spanning the tropics and subtropics (from Iskenderian 1995)
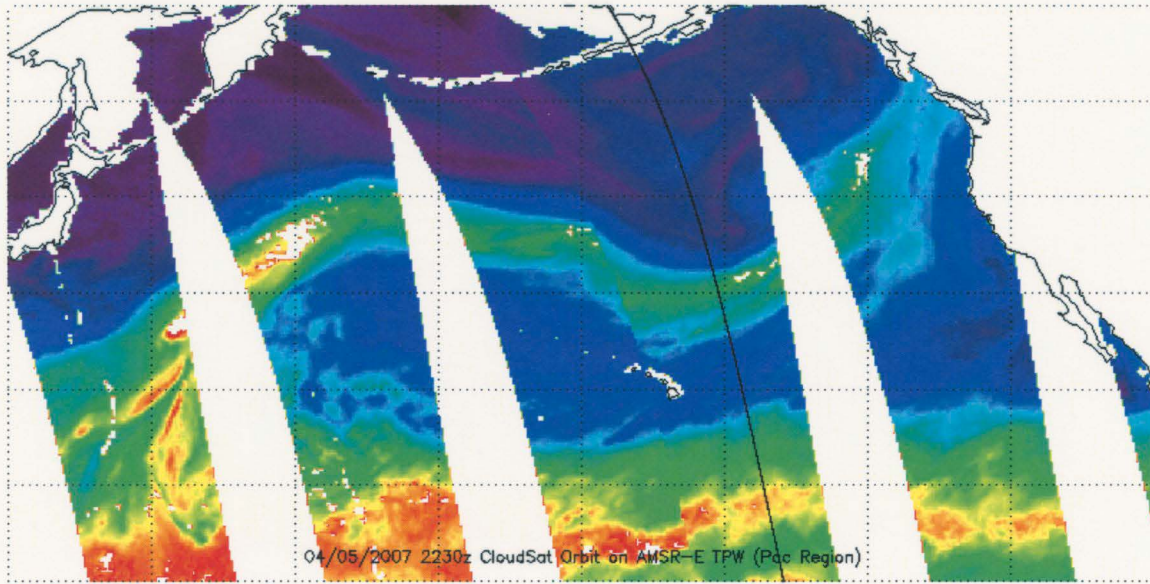
Figure 2.11) Example of an atmospheric river connected with deep tropical moisture
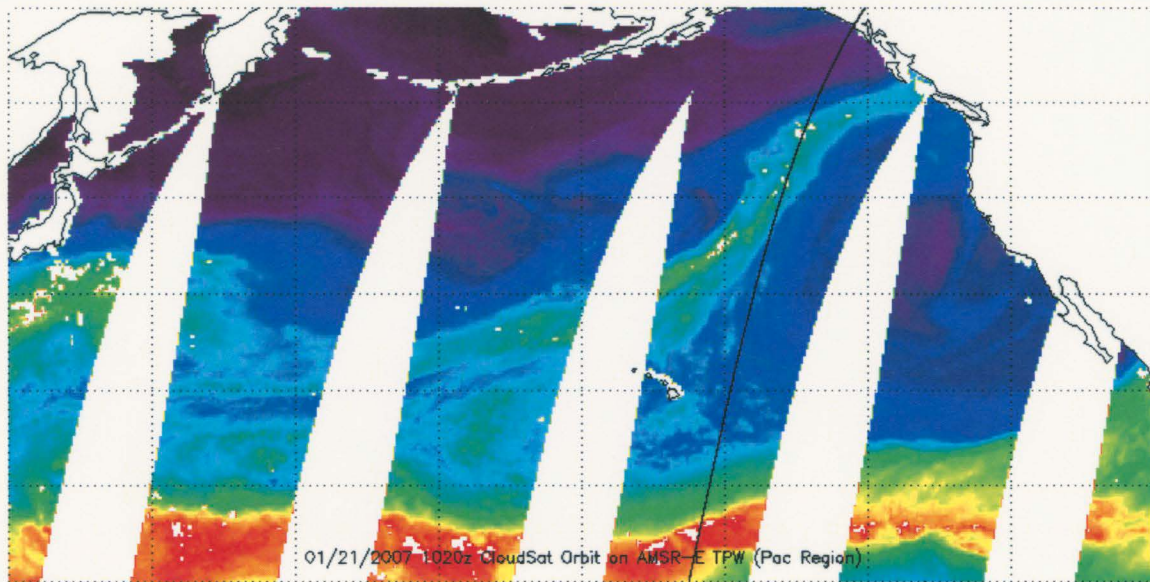
Figure 2.12) Example of an atmospheric river not connected with deep tropical moisture

3. INSTRUMENTS AND PRODUCTS

3.1 A-Train

The A-Train is a series of polar-orbiting satellites placed in the same orbit, close enough to each other to measure the same atmospheric features in the time span of a few minutes. The Aqua satellite is the original and lead satellite, with other satellites launched later on. The A-Train orbits at an altitude of 705km, an inclination in 98.2^{o}, and a period of 98.8 minutes, allowing Aqua (and the A-Train) to observe most of the Earth's surface once in a 24 hour period (Parkinson 2003). The strengths of the A-Train are the combination of large spatial coverage from Aqua and a large array of instruments capable of measuring many different properties of the same meteorological features. In terms of this project, over the winter 2006-2007 seasons the A-Train passed over more than 20 atmospheric rivers in the central and eastern Pacific, enough times to take the amount of measurements necessary for understanding typical river characteristics and variability.

This project uses the CloudSat and Aqua satellites to observe atmospheric rivers. CloudSat is used to observe river cloud structure. CloudSat possesses a unique radar capable of simultaneously measuring a cloud band's base and top height, depth, microphysical properties, all with resolution on the order of a kilometer wide and less than a kilometer depth. These types of measurements cannot all be made at once by other observing systems. In order to place cloud structure in relation to other meteorological

variables, Aqua is used to measure water vapor. Among Aqua's instruments is a microwave radiometer specially designed to measure atmospheric water. Aqua observes atmospheric features only a minute before CloudSat does, eliminating the need to account for time discrepancies. These properties make Aqua a very useful satellite for this project.

3.2 CloudSat and the Cloud Profiling Radar

CloudSat was launched on 28 April 2006, with the primary mission of observing cloud features. CloudSat is a sun-synchronous polar orbiter nestled within the A-Train group of satellites. CloudSat's orbit is carefully controlled to trail the Aqua satellite by about 460km, giving an average time delay between Aqua and CloudSat measurements of about a minute. CloudSat's footprint is much narrower than the Aqua's swath, so there is always Aqua information available to complement CloudSat's measurements (CloudSat Handbook and website) (Fig. 3.1).

3.2.1 Cloud Profiling Radar

CloudSat's primary instrument is the Cloud Profiling Radar (CPR), a 94GHz (W-band, about 3mm) radar designed to detect cloud droplets and ice particles. Unlike traditional precipitation radars, the 94GHz radar beam has a sufficiently small wavelength to scatter off most cloud water particles in a predictable Rayleigh fashion without being severely attenuated by cloud water (Stephens 2002). No major gaseous absorption lines occur near 94GHz, so most of the time gaseous attenuation of the radar beam is fairly minimal. High concentrations of water vapor can attenuate the beam slightly, which is problematic for

observing the tropics. Heavy precipitation can greatly attenuate the beam, sometimes completely. While this makes measurements of cloud properties difficult in high precipitation clouds, this attenuation can also be used to estimate precipitation rates (checking for reference). Most terrestrial surfaces have a predicable echo signal, and heavy precipitation diminishes this signal.

The CPR has a horizontal resolution of 2.5km along-track by 1.4km cross-track for each pulse. The pulse interval yields an effective horizontal resolution of 1.1km for each vertical profile. The CPR's vertical resolution is normally about 500m, but the derived products oversample the radar returns to produce a dataset resolution of 240m (Fig. 3.2). This horizontal resolution allows the CPR to detect most clouds, any cloud with a horizontal extent greater than a small fair-weather cumulus cloud. The vertical resolution allows the CPR to measure vertical structure within the cloud in addition to the cloud's height and depth. This vertical structure information can be used to detect features like embedded convective updrafts and freezing/melting levels.

3.2.2 CloudSat Geometric Profile

The CloudSat Geometric Profile (Geoprof) is a level 2B product that estimates the locations and spatial structures of clouds occurring within its field of view. This study uses the CPR Cloud Mask subproduct found within the Geoprof product, and references the Radar Reflectivity subproduct to help understand ambiguous situations.

The CPR Cloud Mask contains the estimated probable location of clouds for a two-dimensional cross section of the atmosphere within CloudSat's field of view. The cloud mask itself is derived directly from the echo return power from the 1B-CPR product. The

cross-section is divided into bins, with each bin extending 1.1km horizontally and close to 240m vertically. The mask product is 125 bins vertically tall, representing a 25km depth of atmosphere over the oceans. Each bin in the cross-section is assigned a number indicating the probability of a cloud occurring within that bin (Fig 3.3). While the numbers given by the mask have no inherent physical or statistical significance, verification studies are used to help match values in the cloud mask with empirical statistical probabilities (Table 3.1).

The heart of the Cloud Mask product is the Significant Echo Mask (SEM) algorithm. This algorithm is designed to detect the presence of hydrometeors by determining which bins contain more echo power than is likely to be caused by normal sensor noise. The distribution of sensor noise can be measured by examining echo returns above the tropopause, where clouds and other hydrometeors are very unlikely to occur. This noise distribution is then compared to all the bins in the granule. Bins containing echo returns that are much greater than the noise distribution are said to contain a "significant echo", and are flagged as containing clouds. This process works well for thick deep clouds such as the ones occurring along polar frontal boundaries, but problems arise for very thin cirrus clouds which have very low echo powers. Additional statistical methods are applied to distinguish thin clouds from noise (described in literature as "aggressive"), but the SEM still has problems with thin clouds (e.g. the ambiguous cloud in Fig 3.3).

Another problem relevant to this project is the difficulty of detecting very low level stratus clouds. The CPR's signal is heavily scattered by the ground. This scattering is very useful for measuring things like the surface elevation and beam attenuation, but it also interferes with the echos coming from clouds within 1km or so of the surface. In

terms of observing atmospheric rivers, this issue may disrupt detection of any low level stratus normally occurring near polar fronts (if stratus decks are a typical feature).

One more note should be made for the beam attenuation mentioned earlier. Large raindrops, common in heavy precipitation, will scatter and attenuate the beam greatly. This can significantly decrease the return power from the lower regions of convective clouds or storm systems. In addition to this, large amounts of water vapor can slightly attenuate the beam as well, though not as significantly as precipitation. Surprisingly, this is not accounted for in any of the early 2B-Geoprof products. Cloud mask users may have difficulties using the cloud mask for extreme heavy precipitation events, usually tropical in nature. However, we have observed that atmospheric rivers rarely cause the heaviest precipitation needed to completely attenuate the CPR signal, particularly over the oceans. For the purposes of this project, there are only a couple of cases where attenuation may be a problem, which will be noted when necessary.

While it is true that the cloud mask itself is derived directly from CPR measurements, it is important to note that calibration and verification of the cloud mask depends on inputs from ancillary sources, notably MODIS measurements and ECMWF model output (CloudSat Geoprof Desc.). While these datasets have been extensively analyzed and used, it is possible that unknown weaknesses in these datasets can carry over into the cloud mask indirectly.

The Radar Reflectivity product is basically the 1B-CPR's echo product expressed in terms of dBZ instead of raw radar return power. The major difference between the echo and reflectivity products (aside from the oversampling) is the application of the SEM to the reflectivity product, reducing the amount of noise presented in the reflectivity (Fig

3.4). The reflectivity is used in the CloudClass product to identify cloud types. Though this project uses mostly the Cloud Mask and Cloud Class products to characterize cloud, the Radar Reflectivity may be useful for double-checking the output from the former two products and for clarifying ambiguous measurement situations.

Validation for the radar and the Geoprof products (and the Cloud Class product) is done largely by special campaigns such as the Canadian CloudSat/CALIPSO Validation Project (C3VP), which compares ground and aircraft observations with CloudSat observations of clouds over Canada (Hudak 2005). The goal is to rigorously test the algorithms used by the CloudSat products (e.g. the SEM algorithm) with the measurements from a suite of radiometers, radars, imagers, and other instruments. The project is supposed to run for several years, with the data collection period having occurred from October 2006 to March 2007 in southwest Ontario.

3.2.3 Cloud Scenario Classification

The CloudSat Cloud Scenario Classification (Cloud Class) product estimates the type of cloud found in each bin of the GeoProf product. For each cloudy bin identified by the SEM algorithm, one cloud type of eight is assigned to that bin (Fig 3.5). Cloud types are assigned by a number of criteria about spatial scale and echo strength (Table 3.2). Validation work on the Cloud Class algorithm predates the launch of CloudSat, by utilizing ground-based cloud radars and lidars in combination with traditional ground observations (Wang 2001).

There are five primary criteria used to identify cloud types. These criteria are not completely rigid, and one criterion be overridden if other criteria strongly suggest a certain cloud type (Wang 2007).

1) Precipitation is a very important criterion for identifying deep convective clouds and nimbostratus clouds. It is unlikely that other cloud types could produce as much heavy precipitation as a cumulonimbus, for example. Precipitation is identified using attenuation of the radar beam, resulting in decreased surface reflectivity (as described previously).

2) Maximum reflectivity will be greater in a dense cumuliform cloud than a less dense stratus deck with the same physical dimensions.

3) Vertical extent includes the height of the cloud base, the height of the cloud top, and the depth of the cloud. Most cumuliform clouds have low cloud bases, with only altocumulus being far removed from the surface. High reflectivity values extending from near the surface to several kilometers above the surface are usually indicative of a strong convective updraft lifting dense cloud material into the upper troposphere; stratiform clouds do not possess these updrafts. Cirrus clouds do not occur in the lower troposphere. In practice, temperature information is used to help identify the height of the vertical bins, which can vary for several reasons.

4) Cloud horizontal extent is usually greater for stratiform clouds than cumuliform clouds. However, this criterion can be overridden if the other criteria strongly support a certain cloud type. For example, while most

deep convective clouds are only a few tens of kilometers wide, some large

convective systems can exceed a hundred kilometers in width (such as

those occurring within atmospheric rivers). In these cases, the heavy

precipitation, high reflectivity values, and large vertical depth override the

large horizontal width.

5) Cloud temperature is mostly used for identifying high level clouds.

Temperature information is provided by ECMWF output.

At the time of this writing, the Cloud Class product is still in the experimental stage

with ongoing modifications and verification work. Of the work presented in this report,

the Cloud Class results remain the most tentative. The Cloud Class algorithm is designed

to be the most reliable for the entire global atmosphere, so specific meteorological

features may not be well-represented in the product. Specific issues with using the Cloud

Class product for this project will be discussed in relevant sections. However, for the

moment, the current Cloud Class product is the best data set available for answering

questions involving cloud types within atmospheric rivers. Furthermore, the cloud types

often depicted within and around rivers do not run completely contrary to outside

measurements (e.g. AMSR-E) and intuitive expectation, so for this study the preliminary

Cloud Class product is used to some extent.

3.3 Aqua and the Advanced Microwave Scanning Radiometer-EOS

Aqua was launched on 4 May 2002 as a major component of the Earth Observing
System (EOS). Aqua's primary purpose is to take more specialized measurements of
Earth's hydrological cycle, including atmospheric water vapor, as a complement to the
EOS Terra satellite (Parkinson 2003).

3.3.1 The Advanced Microwave Scanning Radiometer-EOS

The Advanced Microwave Scanning Radiometer-EOS [version] (AMSR-E) is a six-
frequency conical scanning passive microwave radiometer with horizontal and vertical
polarization measurements for each frequency (Kawanishi 2003). Measured frequencies
are 6.9, 10.7, 18.7, 23.8, 36.5, and 89.0GHz (Table 3.3). The 50GHz channels used by
other AMSR instruments are not included on AMSR-E for space constraint reasons. The
instrument maintains a constant incidence angle of 55°, yielding a swath width of
1450km. Horizontal resolution varies with frequency, from 43x75km for 6.9GHz to
3.5x5.9GHz for 89.0GHz. AMSR-E uses an external calibration scheme.

3.3.2 AMSR-E Ocean Algorithm

The AMSR Ocean Algorithm is a methodology developed to retrieve several
geophysical variables from AMSR-E measurements simultaneously from a set of semi-
physical linear-regressed equations (using radiosonde data) coupled with a radiative
transfer model. Retrieved variables include total precipitable water (TPW), precipitation,

33

surface wind speed, cloud liquid water, and sea surface temperature. All frequencies are used as input variables.

The Ocean Algorithm TPW grid contains TPW measurements occurring over one 24hr period, separated into ascending (afternoon) and descending (morning) orbital branches. The TPW values range from 0mm to 75mm. Each swath is 1450km wide, with a pixel resolution of 25km x 25km (Fig 3.6). This resolution is much larger than CloudSat's resolution, leading to the "bumpiness" of the TPW curve when CloudSat and AMSR-E data are compared.

The 18.7, 23.8, and 36.5GHz channels are the most influential in estimating TPW within the algorithm (Wentz 2000). Water vapor has a weak absorption band at 22.23GHz, so the 23.8GHz channels would be the most sensitive to atmospheric water vapor, and the 18.7GHz channels slightly less sensitive. 36.5GHz is an atmospheric window frequency, so the 36.5GHz window channels can measure background radiance from the ocean surface for the purposes of removing their influence on the channels sensitive to water vapor (Fig 3.7). In this way, water vapor indices such as TPW can be retrieved from AMSR-E's radiance measurements. Validation of retrieved water vapor is done by comparison with radiosonde data and retrieval information from the SSM/I and TMI radiometers.

The primary issue of concern with the ocean algorithm is its questionable performance when viewing high precipitation environments. In the microwave regime, a water droplet's radiative properties change substantially as it grows from a cloud droplet into a larger raindrop. If precipitation within the field of view does not behave in the way the algorithm predicts (which is possible given the extreme nature of some atmospheric

rivers), then both the TPW and the rain rate products will be affected adversely. Heavier precipitation makes TPW retrievals practically impossible, as well (Fig 3.8). While precipitation will not hide the presence of an atmospheric river or create a false appearance of a river, it often makes accurate measurements of maximum TPW within the river impossible. These data gaps also make defining horizontal coordinate systems based on TPW structure a challenge.

Mask Value	Meaning	% False Detections Goal	Estimated % False Detection via CALIPSO comparison
-9	Bad or missing radar data		
5	Significant return power but likely surface clutter		
6-10	Very weak echo (detected using along-track averaging)	< 50 %	44 %
20	Weak echo (detection may be artifact of spatial correlation)	< 16%	5 %
30	Good echo	< 2 %	4.3 %
40	Strong echo	< 0.2 %	0.6 %

Table 3.1) Description of numerical values found in the CPR Cloud Mask product (from CloudSat Geoprof Description)

Cloud Class	Cloud Features	
High Cloud	Base	> 7.0 km
	Rain	no
	Horiz. Dim.	10³ km
	Vert. Dim.	moderate
	LWP	= 0.
As	Base	2.0-7.0 km
	Rain	none
	Horiz. Dim.	10³ km, homogeneous
	Vert. Dim.	moderate
	LWP	~ 0, dominated by ice
Ac	Base	2.0-7.0 km
	Rain	virga possible
	Horiz. Dim.	10³ km, inhomogeneous
	Vert. Dim.	shallow or moderate
	LWP	> 0
St	Base	0-2.0 km
	Rain	none or slight
	Horiz. Dim.	10² km, homogeneous
	Vert. Dim.	shallow
	LWP	> 0.
Sc	Base	0.-2.0 km
	Rain	drizzle or snow possible
	Horiz. Dim.	10³ km, inhomogeneous
	Vert. Dim.	shallow
	LWP	> 0.
Cu	Base	0-3.0 km
	Rain	drizzle or snow possible
	Horiz. Dim.	1 km, isolated
	Vert. Dim.	shallow or moderate
	LWP	> 0.
Ns	Base	0-4.0 km
	Rain	prolonged rain or snow
	Horiz. Dim.	10³ km
	Vert. Dim.	thick
	LWP	> 0.
Deep convective clouds	Base	0-3.0 km
	Rain	intense shower of rain or hail possible
	Horiz. Dim.	10 km
	Vert. Dim.	thick
	LWP	> 0.

Table 3.2) Cloud characteristics used to determine Cloud types (from Wang 2005).

Parameter	Performance and characteristics						
Center Frequency (GHz)	6.925	10.65	18.7	23.8	36.5	89.0(A)	89.0(B)
Bandwidth (MHz)	350	100	200	400	1000	3000	3000
Polarization	Vertical and Horizontal polarization						
NEΔT (K) [1]	< 0.34	< 0.70	< 0.70	< 0.60	< 0.70	< 1.20	< 1.40
NEΔT (K), as built [1], V-pol/H-pol	0.32/0.34	0.49/0.57	0.55/0.47	0.56/0.54	0.51/0.41	0.89/1.01	1.18/0.91
Dynamic range (K)	2.7 to 340						
Main beam efficiency (%), as built [2]	95.1	94.8	95.8	94.8	93.9	94.5	93.7
Cross polarization (%), as built [2]	0.34	0.29	0.32	0.89	0.43	0.77	0.68
Feed-horn spillover (%), analysis [2]	3.6	2.8	2.2	3.2	2.4	2.4	2.6
Incidence angle (deg.)	55.0						54.5
Off-nadir angle (deg.)	47.5						47.0
Beam width (deg.)	2.20	1.50	0.80	0.92	0.42	0.19	0.18
IFOV (km) Cross-track x along-track	43x75	29x51	16x27	18x32	8.2x14	3.7x6.5	3.5x5.9
Sampling interval (km), Along-track	10.1					4.1/6.0 (B→A/A→B)	
Sampling interval (km), Cross-track	9.0					4.5	4.4
Swath width (km)	1450						
Integration time (msec)	2.5					1.2	
Digital quantization (bits)	12	10					

Table 3.3) AMSR-E frequencies and related properties (from Kawanishi 2003)
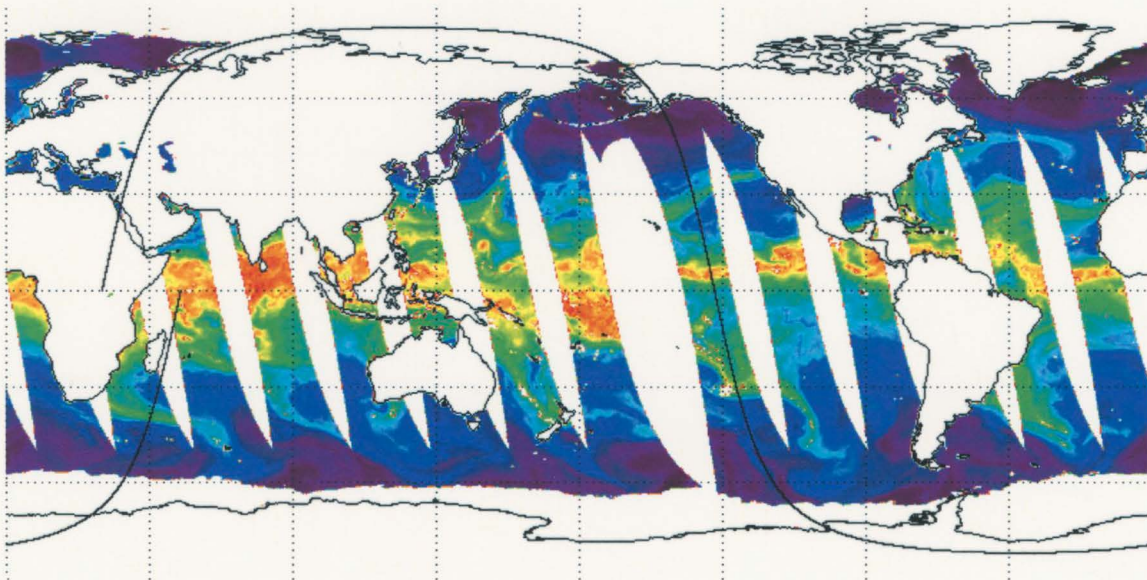
Figure 3.1) CloudSat's swath (black line) falls well within AMSR-E's swath during an ascending pass over the Pacific.
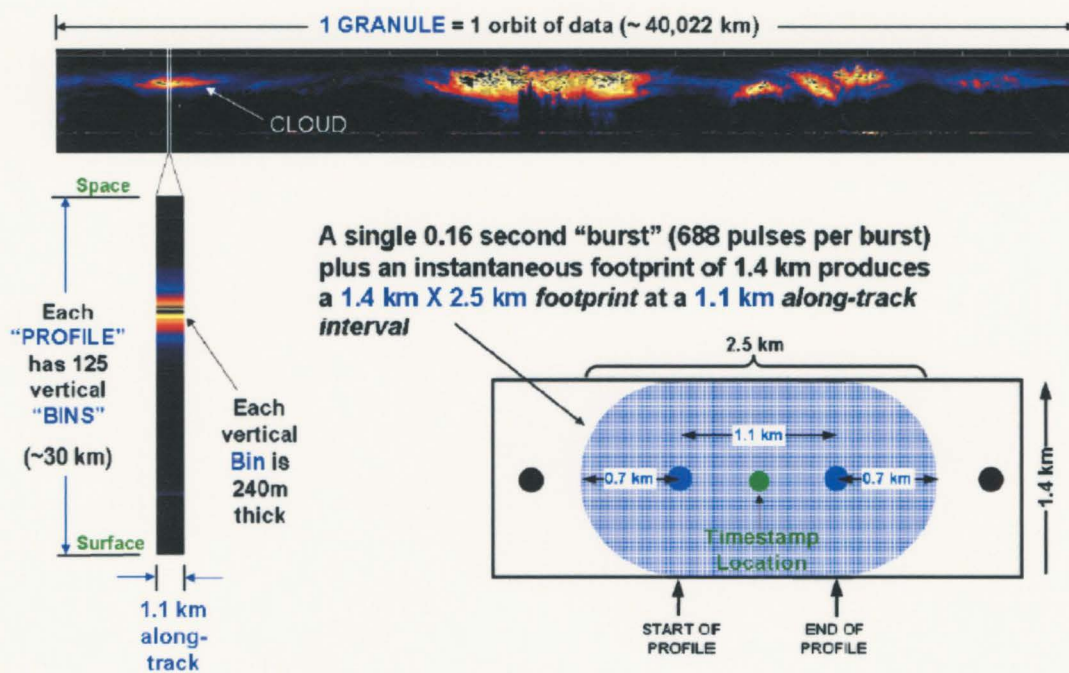
Figure 3.2) CloudSat's footprint and vertical resolution (from CloudSat Handbook)

Figure 3.3) Example cloud mask output from the northern Pacific. Note the ambiguity with the high cloud in the middle of the image.
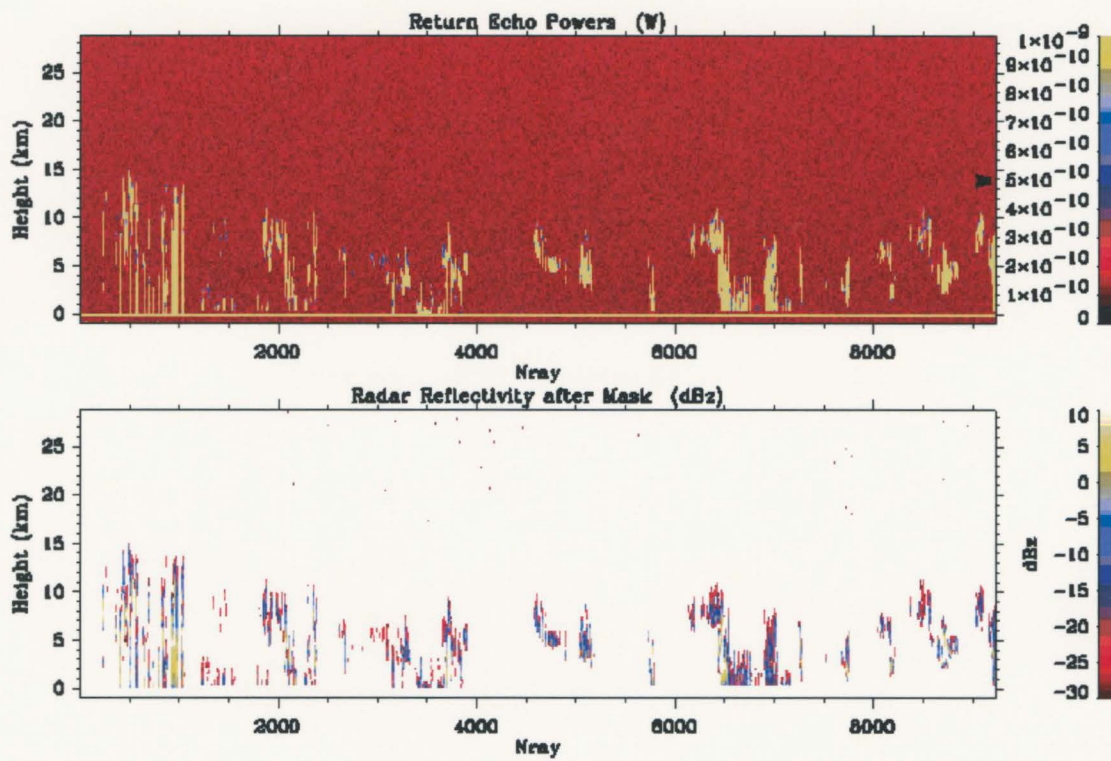
Figure 3.4) Relationship between echo power and reflectivity (from Geoprof Description).
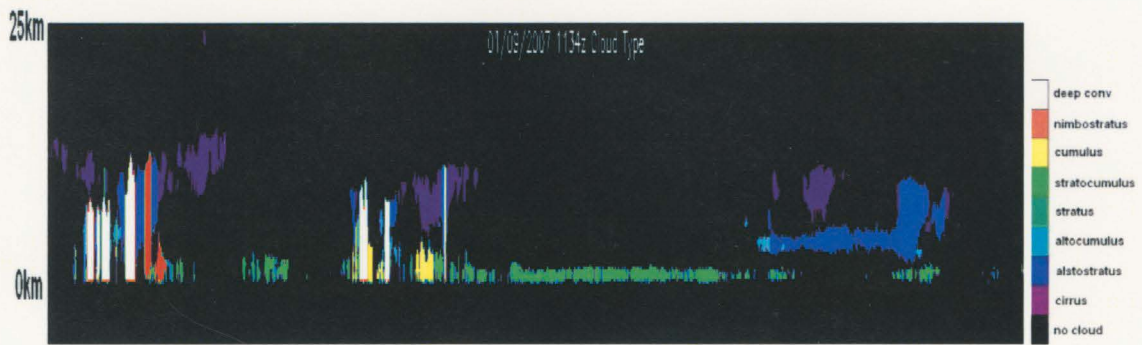
Figure 3.5) Example of Cloud Class product for the northern Pacific Ocean
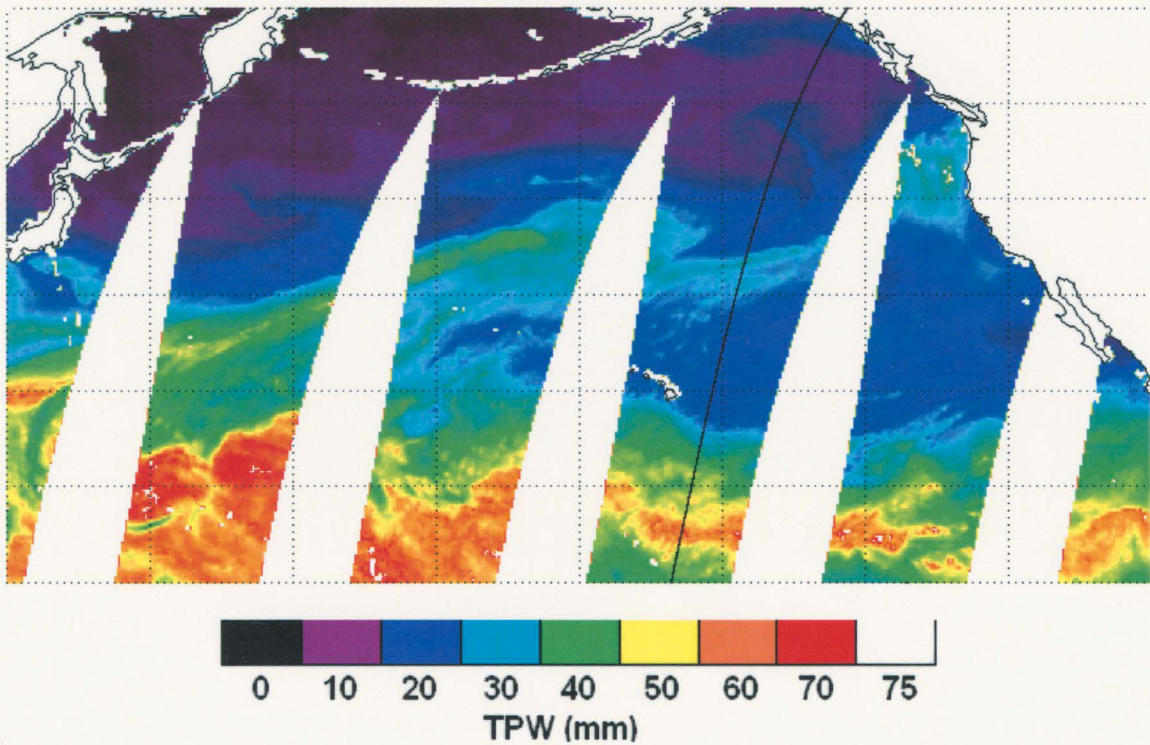
Figure 3.6) AMSR-E TPW map of the north Pacific. The white strips are areas not covered in AMSR-E's 12hr swath. One of CloudSat's passes is marked with the black line.
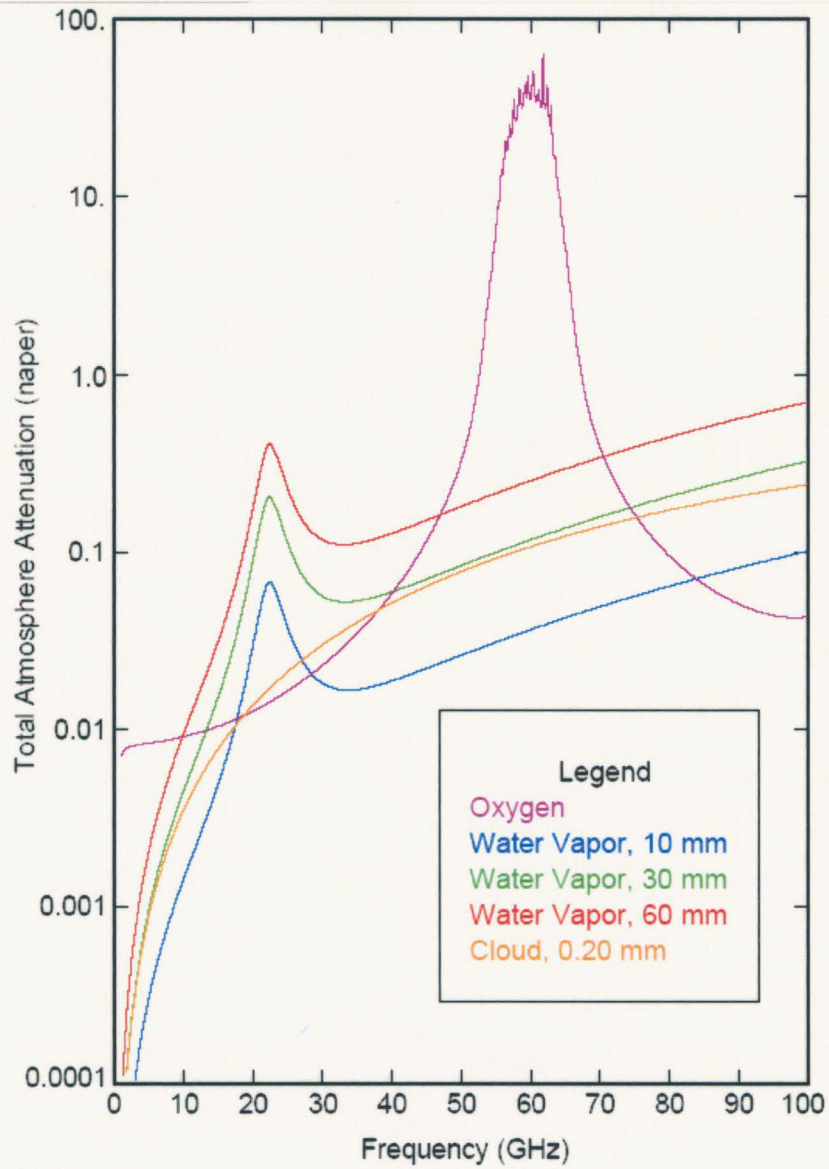
Figure 3.7) Attenuation of microwave radiation by water vapor (from Wentz 2000).
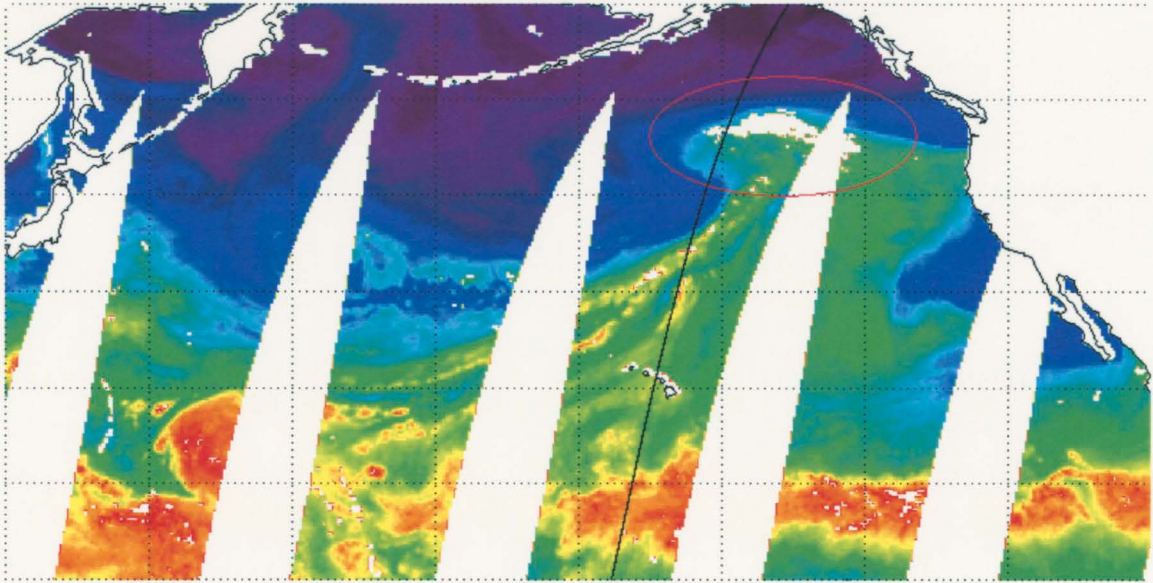
Figure 3.8) Precipitation-induced retrieval failure for TPW in a developing extratropical cyclone and atmospheric river (red ellipse).

4. CASE STUDIES

4.1 River Identification

For this research project, atmospheric rivers were identified using the planer view TPW map of the northeast Pacific as measured by the AMSR-E instrument. The primary identification criteria are as follow:

1) A river's core contains a moisture structure with TPW values significantly greater than the surrounding areas.

2) A river's moisture axis must contain a maximum TPW value greater than or equal to 20mm.

3) The moisture axis must be greater than 2000km along its major dimension (hereby referred to as a river's "length").

4) The moisture axis must be less than 1000km along its minor dimension (hereby referred to as a river's "width").

5) The moisture axis must extend into the northeast Pacific region, possibly also extending into but not confined within the tropics or lower subtropics.

The first four criteria were used for identification purposes by Ralph et al when working with CALJET observations. The criteria are not universally used for all atmospheric river research, but there are no serious complaints about these criteria in the literature either.

The first criterion recognizes the atmospheric river as being first and foremost a region of high water vapor concentration. The second and third criteria limit significant moisture masses to the characteristic filamentary structure of the atmospheric river (Fig. 4.1).

However, the narrow width requirement in particular can occasionally be difficult to handle in certain river events where the southern gradient region of the moisture band can be diffuse (e.g. the November 6th case). The fourth criterion is needed to separate atmospheric rivers from other filamentary water vapor structures occurring in the tropics (e.g. upper level moisture plumes) as well as the ITCZ itself. The limit to the eastern Pacific is because the bulk of in situ river research occurs in the eastern Pacific, and this research aims to stay consistent with the current body of knowledge for the time being.

For this project, it is necessary to determine when a river event begins and ends, in order to divide up the observational data into individual river events. In the majority of cases this can be accomplished manually without resorting to a hard set of rules. One river event is defined as the period from when an individual moisture mass converges into a singular filamentary river structure meeting the primary identification criteria until the time the filamentary structure fails at least one of the criteria. Most river events occurring during the 2006-2007 season followed this definition closely. However, like many meteorological features (like polar fronts), rivers are not always discrete entities. It is possible for two rivers to merge into each other, or for one river to break in half when a low pressure region forms near its midpoint. It is also possible for a river to temporarily fail the primary criteria for a short period of time (up to a day) but recover afterwards, while obviously remaining the same atmospheric feature. The 9th and 13th river events are divided into two parts each for this reason. These occurrences do not separate into individual cases easily, and there is no standard methodology currently existing to define individual river cases, so choosing cases becomes more subjective. These particular cases are noted.

4.2 River Dataset

The data set used to examine atmospheric rivers contains 22 individual river events occurring between November 2006 and April 2007. Two of the river events are divided into two parts for reasons listed previously, giving a total of 24 formation-to-dissipation periods. Table 4.1 lists each river event and relevant information.

The A-Train orbits the planet rapidly enough that each river event almost always has several satellite overpasses between its formation and dissipation. Some of these passes occur with CloudSat's field of view moving more or less along the river's length. These passes are not usable for composite plots or inter-river cloud comparisons, but they can provide some information about the cloud variation occurring along a river's moisture axis. Other passes occur at a great enough angle to the moisture axis that they can be used for cross-sectional comparison purposes. Most of the 24 cases have multiple usable passes. Because of this, it is possible to use CloudSat data to get a rough idea of time evolution of a river's cloud structure. The methodology for accomplishing a time evolution is as follows:

1) For each case, choose a CloudSat pass closest to the river's maximum intensity. Maximum intensity is found as follows:

   a. For all passes for one case, choose the passes with the tightest TPW gradients.

   b. Out of those passes, choose the pass with the highest central TPW values.

c. If there is more than one pass with similar maximum TPW values (uncommon), choose the one with CloudSat passing the closest to perpendicular with the main moisture axis.

2) For all cases, the maximum intensity passes are placed into one group, the "best" group.

3) All passes occurring before the maximum intensity passes for each particular river are placed into a second group, the "before" group.

4) All passes occurring after the maximum intensity passes for each particular river are placed into a third group, the "after" group.

In this way the passes all fall neatly into a rough time-based category system without the need for a rigorous time-based coordinate system. It is a basic system, and is partly dependent on the methodology used for choosing the "best" case, but it still provides a useful first look at a river's time evolution, and may provide some insight into the time evolution of other physical processes occurring within the river as well.

4.2.1 Co-Locating CloudSat and AMSR-E

Using two satellites in the A-Train makes co-location relatively simple compared to other satellites. For temporal purposes, CloudSat trails Aqua by only a minute or so. Atmospheric rivers are somewhere between mesoscale (100km order of magnitude) and synoptic scale (1000km order of magnitude) events, with a time period much greater than a few minutes. For this reason, it is reasonable to assume for this project that CloudSat and AMSR-E measurements are taken simultaneously. For spatial co-location, with CloudSat's footprint being much smaller than AMSR-E's footprint, TPW for each

CloudSat profile is taken from the AMSR-E TPW gridpoint that corresponds to CloudSat's latitude and longitude at the time of the profile. This can lead to errors of a few kilometers towards the edges of AMSR-E's gridpoints where sudden changes of TPW are possible, but these errors are small compared to the typical river width of several hundred kilometers.

4.2.2 Eliminating Angle Independence

Because of the A-Train's orbital geometry and the atmospheric rivers' variable orientations, CloudSat's orbital track does not pass over all rivers at the same angle to the river's moisture axis. Because of this, the measurements within the river can become elongated within the datasets as the crossing angle becomes smaller (Fig. 4.2). For inter-river cloud comparisons, it is necessary to eliminate angle dependence so that the results more accurately reflect the real atmosphere. Fortunately, CloudSat's ground track curvature is small compared to the width of the rivers, so correcting for angle is a matter of fundamental trigonometry.

4.3 Individual River Cases

The following section presents four river events chosen from the twenty-two total river events as case studies. It may be useful to see some data from individual observations to better interpret the multi-river plots. The cases were selected to show a variety of river and cloud structures, as to not present an apparent artificial bias towards any one particular cloud structure. The CloudSat observations are presented in the physical

length-based coordinate system for simplicity (coordinate systems are discussed in detail in the multi-river chapter).

4.3.1 5-7 Nov 2006

This river event was the strongest occurring in the 2006-2007 river season. As noted earlier, this river cased a large amount of flooding in the Washington/Oregon area, breaking several local records. Observations of this river are shown in Fig. 4.5-4.8.

This river began as a large tongue of moisture covering much of the northeast Pacific, which eventually converged into a very wide moisture band. Large amounts of deep clouds formed throughout the early moisture tongue, and convection quickly developed along the frontal boundary as the river structure formed (Fig). During the river's mature phase, the convective clouds along the river converged into a concentrated band spanning much of the river's length. During the river's decline, deep clouds dissipated along much of the river's length, only lingering along the coastline.

4.3.2 14-17 Nov 2006

This river event was notable for the lack of deep cloud formation despite possessing typical river TPW values and structure. High clouds were limited to the river's landfall region, likely related to orographic lifting. This river produced some moderate rain along the Oregon coastline, but nothing as severe as had occurred in the Nov. 6th case. Observations of this river are shown in Fig. 4.9-4.11.

The river formed as a moisture band in the subtropics (possibly a "moisture plume"), which entered the midlatitude Pacific basin and merged with an extratropical cyclone. At

this time a band of low level clouds formed along the frontal boundary, producing shallow convection. These clouds persisted over the river's lifespan, but never developed into a deep cloud band. The clouds dissipated when the river began showing signs of weakening, leaving only very shallow stratiform cloud behind.

4.3.3 7-12 March 2007

This river could be considered a "typical" river case, possessing moderate TPW values and a well-defined filamentary structure. There were no severe rain reports associated with this landfall. Observations of this river are shown in Fig. 4.12-4.14.

The river began as a moisture tongue extending out of the subtropics, converging into a river structure over a couple of days. There was considerable deep cloud formation and convection within the moisture tongue, even before taking on a river structure. As a mature river, a band of deep convective clouds spanned much of the river's length. As the river weakened, the width of the deep cloud band considerably decreased, leaving behind a deck of mid-level and high level clouds.

4.3.4 21-25 March 2007

This river was another example of a "typical" river case. The river spanned across much of the northern Pacific region, but was fairly narrow in width by the time it entered the eastern Pacific region. There were no severe weather reports associated with this river. Observations of this river are shown in Fig. 4.15-4.18.

The river began in the western Pacific, entering the northeast Pacific fully-developed. This river contained a deep cloud band like most other rivers, but strong convective

clouds were not as apparent in this river as they were in many other river cases. This may suggest that the convective cells possessed weaker updrafts, or that the deep clouds were formed largely through non-convective processes, e.g. isentropic lifting. Later in its life, the deep cloud band dissipated, leaving a high level cloud deck over the weakening river.

4.4 Case Studies and Vertical Temperature Profiles

While the main purpose of this project is to observe clouds within atmospheric rivers, it may be useful to examine vertical sounding profiles taken near rivers to complement observations of clouds. As was shown previously, rivers often contain deep convective systems. While many variables influence cloud formation, deep convective systems form most often in regions of high vertical instability. The 14-17 Nov river event did not produce deep convection like the other three cases presented, so it's possible that the pre-frontal environment lacked the instability needed for deep convection. Ideally, for this purpose the best place to take soundings is just ahead (i.e. south) of the river and polar front. The river draws most of its moisture and warmth from the warm sector, so the warm sector's vertical profile is most relevant to deep convection within the river. Of course, the environment within the river is usually already "contaminated" by existing deep convection and other activity, so the sounding needs to be taken in advance of the river's position.

Unfortunately, it is difficult to obtain soundings representative of the pre-river environment from normal land-based radiosonde stations because of both land contamination (e.g., orographic lift) and the variable location of river landfalls on the

coast. Also, because this project focuses on clouds occurring over the ocean, it is ideally more desirable to take soundings within ocean air masses. Fortunately, it is possible to use the sounding ability of the Aqua satellite to obtain temperature soundings in the pre-river environment for all river events. These soundings are derived from measurements taken by the Atmospheric Infrared Sounder (AIRS) and the Advanced Microwave Sounding Unit (AMSU), both mounted on Aqua (Aumann 2003). The soundings used in this project were taken near CloudSat's orbital track a few hundred kilometers ahead (south) of the rivers' central moisture axes, far enough that the clouds within the river do not interfere with the retrieval. Clouds can be problematic for IR-based soundings, so the sounding locations used in this project were taken in fairly cloud-free locations (which is usually the case in the pre-river environment). Most other accuracy issues for the soundings involve land emissivity effects, which are not a problem over the ocean (Chahine 2006).

Figure 4.19 shows four AIRS-derived temperature soundings taken during the maturity phase of each river in the presented case studies. In general, vertical instability is a function of both temperature and moisture, but the AMSR-E observations of these cases show that moisture is abundant in all four river events. In terms of temperature, larger environmental lapse rates create greater environmental instability, so it is reasonable to expect greater deep convective activity in environments with higher lapse rates. Between the four sounding, the largest difference in lapse rates occurs between the 850mb and the 700mb levels. The 15 Nov event (the event lacking high cloud and deep cloud development) had the lowest lapse rates in this region, with a 3.7K change between 850mb and 700mb. The 6 Nov case had a 6K change, the 10 Mar case had a 6.5K change,

and the 23 Nov case had a 7.8K change. The pre-river environments before and after maturity show the same general differences between the events, with the 15 Nov case having the lowest lapse rates. These soundings suggest that the lack of instability just above the planetary boundary layer contributed to the lack of deep convection occurring in the 15 Nov event. However, it is also apparent that temperature lapse rates are not the only contributing factor to deep convection, as the 6 Nov event had lower lapse rates than the March events.

case number	dates	comments
1	11/5 - 11/7	record-setting event
2	11/11 - 11/14	merged with #3
3	11/14 - 11/17	
4	11/19 - 11/20	missing AMSR-E data 11/17 - 11/19
5	12/12 - 12/14	
6	12/25 - 12/26	
7	12/31 - 1/04	
8	1/04 - 1/06	borderline case
9	1/06 - 1/10	almost two cases - central TPW value fell below 2cm for a day, but moisture maintained filamentary shape
10	1/17 - 1/19	
11	1/18 - 1/23	
12	2/01 - 2/04	
13	2/05 - 2/11	almost two cases - moisture axis temporarily loses filamentary shape, but recovers next day
14	2/13 - 2/17	river develops exaggerated "kink" in later stages
15	2/18 - 2/19	
16	3/06 - 3/07	
17	3/07 - 3/12	several filamentary structures develop and fail before main river forms
18	3/13 - 1/17	missing CS data 3/17 - 3/21
19	3/21 - 3/25	may be related to event occurring during data blackout
20	3/27 - 3/30	river disintegrated into moisture tongue
21	4/01 - 4/03	merged with #21
22	4/02 - 4/08	
-	-	data availablility was lacking at this point

Table 4.1) List of cases used in this project, with specific comments of the river's characteristics when necessary.
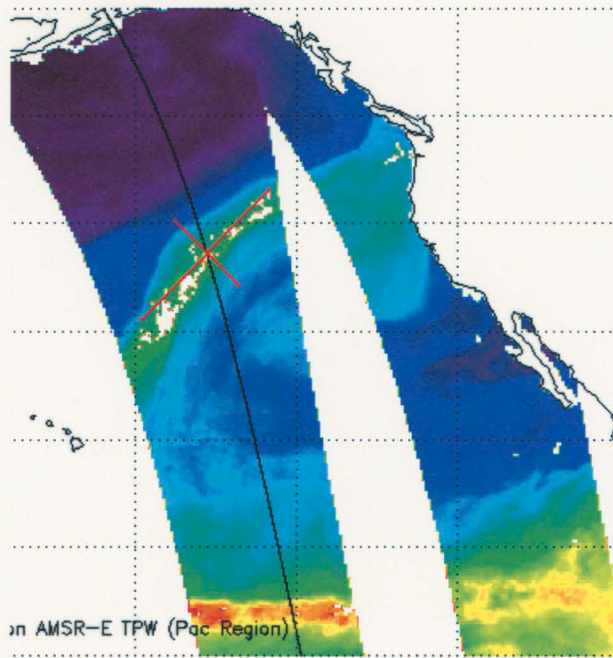
Figure 4.1) The physical dimensions of an atmospheric river. The red lines represent the distance constraints defining the river. The line along the moisture axis denotes a 2000km length, and the line across the moisture axis denotes a 1000km length.
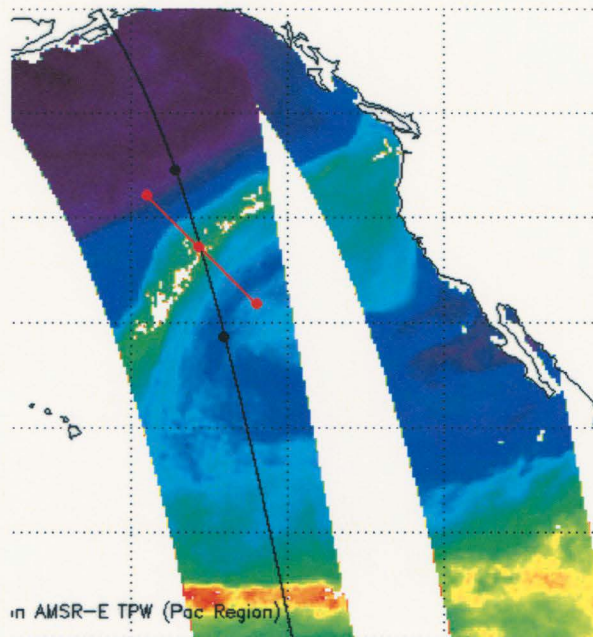

Figure 4.2) Reforming the CloudSat data to eliminate angular dependence. The red line is perpendicular to the moisture axis. The example data points on the CloudSat orbit (marked with black dots) are projected onto the perpendicular line (marked by red dots), reducing the distortion in the CloudSat data.
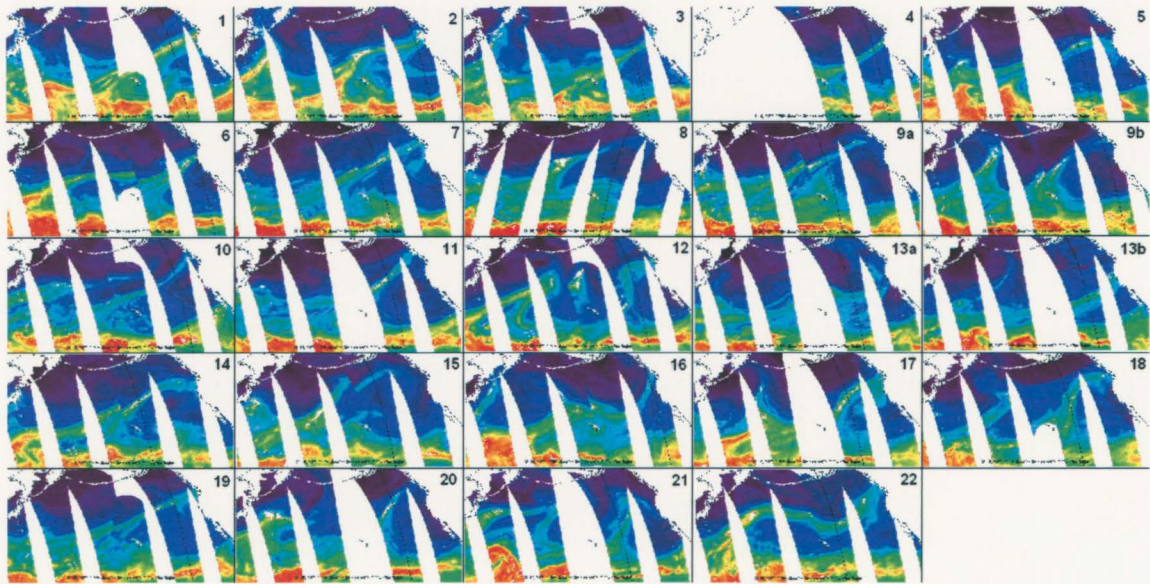
Figure 4.3) Mosaic of the twenty-two river events (including each half of the two-stage events) used in this project.
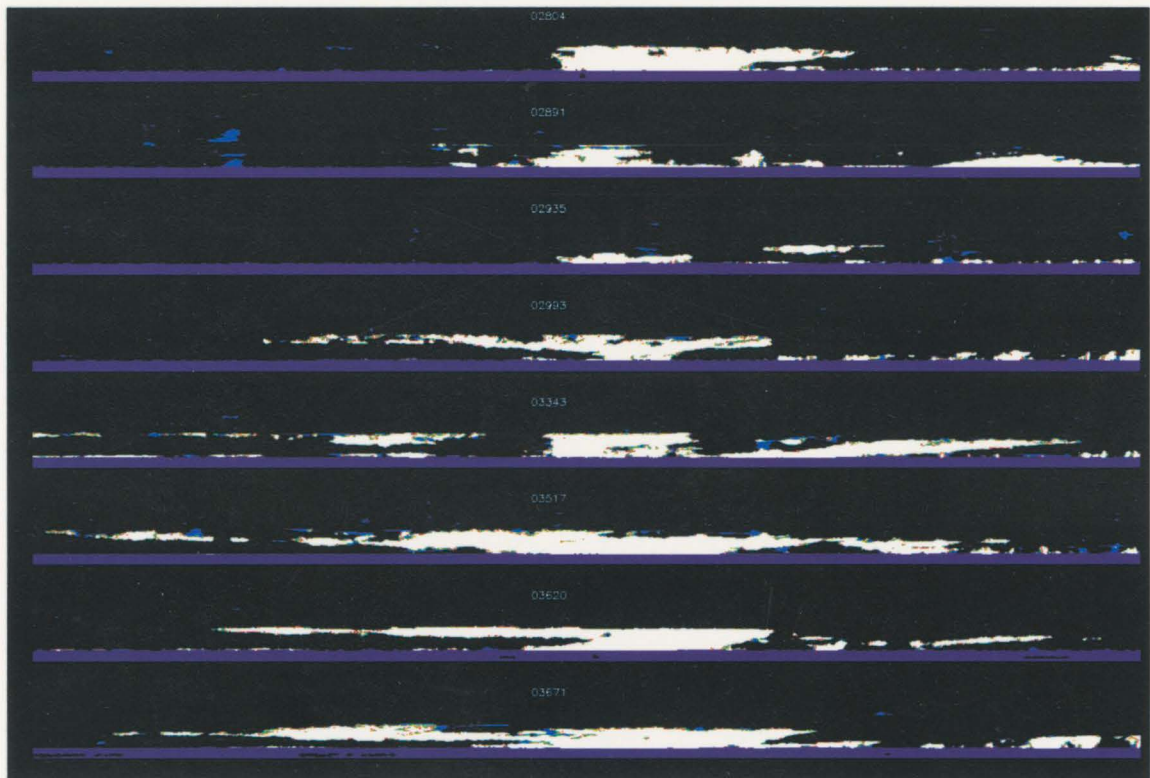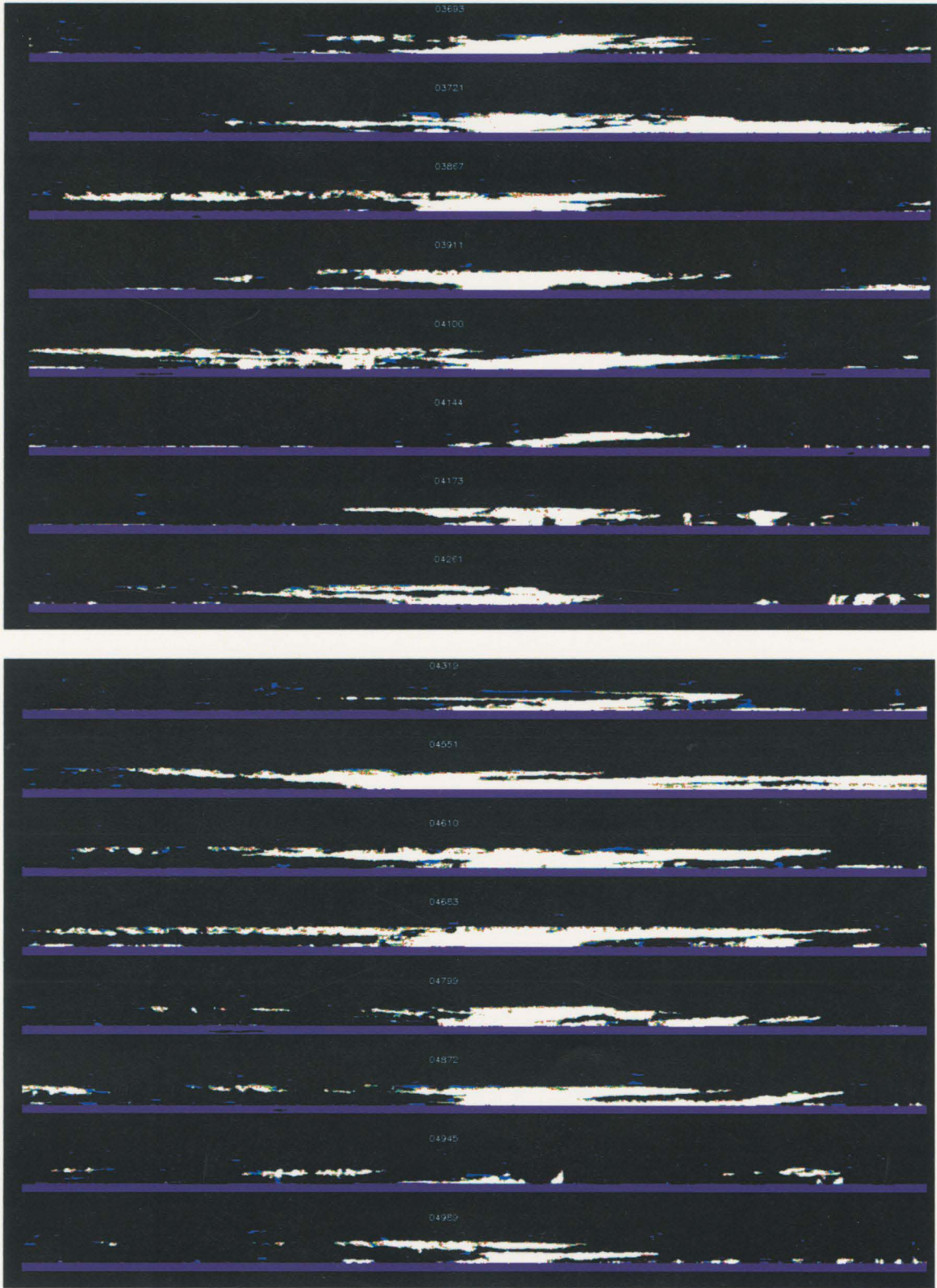
Figure 4.4) Mosaic of the cloud masks for the 22 river cases.
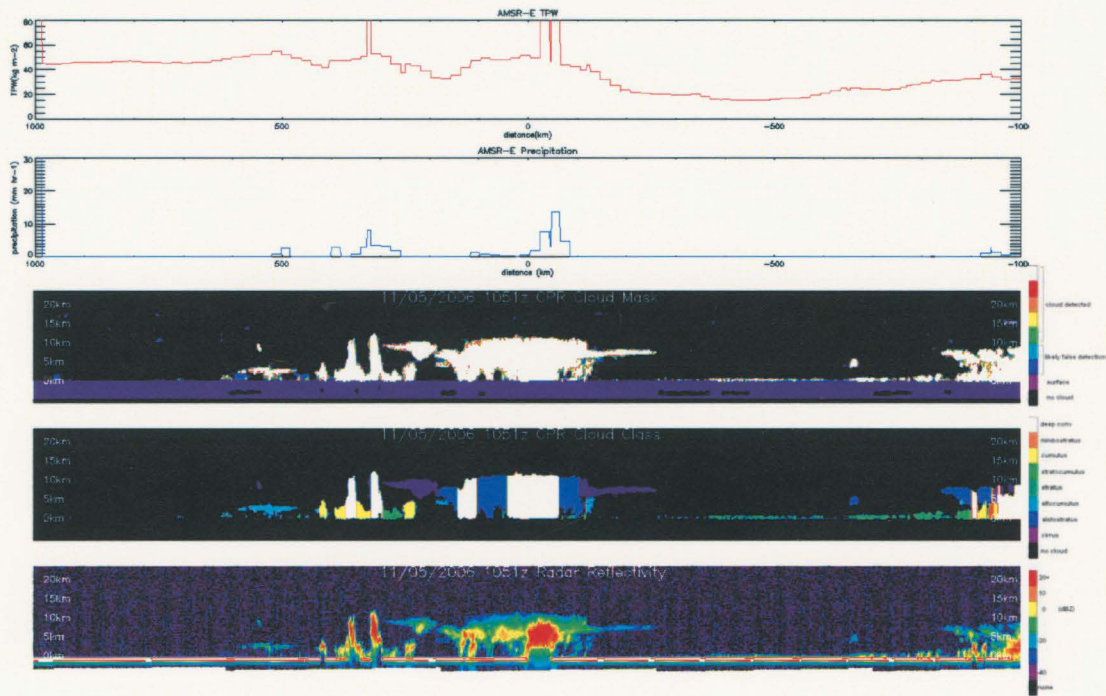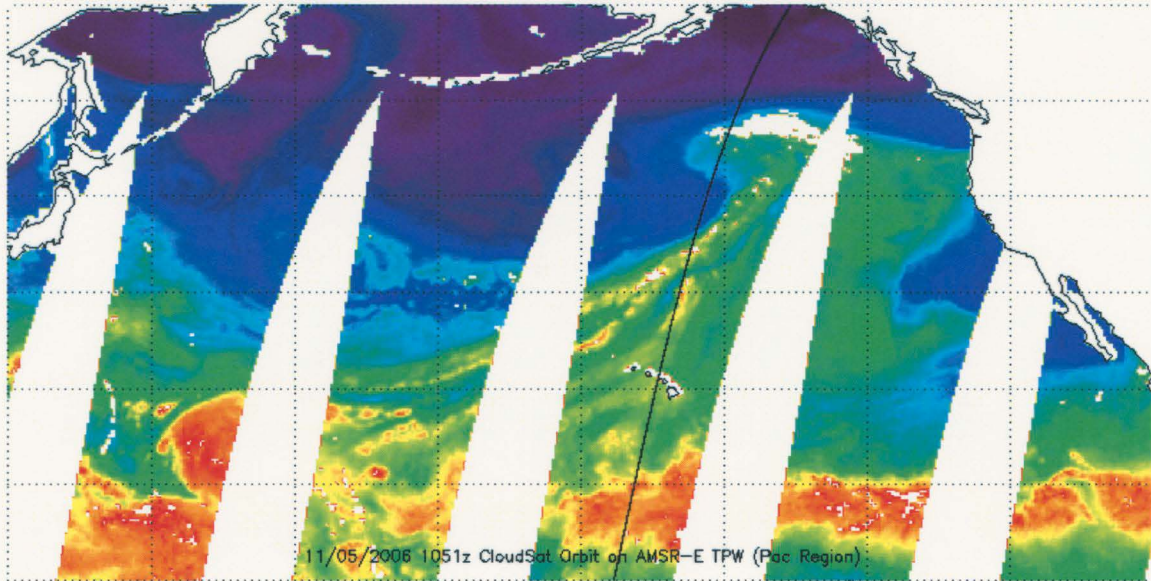
Figure 4.5) Observation on 5 November 2006, morning pass.

The TPW map shows a large tongue of moisture in the eastern Pacific, with a moisture convergence zone forming along its northwestern boundary. Deep convective clouds are forming within the convergence zone.
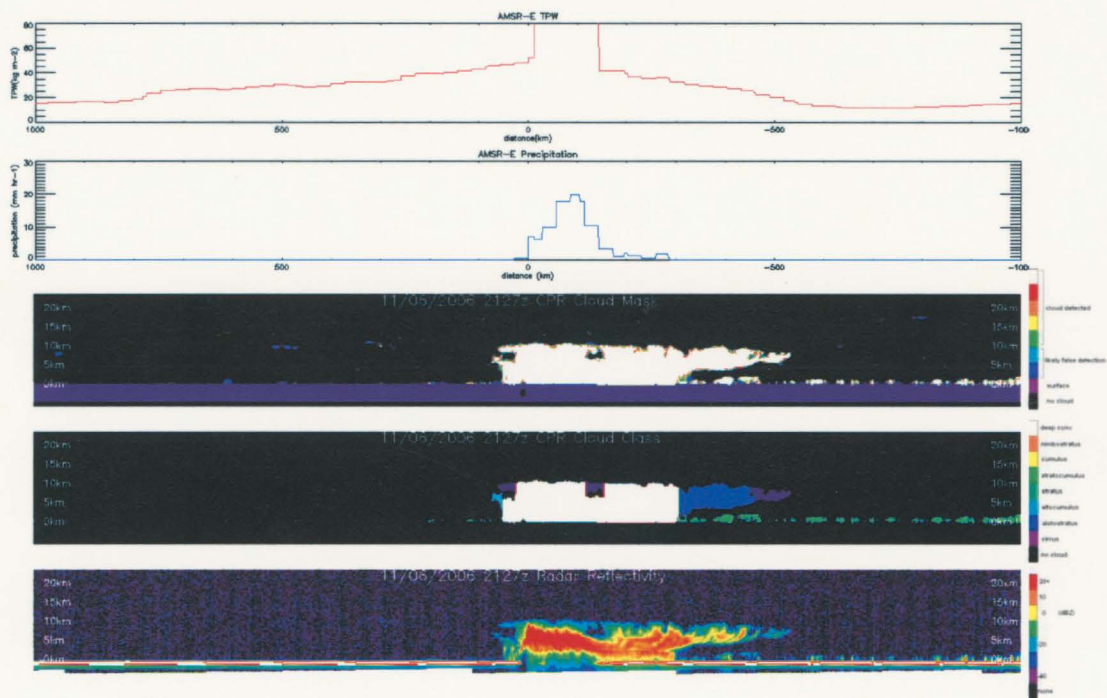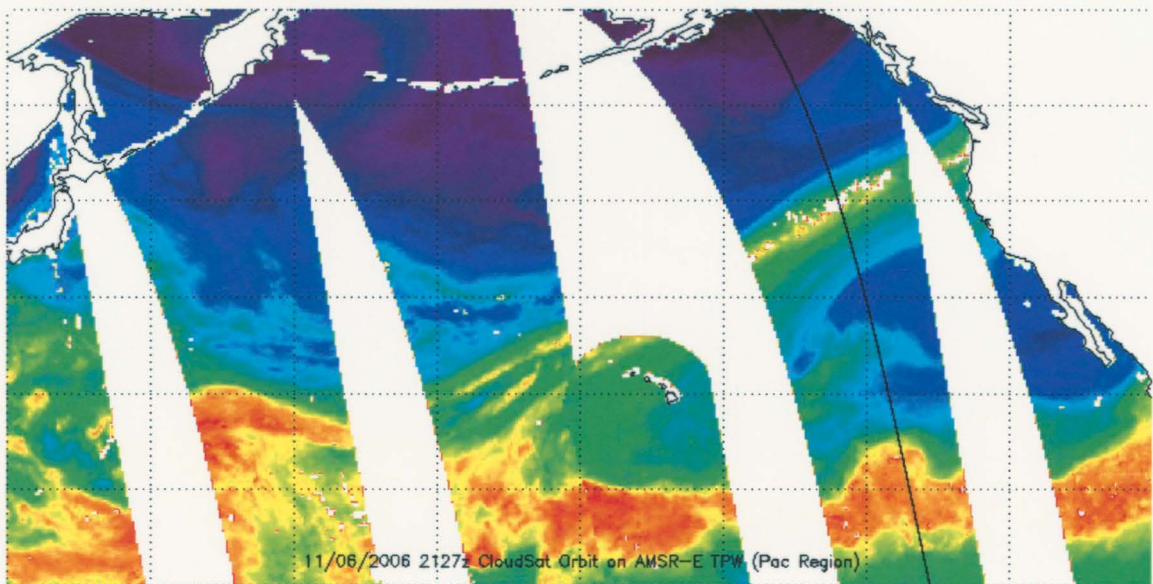
Figure 4.6) Observation on 6 November 2006, afternoon pass.

The moisture tongue has converged into a wide atmospheric river, with a maximum width approaching the 1000km limit. The CloudSat pass captures a substantial convective system within the river, with a width over 300km.
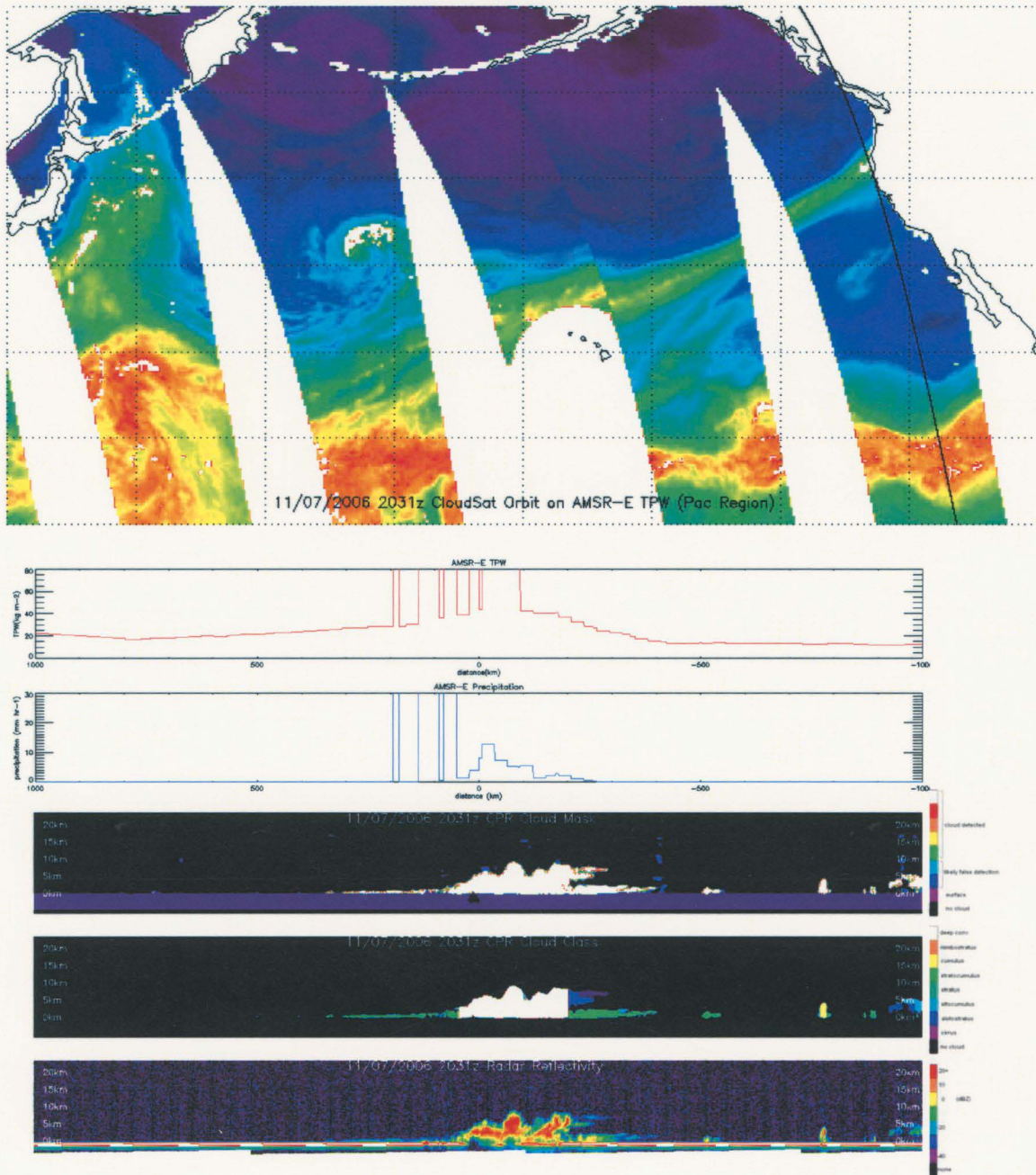
Figure 4.7) Observation on 7 November 2006, afternoon pass.

At this time the river is weakening, decreasing in both width and in maximum TPW. This CloudSat pass captures what is likely orographically-induced precipitation at landfall. The clouds are probably not classical deep convective clouds as the cloud type product indicates, but are producing heavy enough precipitation to confuse the cloud type algorithm.

59
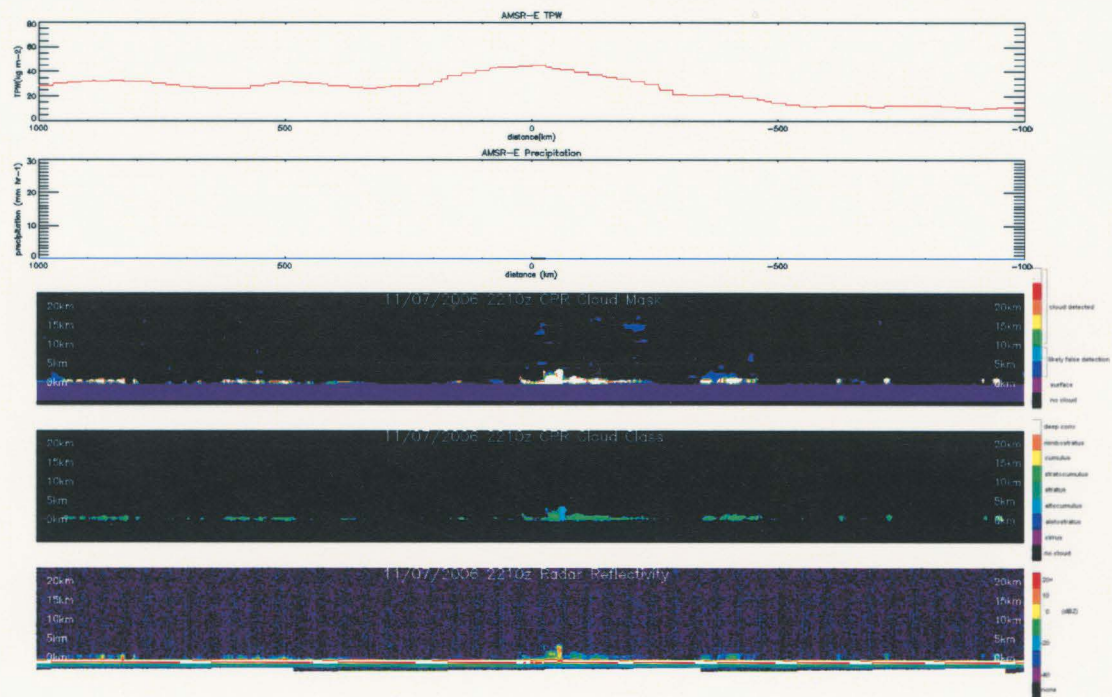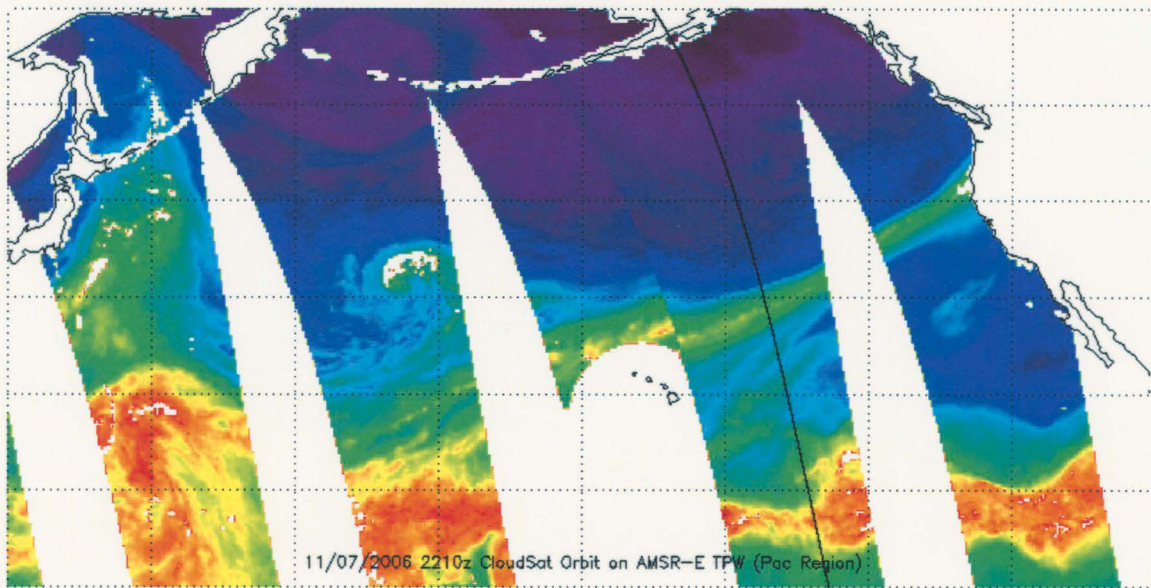
Figure 4.8) Observation on 7 November 2006, afternoon pass.

This observation is taken about an hour and a half after the previous observation (Fig. 4.7). Although the river moisture is till evident in the TPW map, there are no deep clouds evident within the river.
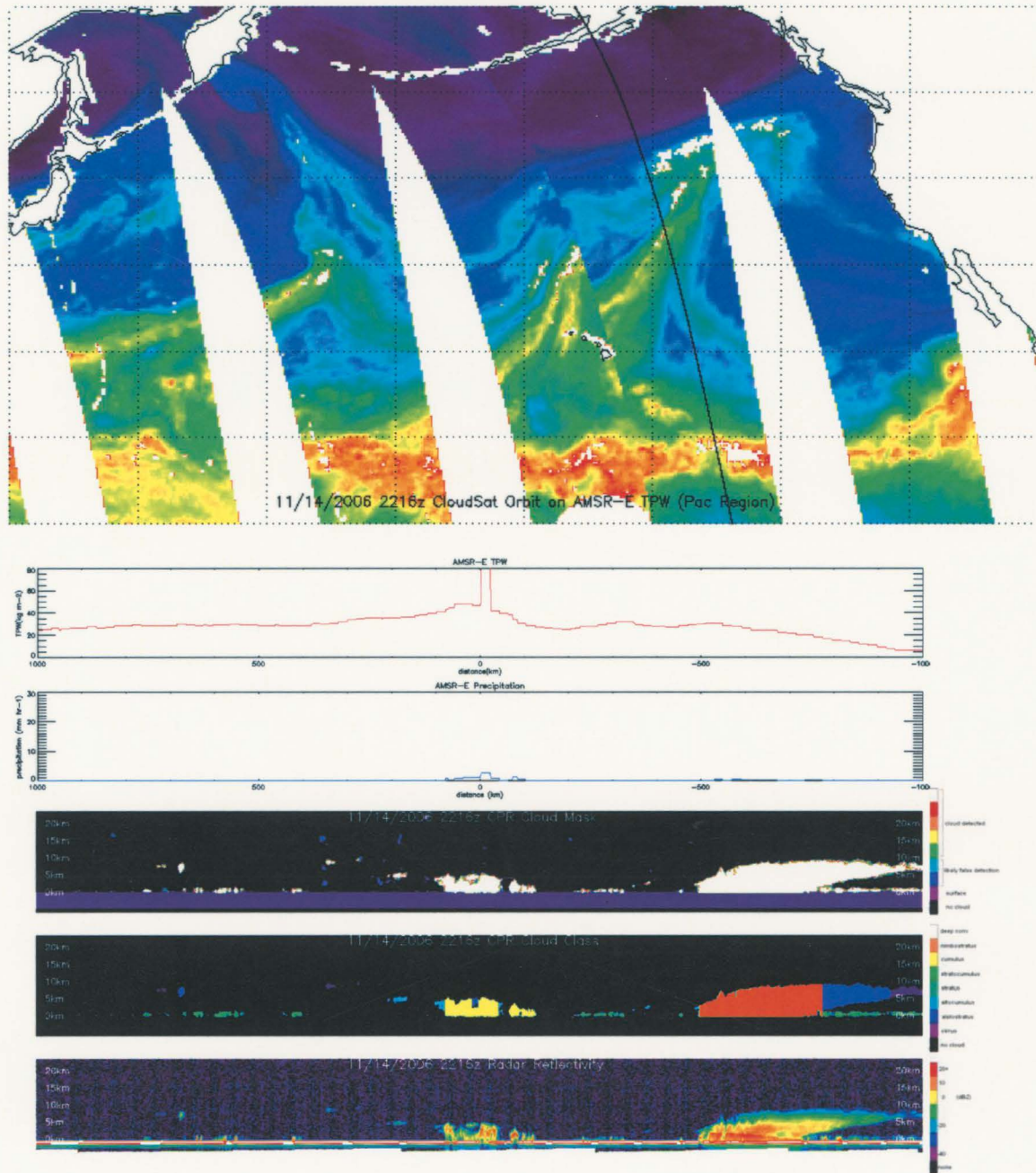
Figure 4.9) Observation on 11 November 2006, afternoon pass.

The TPW map shows a developing river approaching the west coast. CloudSat detects a band of shallow convective clouds forming within the river. The clouds to the north of the river in the cross-section are probably not related to the clouds within the river.
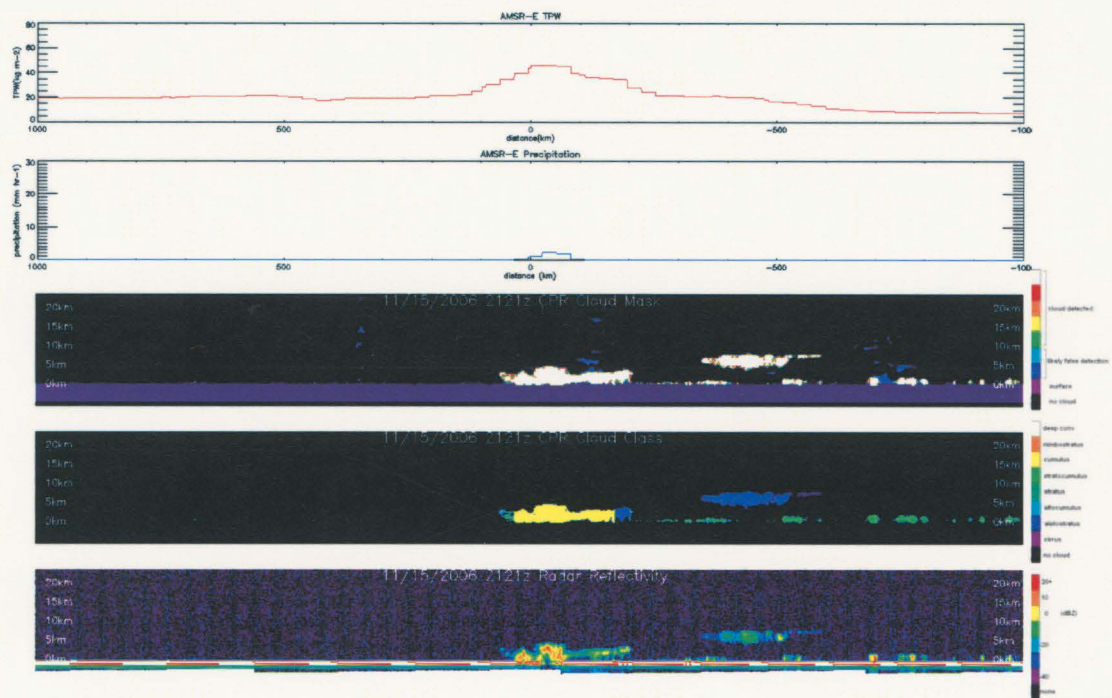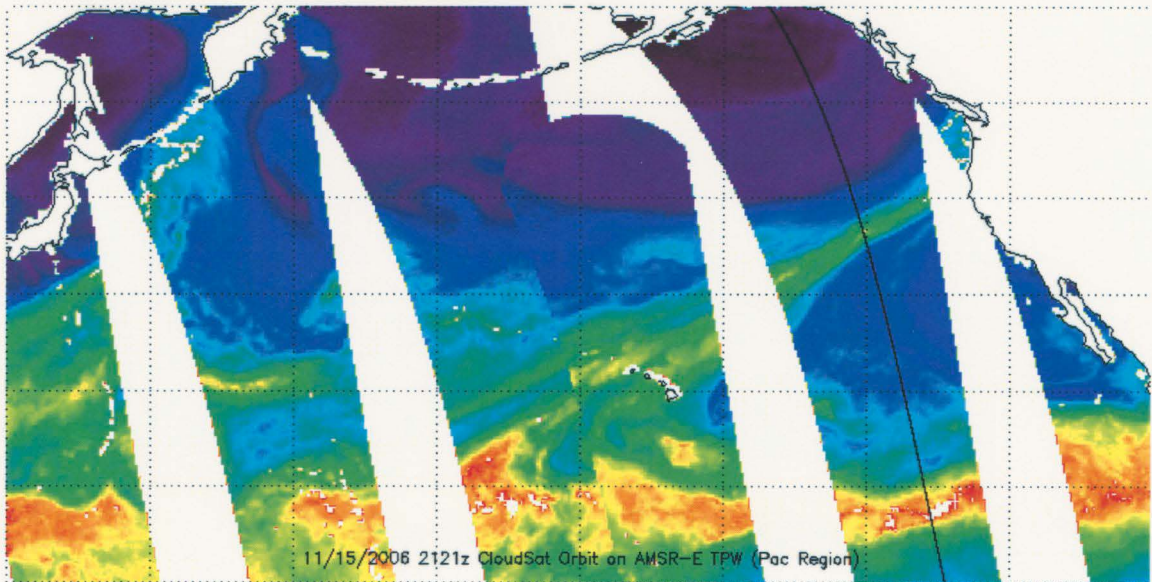
Figure 4.10) Observation on 15 November 2006, afternoon pass.

The river has made landfall. There is heavy precipitation occurring on land at the time of this observation, but deep clouds and high clouds have failed to form along the river away from land.
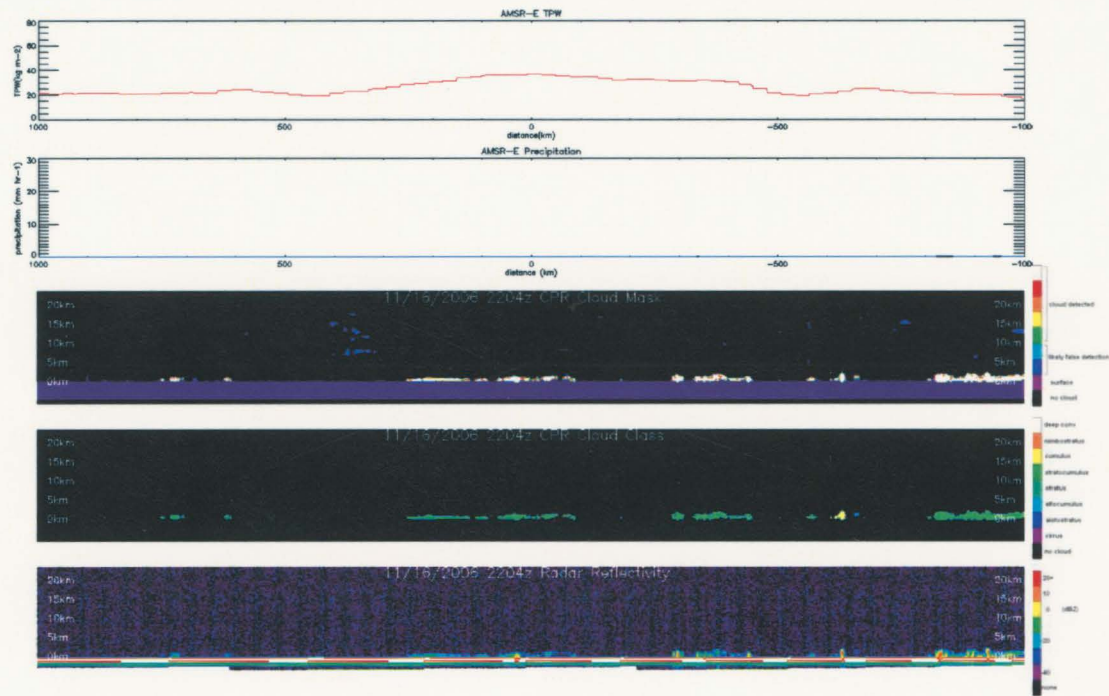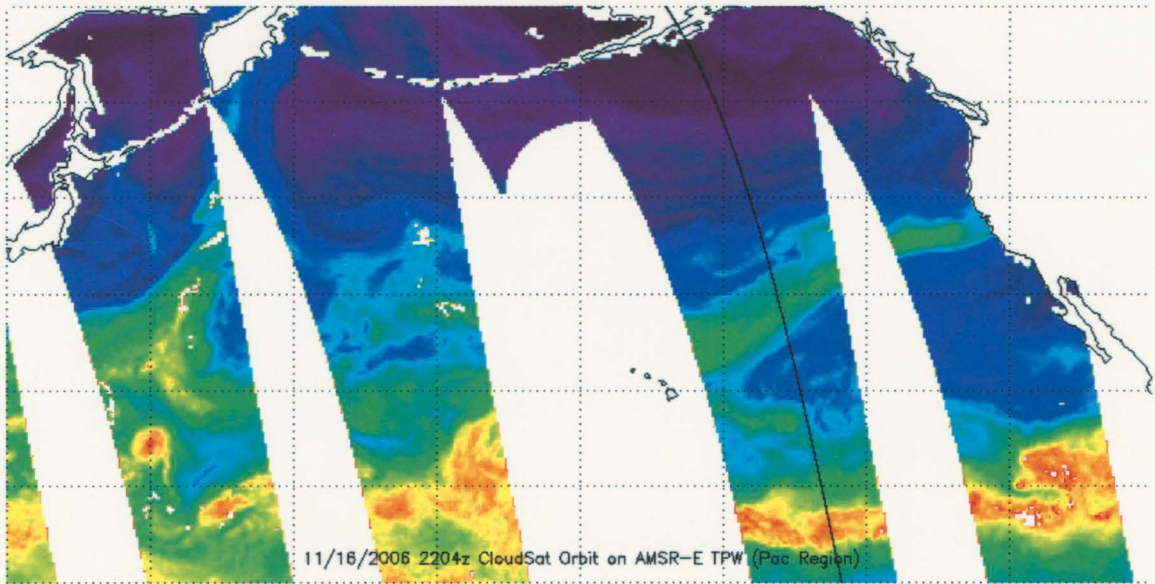
Figure 4.11) Observation on 16 November 2006, afternoon pass.

The river has begun weakening, losing its sharp TPW gradients and its high maximum TPW values. The shallow convective clouds have been eroded, leaving no cloud signature behind.
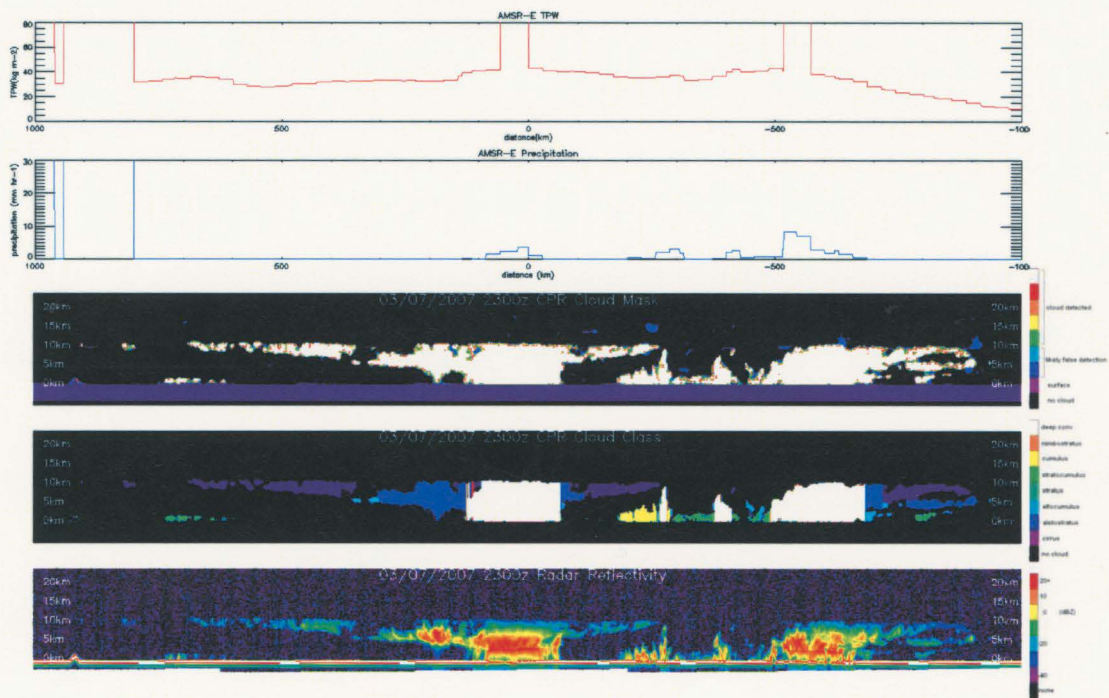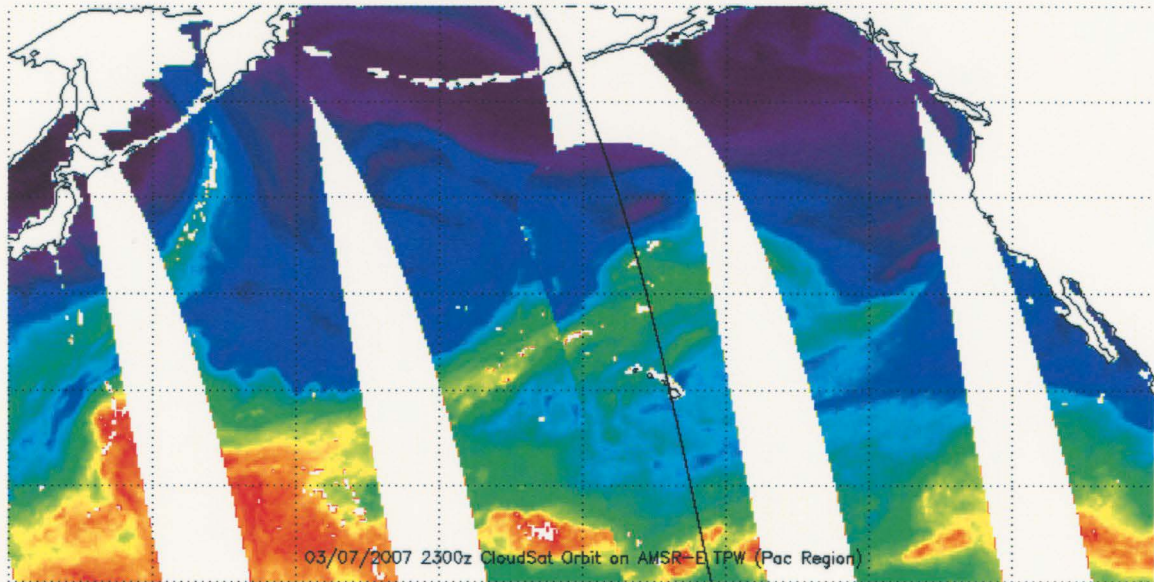
Figure 4.12) Observation on 7 March 2007, afternoon pass.

The TPW map shows a wide moisture tongue entering the eastern Pacific. Deep convective clouds have formed within the moisture tongue well ahead of the approaching polar front.
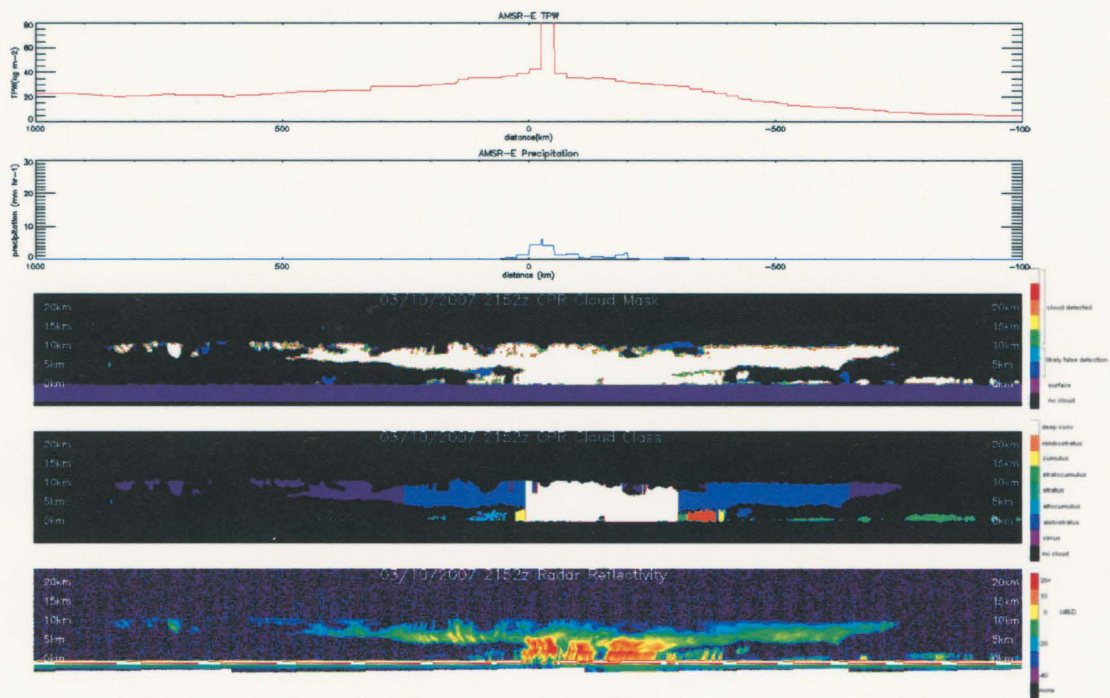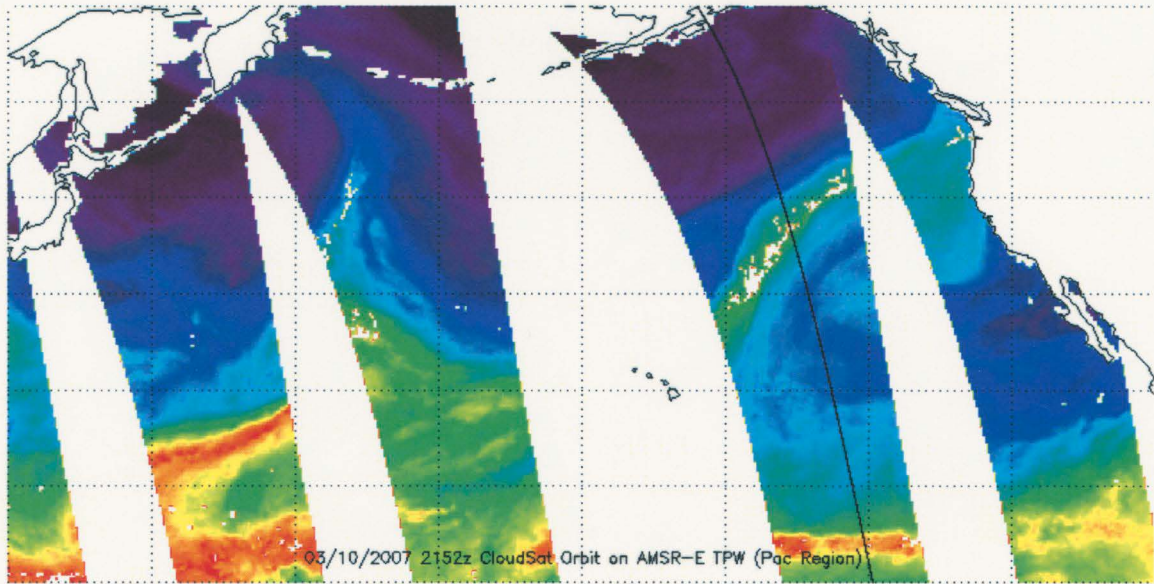
Figure 4.13) Observation on 10 March 2007, afternoon pass.

The river is making landfall along the west coast. The river contains a wide deep convective cloud band similar to the one occurring in the first case study. However, the high level cloud band (possibly a large convective anvil) is much larger for this river that is was the first river.
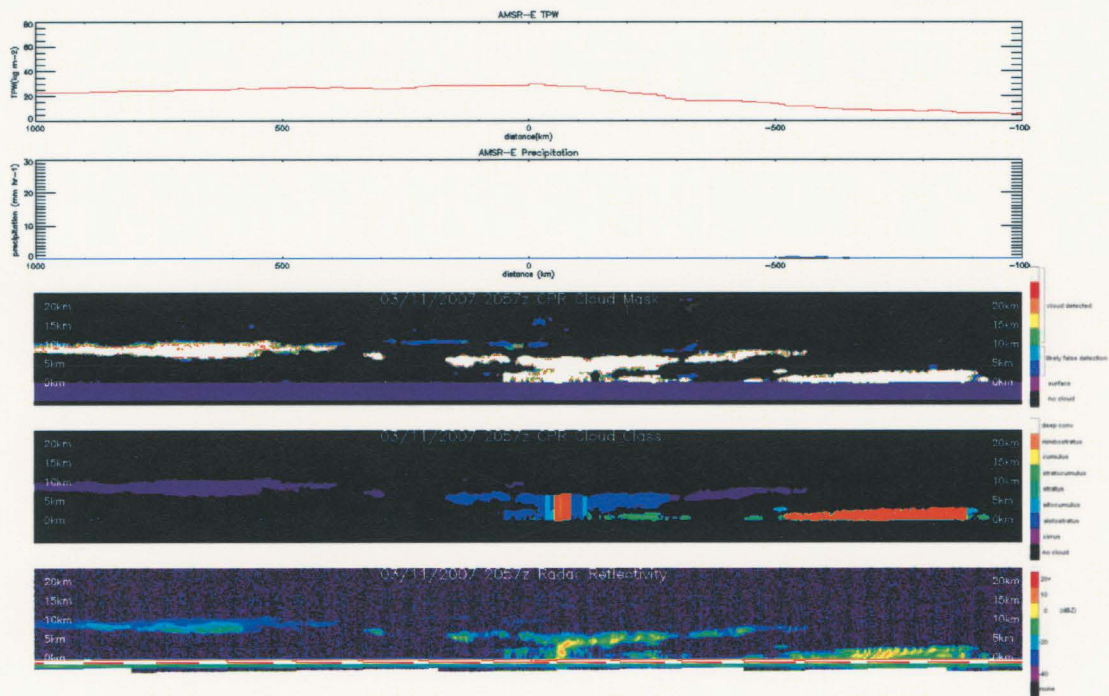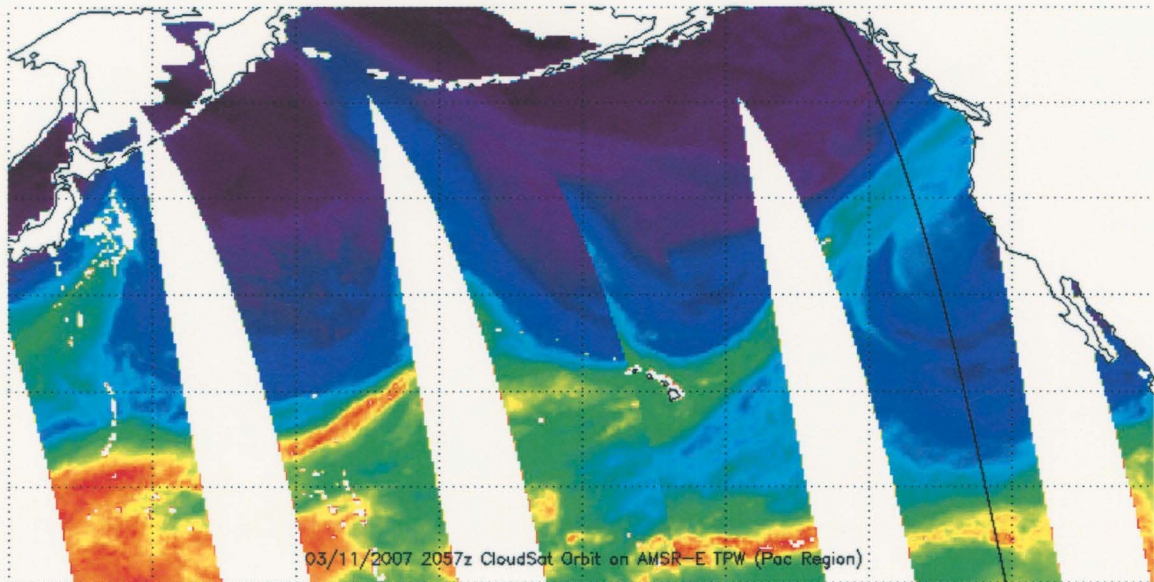
Figure 4.14) Observation on 11 March 2007, afternoon pass.

The river is weakening, most noticeably in the tip near land. Some deep clouds persist within the river, possibly a remnant weak convective updraft.
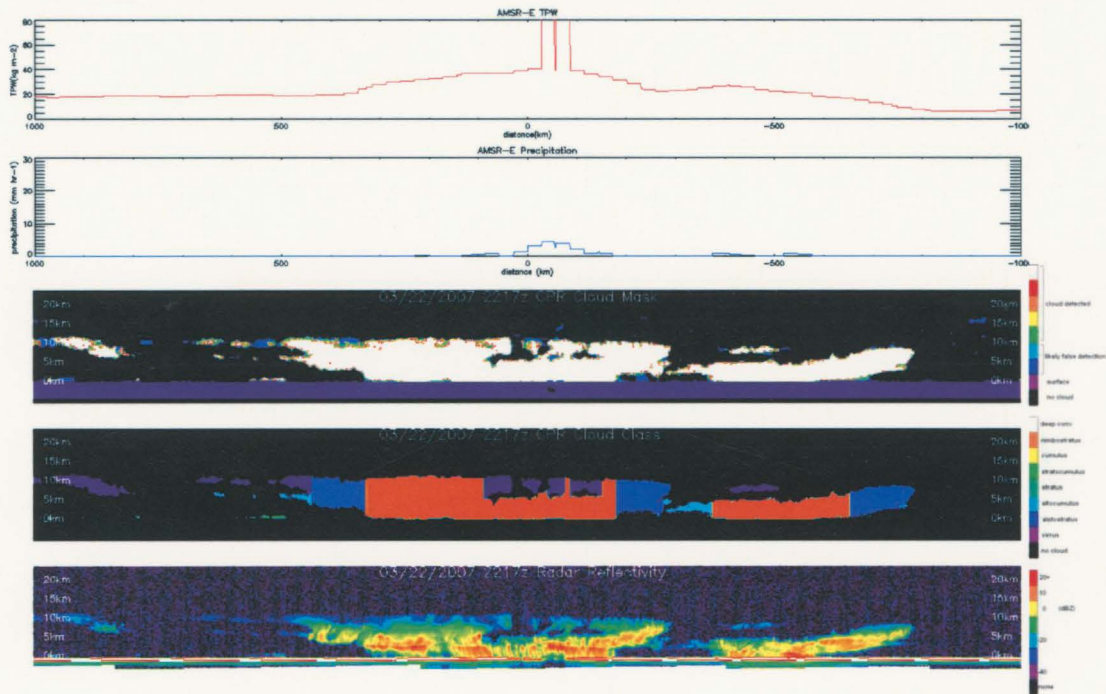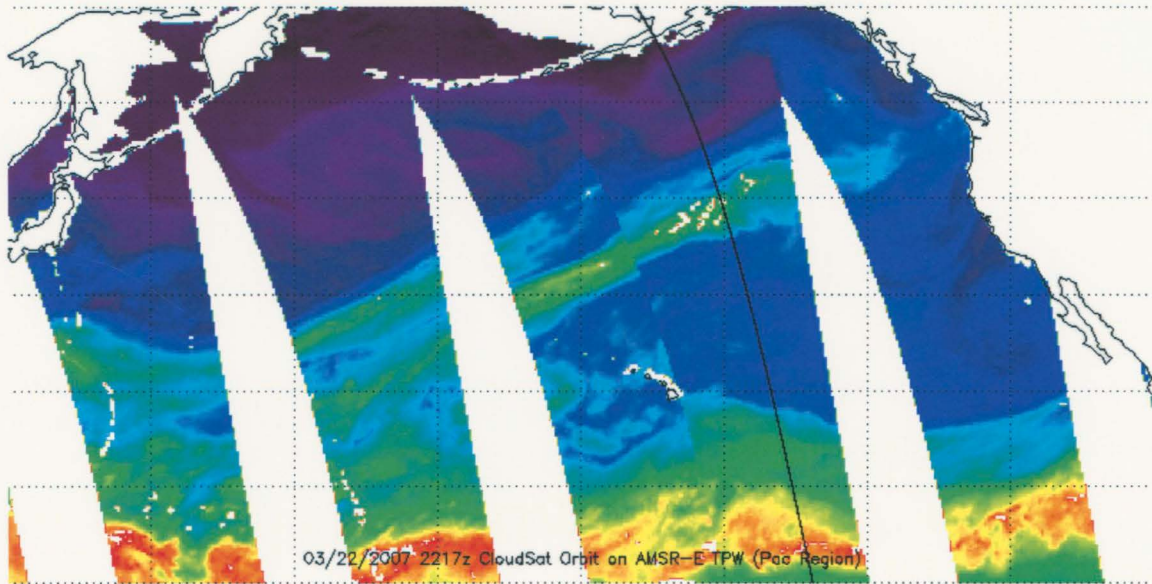
Figure 4.15) Observation on 22 March 2007, afternoon pass.

The river seen in the TPW map is fully formed and has entered the eastern Pacific (note the apparent disconnect between the river and tropical moisture). A wide band of deep clouds has formed within the river, possibly with some embedded deep convection (the complete surface attenuation is indicative of localized heavy precipitation).
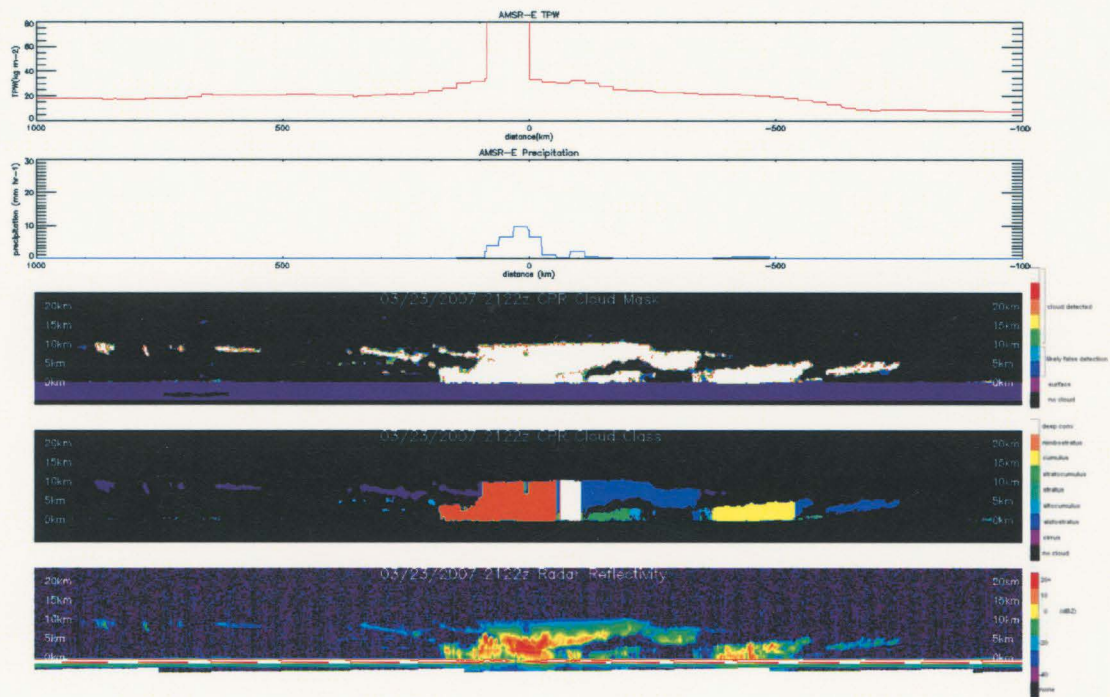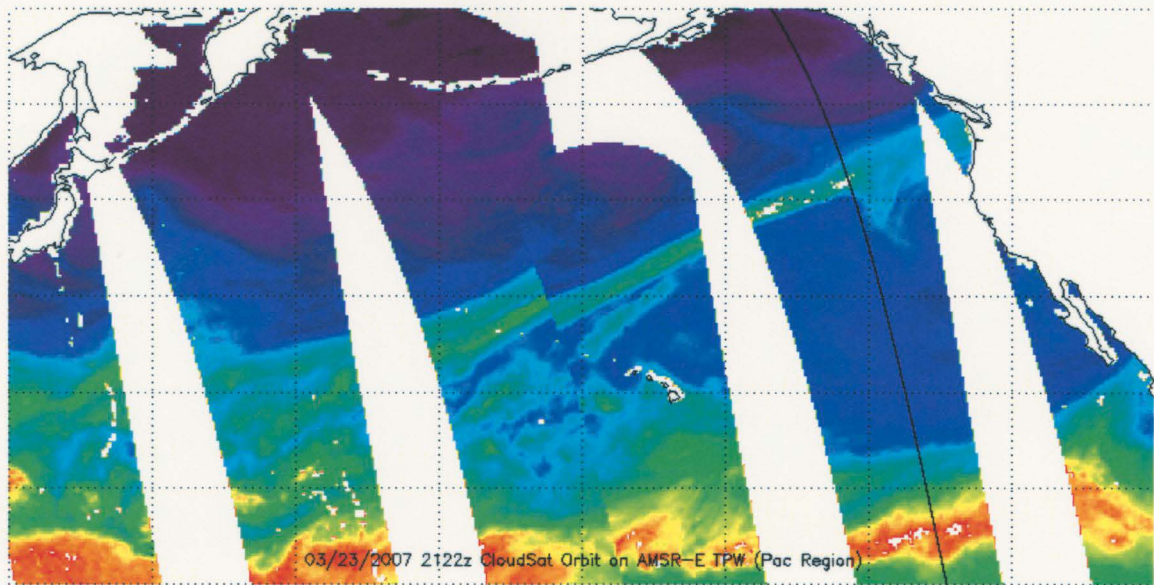
Figure 4.16) Observation on 23 March 2007, afternoon pass.

The river has made landfall. The deep cloud band has an average width despite the river's abnormally narrow width. The deep convection region is likely a false detection; the reflectivity image shows a significant break in the cloud column, which is narrow enough for the cloud type algorithm to overlook.
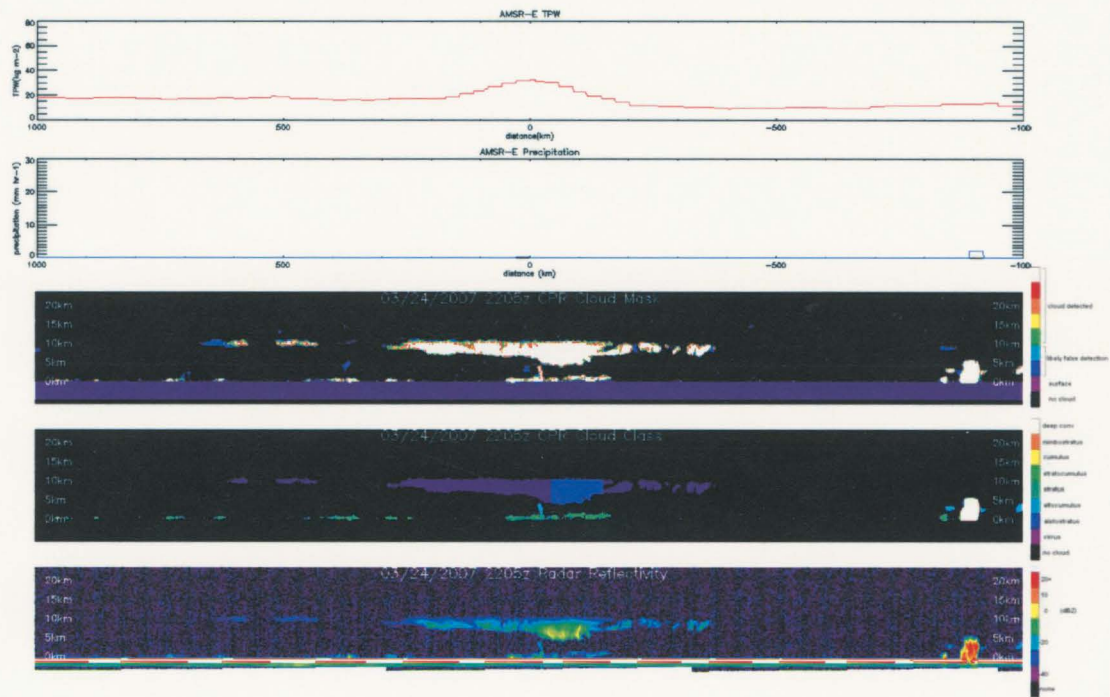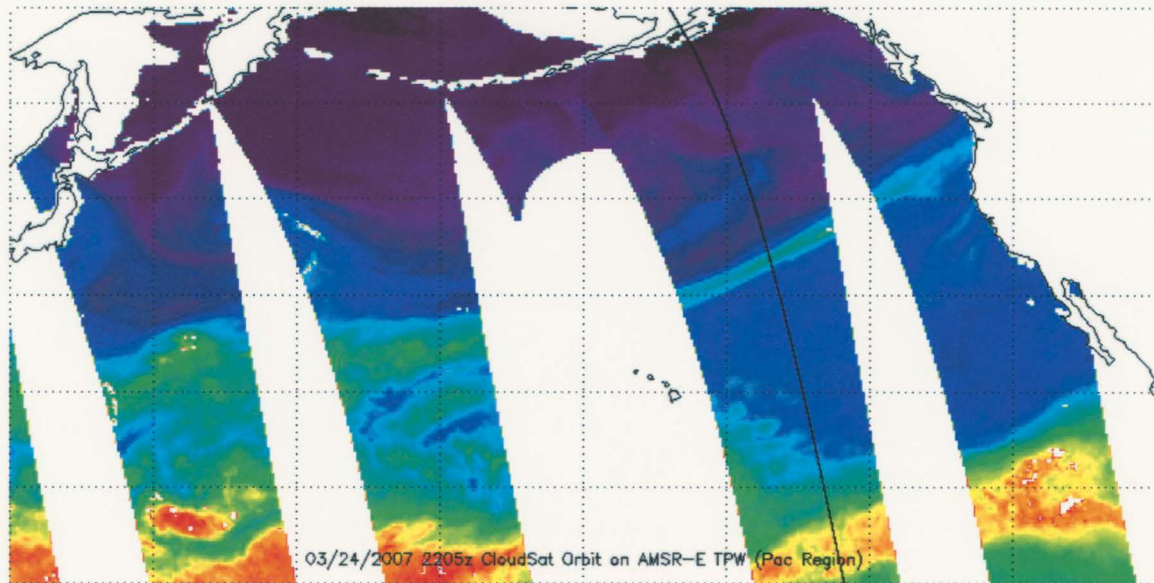
Figure 4.17) Observation on 24 March 2007, afternoon pass.

The river is narrowing and decreasing in maximum TPW. Unlike the first two case studies, this particular river retains a high level cloud band even after the deep cloud layer has been eroded.
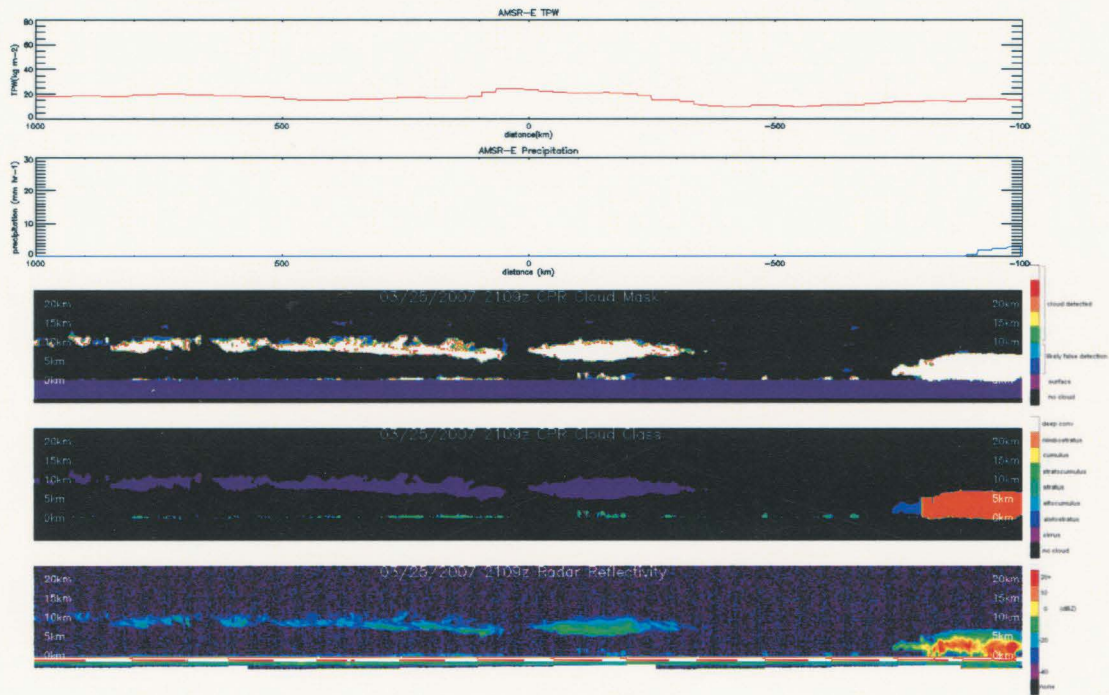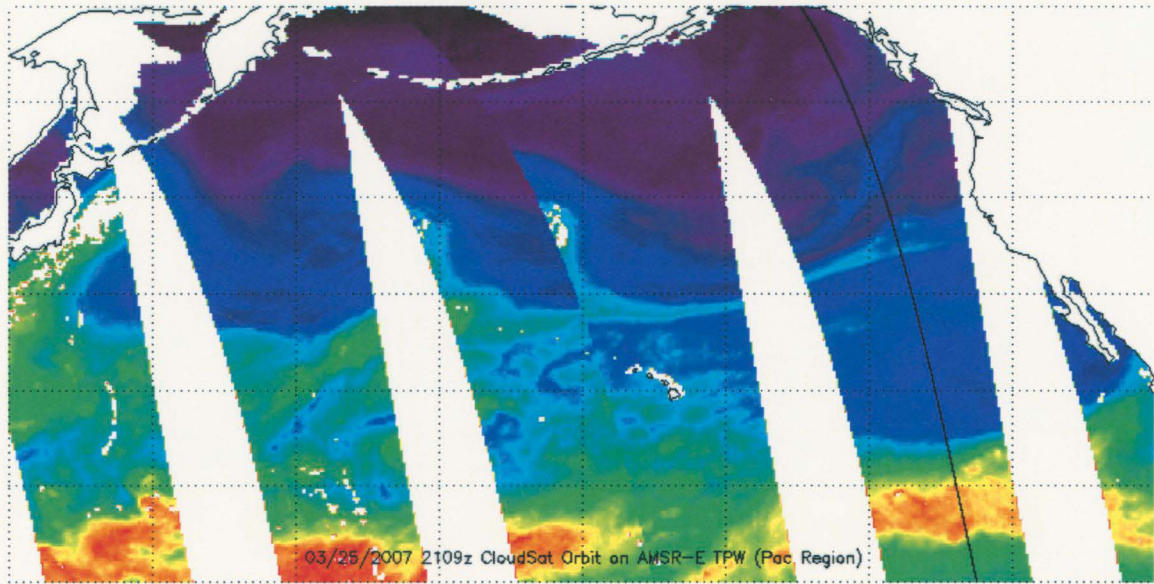
Figure 4.18) Observation on 25 March 2007, afternoon pass.

The TPW signal is too weak to classify this structure as a river at this time. However, the high cloud band identified in the previous observation still persists near the river's former location.
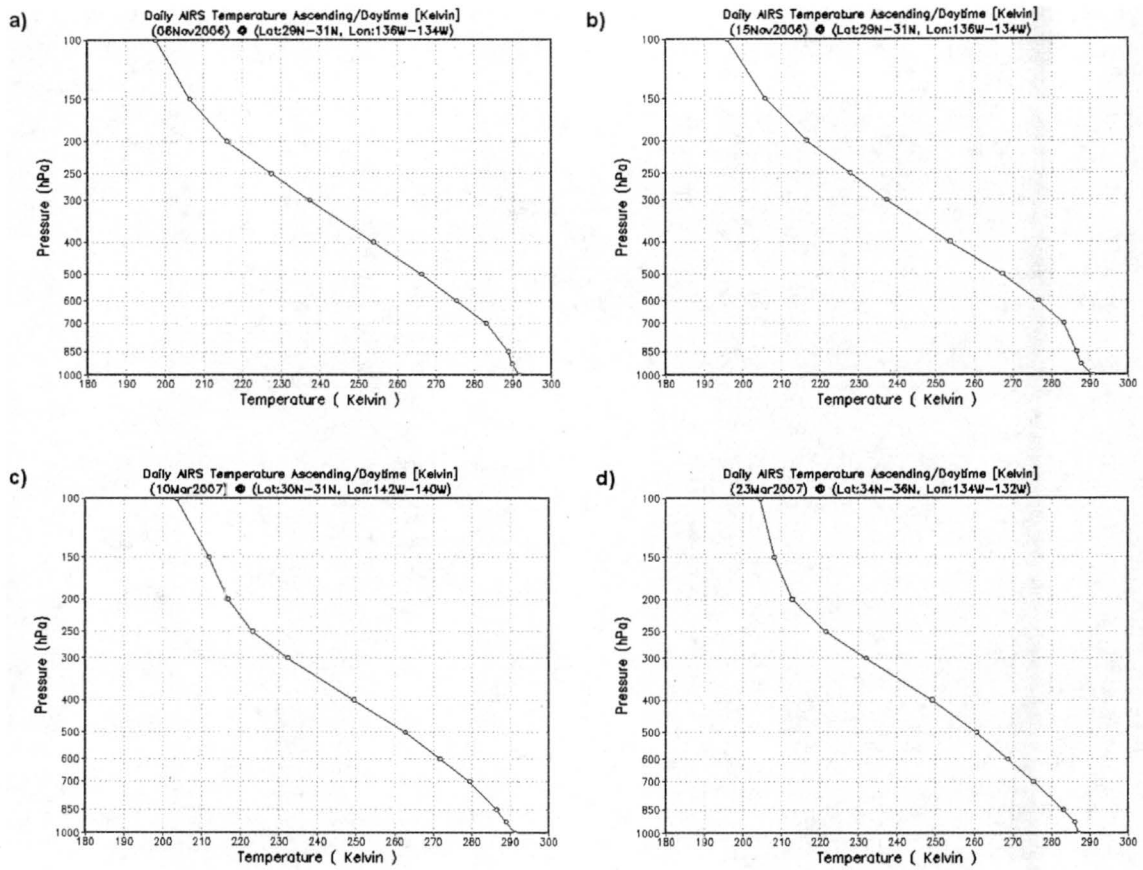
Figure 4.19) AIRS soundings of the pre-river environment taken at river maturity for the river events on a) 6 Nov 2006, b) 15 Nov 2006, c) 10 Mar 2007, and d) 23 Mar 2007 (images generated with NASA's Giovanni tool)

5. MULTI-RIVER COMPOSITES AND STATISTICS

5.1 River-Relative Coordinate Systems

In order to match up the granules from several passes to examine composites and statistical properties of cloud structure, it is necessary to devise a coordinate system across the river for spatially co-locating the granules relative to the rivers they intercept. The coordinate system needs both an origin and a set of boundaries marking the ends of the river. For this project, the coordinate systems used are determined by the river's TPW structure within CloudSat's field of view as measured by AMSR-E. The idea is to use the quantity defining the river to orient the CloudSat observations. There are two types of "river-relative" coordinate systems used for this project.

5.1.1 Physical Length Coordinate System

As the name suggests, the physical length coordinate system uses physical length (e.g. kilometers) as the horizontal coordinate. The strength of this coordinate system is that it is uses a very common coordinate, so understanding and visualizing the data in respect to other meteorological features may be easier for many people. The primary weakness of this method is the possibility of dependence between the cloud band's width and the river's width. If the cloud band's width is entirely dependent on the river's width, any inter-river cloud comparison will just be a comparison of rivers' widths.

Fig. 5.1 shows the layout of the physical length coordinate system. The origin is set as the beginning of the northern TPW gradient, where the TPW values begin to drop significantly in the frontal transition zone. For the ideal river consisting of a single TPW maximum with well-defined gradient regions to the north and south, the origin should sit about in the middle of the moisture axis. The northern half of the coordinate system would cover the polar frontal transition zone, and the southern portion would cover the frontal warm sector. The boundaries of the coordinate system are set a constant 1000km to either side of the origin, for a total horizontal axis length of 2000km. This length should allow for the river (width less than 1000km) to fit easily within the coordinate system, as well as allow any commonly-occurring clouds just outside of the river to be included in inter-river comparisons.

5.1.2 Gradient Independent Coordinate System

The gradient-independent coordinate system uses the rivers' northern TPW gradient to define a common horizontal coordinate. All rivers have TPW gradients along their northern and southern boundaries, with the northern gradient usually being sharper and more well defined than the southern. Unfortunately the southern gradient region tends to be less well defined and containing many more anomalous high TPW structures, making gradient identification a difficult problem. For this reason, the northern gradient's width can be used as a unit length of the horizontal coordinate. Each river's width can be normalized by its northern gradient width, making inter-river comparisons possible without possible interference from river width variation. One weakness of this system is the opposite of the physical length coordinate system, in that there may not be a total

73

dependence between river width and cloud band width either. The second weakness occurs in uncommon passes where the northern gradient is poorly defined on contains several maxima, making boundaries ambiguous.

Fig. 5.2 shows the layout of the gradient-independent coordinate system. The horizontal coordinate length is determined by the distance between the beginning of the northern gradient and the end of the northern gradient. This distance is one unit of length along the horizontal axis. The coordinate system can be any number of units long, and in this project the horizontal axis is set at five units long. The boundaries extend from one unit length north of the TPW gradient to three units south of the gradient. This allows the coordinate system to capture clouds both within and around the river, similar to the physical length system.

5.1.3 Caveat

Unfortunately, as we strive to obtain composites of many atmospheric rivers, there is no single coordinate system that is most important for all atmospheric rivers. River moisture structures are highly variable in space and time, often containing multiple moisture maxima and large moisture gradients and other temporary anomalies, making it difficult to establish a good common basis for orienting a common coordinate system. For this project, the relative usefulness of each coordinate system is investigated in section 5.3.

5.2 Cloud Mask Composites

The cloud mask composites are calculated with a fairly straightforward averaging method. Each pass being used in the average has its pixels classified as "cloud" or "no cloud" based on the CPR Cloud Mask product, with a value of 20 being the threshold for assigning the "cloud" status (see Table 3.1). All passes are then averaged pixel-by-pixel to give a frequency composite plot.

5.2.1 Average Cloud Mask

The average cloud structure for all rivers (Fig. 5.3) was calculated using the total 92 observations of rivers, with no regard for time relative to the river's lifespan. It should be noted that CloudSat's narrow field of view may cause some observations to miss clouds for rivers possessing broken convective lines and other such asymmetric features.

Results show that almost all atmospheric rivers contain low level clouds throughout their lifespans, centered around the cross-sectional TPW maximum. Cloud formation along the polar front is reasonable given the lifting mechanisms occurring along a polar front. Even without the lifting and/or instability necessary for deep cloud formation, boundary layer cumulus and shallow convection are possible. Low level clouds also often form north of the river itself, behind the cold front. These are probably normal post-frontal cumulus clouds, resulting from cold polar air flowing over the warmer ocean water.

Deep clouds occur in about half of the 92 observations. These deep cloud bands are usually about 200-400km wide, and about 8-10km in vertical extent. The overall shape of

the cloud structure is similar to the cloud structure found in the tails of "comma" clouds associated with extratropical cyclones, e.g. as seen in Carlson 1991 (recall that atmospheric rivers are themselves associated with extratropical cyclones). However, the deep cloud bands seem to be much wider in the typical atmospheric rivers than in the typical midlatitude cyclone, with the average cyclone cloud width of about 50-100km. The low level jet found within atmospheric rivers may be responsible for this difference. As discussed previously, an atmospheric river contains a low level jet that does not form along frontal zones over land. The low level jet provides an additional lifting mechanism for cloud formation ahead of the polar front that is not present for polar fronts over land. So while cloud structure within atmospheric rivers may not be fundamentally different than cloud structure associated with extratropical cyclones in general, it may be enhanced spatially.

High clouds frequently occur above and around atmospheric rivers. These clouds could be the result of "blowoff" from deep clouds occurring within the river, or they could be high clouds originating outside the river (e.g. tropical convection) and transported over the river. Unfortunately it is very difficult to tell exactly what causes the high clouds using CloudSat observations alone.

5.2.2 Time Evolution of Cloud Mask

The following three composite plots are calculated from the three time-based categories of river observations (described in Chapter 4). The purpose of these plots is to display the changes in cloud structure during a river's formation, maturity, and

dissipation. There are a few important notes about interpreting the composite images, which are described when appropriate.

5.2.2.1 River Formation

The "before" category (Fig. 5.4) contains river observations occurring early in a river's life, which includes the formation period. At first glance the before group average mask looks much like average mask of all observations. Almost all rivers will possess low level clouds during their early stages, which is understandable for the reasons presented previously. In the previous chapter it was noted that deep clouds and convection sometimes form ahead of a polar front even before the river itself fully forms, which is reflected in the existence of deep clouds in about half of the "before" river cases.

It should be noted that of the three categories of time evolution, the "before" category is probably less representative of the river's early life than the other two categories are representative of their life stages. This is because many rivers are relatively short at formation, not considerably longer than 2000km. Because rivers are not always oriented perpendicular to CloudSat's orbit, the short young rivers often pass completely between CloudSat orbits, evading observation. The river is more likely to be observed only after it has increased in length, at which point it may already be close to maturity. So even though the "before" group has the most observations of the three categories, the observations may be biased towards the middle of the river's life instead of the earliest stages.

5.2.2.2 River Maturity

The "best" category (Fig. 5.5) contains river observations occurring when the river appears to be the most mature in its life span. The most obvious feature of the average mask for the "best" group is the much higher frequency of deep cloud formation than in the other two categories. This suggests that the time of the river's most 'intense' appearance on the TPW map is concurrent with the strongest vertical motion within the river. It is also notable that that region of high cloud frequency is further to the north than it is in other cloud mask averages, occurring over the river's northern gradient. This is probably caused by the sloping shape of the polar frontal zone and the region of high moisture (covered in chapter 2). The occurrence of high clouds also increases from the "before" group to the "best" group, supporting a connection between high clouds over the river and activity within the river.

5.2.2.3 River Dissipation

The "after" category (Fig. 5.6) contains river observations occurring in the river's later life, which includes the weakening and dissipation stages. The occurrence of deep clouds is greatly decreased for observations in the "after" group, and deep cloud formations are notably eroded in the mid-troposphere. This indicates a shutdown of lifting mechanisms occurring within the river. As the polar front temperature gradient decreases, the pressure gradient force driving the low level jet weakens. Without the lifting mechanisms associated with the frontal jet, deep cloud formation and maintenance ceases. This process isn't quite straightforward because of the front/river feedbacks described in Chapter 2. At the end of a river's life, the deep cloud formation is severed into a low-

level cloud band and an upper level cloud band. The average mask indicates that the low level clouds are almost always present (typically as cumulus fields), but the upper level cloud band does not always persist. This is apparent when looking at the individual observations, as shown in the case studies.

It should be noted that rivers do not always decay uniformly, in the same manner as a hurricane would weaken. Occasionally a river can break apart somewhere along its length, with one end of the river dissipating while the other maintains its river status. These particular rivers are mentioned in chapter 4, but such asymmetries are not accounted for in this classification scheme. However, disruptions along the entire river's length are taken into account, which occurred in two of the 22 river events.

5.3 Cloud Mask and TPW

The only reliable AMSR-E measurement for comparison with CloudSat is the TPW product. Other measurements that would be interesting to compare would be surface wind speed and precipitation. Wind speed could be used to estimate surface convergence below the low level jet, assuming that jets follow the model presented in chapter 2. Wind speed measurements suffer greatly in very cloudy precipitation environments, rendering them almost useless in the majority of river observations. Precipitation could be used to identify areas of likely convective activity, which then could be matched with cloud properties. Precipitation does not suffer greatly, but there is one significant problem with using precipitation: CloudSat products also use precipitation in their calculations. This mostly affects the Cloud Class product, which is often highly dependent on CloudSat-

estimated precipitation for classifying deep convective clouds. There is possibly enough overlap that using precipitation would essentially be measuring the same atmospheric feature twice. So for this project, TPW is the only quantity used for comparisons.

In the four scatter plots, the rivers' TPW is characterized in two ways: the river's gradient width, and the river's maximum TPW. The rivers' gradient lengths were calculated during the creation of the river-relative coordinate systems, and the maximum TPW value is found from TPW data from within the northern TPW gradient and one gradient length south of the TPW gradient (from -1 to 1 in the coordinate system). Similarly, the clouds are calculated in two ways: the cloud band's horizontal width, and the cloud band's total vertical depth. The cloud width is the average continuous horizontal extent of the cloud mask for all vertical level, beginning at the origin of the gradient-based coordinate system. The vertical cloud height is the total count of the greatest number of cloudy bins occurring in one vertical profile (one bin wide).

5.3.1 River Width versus Horizontal Cloud Extent

The first scatter plot (Fig. 5.7) compares the width of the river's northern TPW gradient with the width of the cloud band for all 92 observations and the three time-based categories. As discussed earlier, potential relationships between cloud width and river width may bias frequency plots using physical length coordinates, which is the reason two river-relative coordinate systems are used. The plots are presented to show whether any such relationships are represented in the data. The clustering of data points along the 200km TPW value is an artifact of the gradient identification algorithm, which has difficulty dealing with features less than a couple hundred kilometers wide. The plots do

not suggest a strong relationship between river width and cloud width at any point in the river's life span. There is little apparent correlation between river width and cloud width, so using a physical length-based coordinate system with river observations should not be greatly affected by river width. This is somewhat apparent in the frequency plots presented previously, as the plots in the two coordinate systems are similar in appearance despite elimination of river width dependence in one.

5.3.2 River Width versus Vertical Cloud Extent

The second scatter plot (Fig. 5.9) compares the width of the river's northern TPW gradient with the total height of the cloud band. As before, there is no apparent significant correlation between the two variables.

5.3.3 Maximum TPW versus Horizontal Cloud Extent

The third scatter plot (Fig. 5.9) compares the maximum TPW value occurring within the river with the width of the cloud band. As before, there is no apparent significant correlation between the two variables.

5.3.4 Maximum TPW versus Vertical Cloud Extent

The fourth scatter plot (Fig. 5.10) compares the maximum TPW value occurring within the river with the total height of the cloud band. Previous research has suggested a relationship between a river's moisture content and the occurrence of deep convection. If this is true, then there may be a relationship between the occurrence of tall deep clouds

and TPW values within the river. Once again, such a relationship is not readily apparent in the data.

5.4 Cloud Type Statistics

The following statistics were created to explore the types of clouds occurring within rivers, and possible relationships between TPW values and the occurrence of specific cloud types.

5.4.1 Single Cloud Types

The first set of statistics is the frequency of occurrence of each of the eight cloud types within the observed atmospheric rivers. Each frequency is the ratio of the number of rivers containing the cloud type in question to the total number of rivers. The region defined as "within" the river is centered at the beginning of the TPW gradient, and extends one gradient length north and one gradient length south of the origin (from -1 to 1 in the gradient-based coordinate system). This choice of domain contains the vast majority of deep clouds associated with the rivers. The frequency calculations include a minimum threshold of number of bins containing each cloud type. The Cloud Class algorithm sometimes assigns questionable cloud types to a few bins around the edges of clouds (where threshold reflectivity values may confuse the algorithm), so a river must contain more than 50 bins of a cloud type in order to be counted as containing that specific cloud type.

Table 5.1 shows the results of these calculations. Deep convective cloud frequency has the strongest dependence on time, occurring most frequently at a river's peak and rarely during its dissipation. Nimbostratus clouds occur in about half of the cases in each category, suggesting that rivers are often capable of producing vertical motion and significant precipitation even in their formation and dissipation periods. Shallow convection has slight time dependence as well, although it should be noted that shallow convection is often "attached" to the leading edge of nimbostratus or deep convective cloud bands instead of being isolated. Stratocumulus are a common occurrence, both in the form of weakly forced clouds surrounding deep cloud bands and as cold air cumulus behind the front. The three categories of high clouds have high frequencies of occurrence, and this is supported by examination of the individual observations. High clouds are often attached to the tops of deep convective and nimbostratus clouds, where updrafts weaken considerably and clouds disperse in upper level airflow.

5.4.1 Combined Cloud Types

To help remove some of the ambiguity between similar cloud types, the individual cloud types can be combined and their frequencies calculated together. For example, both deep convective clouds and nimbostratus clouds are fairly similar in properties to the point that distinguishing between a weaker convective cloud and a stronger nimbostratus cloud may be very difficult. So by combining the deep convective mask with the nimbostratus mask, they form one category representing deep cloud formation from strong rising motion. Other similar cloud types can be combined in the same manner. In this project, the following five categories of clouds are used:

1)   Deep convective and nimbostratus – these are deep clouds that usually require strong upwards motion along the polar front through several kilometers of atmosphere to form and persist.

2)   Deep convective and cumulus (congestus) – these are the two convective cloud types that may indicate vertical instability, and usually produce the heaviest precipitation of the three precipitating cloud types.

3)   Deep convective, nimbostratus, and cumulus – these cloud types cause most of the precipitation within rivers, and are usually indicative of strong forcing and rising motion, even if they are incapable of growing vertically.

4)   Stratocumulus and stratus – these are low level clouds, usually not associated with any strong forcing or rising motion. Unfortunately, the Cloud Class product handles stratus clouds very poorly.

5)   Altocumulus, altostratus, and cirrus – these are high clouds.

The results are shown in Table 5.2. As seen in the case studies, deep clouds are a very common – but not ubiquitous – feature within atmospheric rivers. Most rivers possess enough forcing to support strong vertical water vapor transport. Convective activity has time dependence, particularly in the river's later stages when frontal forcing weakens. High clouds are very common, as deep clouds (even well-developed shallow convection) will often create high clouds around their tops.

5.4.3 Deep Convection and TPW

One finding from the CALJET experiment (Ralph 2004) was that the frequency of deep convection was related to the maximum TPW values within the rivers. They found

84

that rivers with higher TPW values form convection more often. This finding can be tested using CloudSat data. By categorizing the river observations by maximum TPW, and then finding the frequency of occurrence of deep convective clouds for each category, it is possible to see if the CALJET findings are apparent in the CloudSat dataset. Deep convection should occur most often in rivers with higher TPW (above 40mm), and less common in rivers with minimal TPW.

Table 5.3 shows the results of this process. The rivers were binned into four categories based on maximum TPW within the river: 20mm-30mm, 31mm-40mm, 41mm-50mm, and above 50mm. The frequency is the ratio of the number of rivers in each bin containing convection with the total number of rivers in that bin. The results indicate that convection is indeed probably related to maximum TPW values. Rivers with minimal TPW values rarely contain convection, and rivers with extremely high TPW values almost always contain convection (the "after" group had no cases of 50mm+ TPW).

Cloud Type	frequency
convective	0.336957
nimbostratus	0.521739
cumulus	0.271739
stratocumulus	0.891304
stratus	0
altocumulus	0.728261
altostratus	0.913043
cirrus	0.836957

a) "all" group

Cloud Type	frequency
conv:	0.361111
ns:	0.555556
cu:	0.333333
sc:	0.833333
st:	0
ac:	0.833333
as:	0.972222
ci:	0.833333

b) "before" group

Cloud Type	frequency
conv:	0.541667
ns:	0.541667
cu:	0.25
sc:	0.916667
st:	0
ac:	0.583333
as:	0.958333
ci:	0.833333

c) "best" group

Cloud Type	frequency
conv:	0.15625
ns:	0.46875
cu:	0.21875
sc:	0.9375
st:	0
ac:	0.71875
as:	0.8125
ci:	0.84375

d) "after" group

Table 5.1) Frequency of occurrence of the eight cloud types within atmospheric rivers.

Cloud Group	frequency
conv/ns:	0.76087
conv/cu:	0.5
conv/ns/cu:	0.847826
sc/st:	0.891304
ac/as/ci:	1

a) "all" group

Cloud Group	frequency
conv/ns:	0.777778
conv/cu:	0.555556
conv/ns/cu:	0.888889
sc/st:	0.833333
ac/as/ci:	1

b) "before" group

Cloud Group	frequency
conv/ns:	0.916667
conv/cu:	0.625
conv/ns/cu:	0.958333
sc/st:	0.916667
ac/as/ci:	1

c) "best" group

Cloud Group	frequency
conv/ns:	0.625
conv/cu:	0.34375
conv/ns/cu:	0.71875
sc/st:	0.9375
ac/as/ci:	1

d) "after" group

Table 5.2) Frequency of occurrence of the five groups of cloud types within atmospheric rivers.

TPW bin	frequency
conv freq for 20-30mm	0.12
conv freq for 30-40mm	0.431373
conv freq for 41-50mm	0.833333
conv freq above 50mm	0.75

a) "all" group

TPW bin	frequency
conv freq for 20-30mm	0.1
conv freq for 30-40mm	0.444444
conv freq for 41-50mm	0.833333
conv freq above 50mm	1

b) "before" group

TPW bin	frequency
conv freq for 20-30mm	0.2
conv freq for 30-40mm	0.666667
conv freq for 41-50mm	0.666667
conv freq above 50mm	1

c) "best" group

TPW bin	frequency
conv freq for 20-30mm	0.1
conv freq for 30-40mm	0.222222
conv freq for 41-50mm	1
conv freq above 50mm	0

d) "after" group

Table 5.3) Frequency of occurrence of deep convective clouds by maximum river TPW.
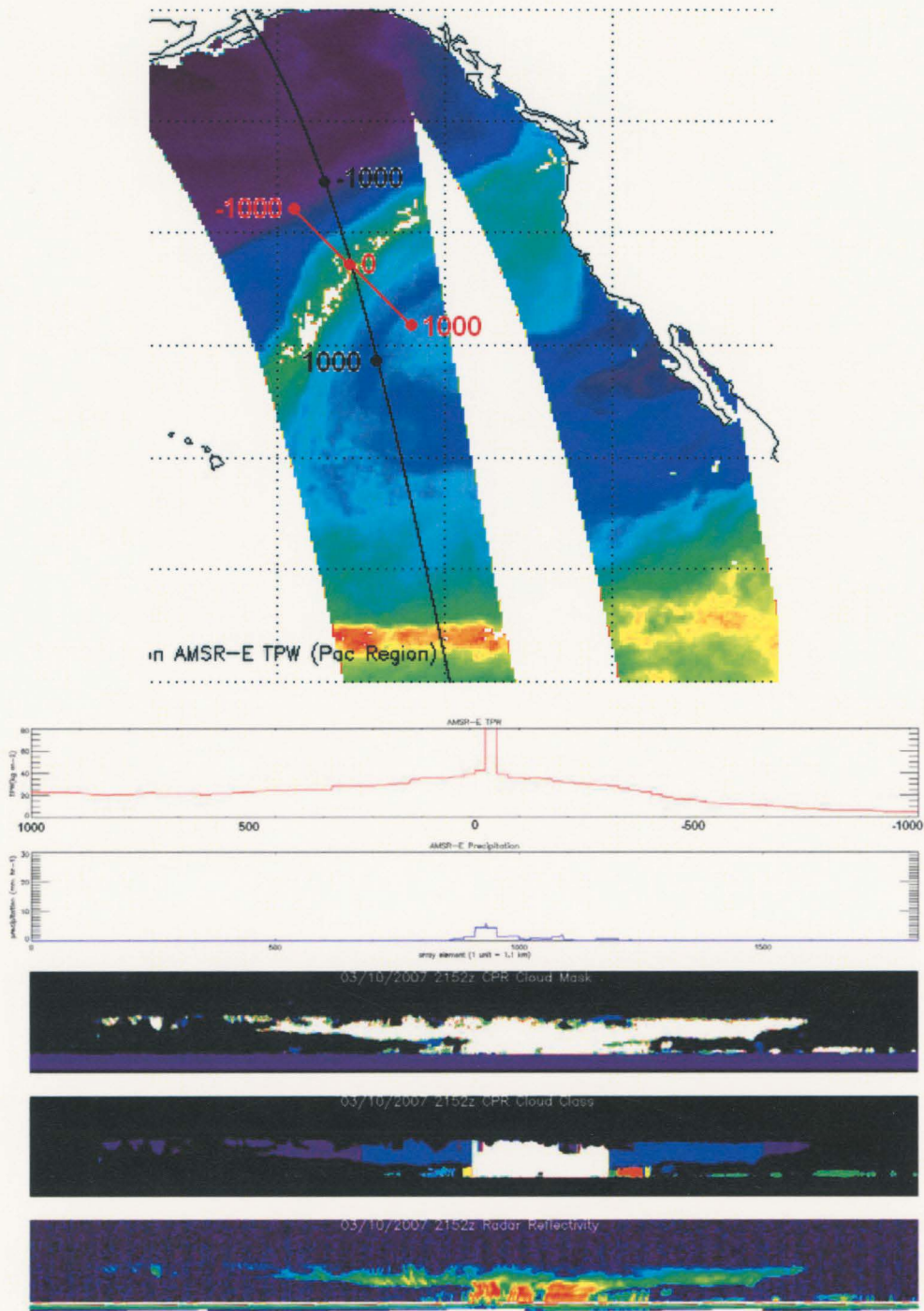
Figure 5.1) River-relative coordinate system based on physical length. The red line represents a 2000km long 90° cross-section of the river to which the data are mapped. The corresponding endpoints on CloudSat's orbit are marked with the black dots.
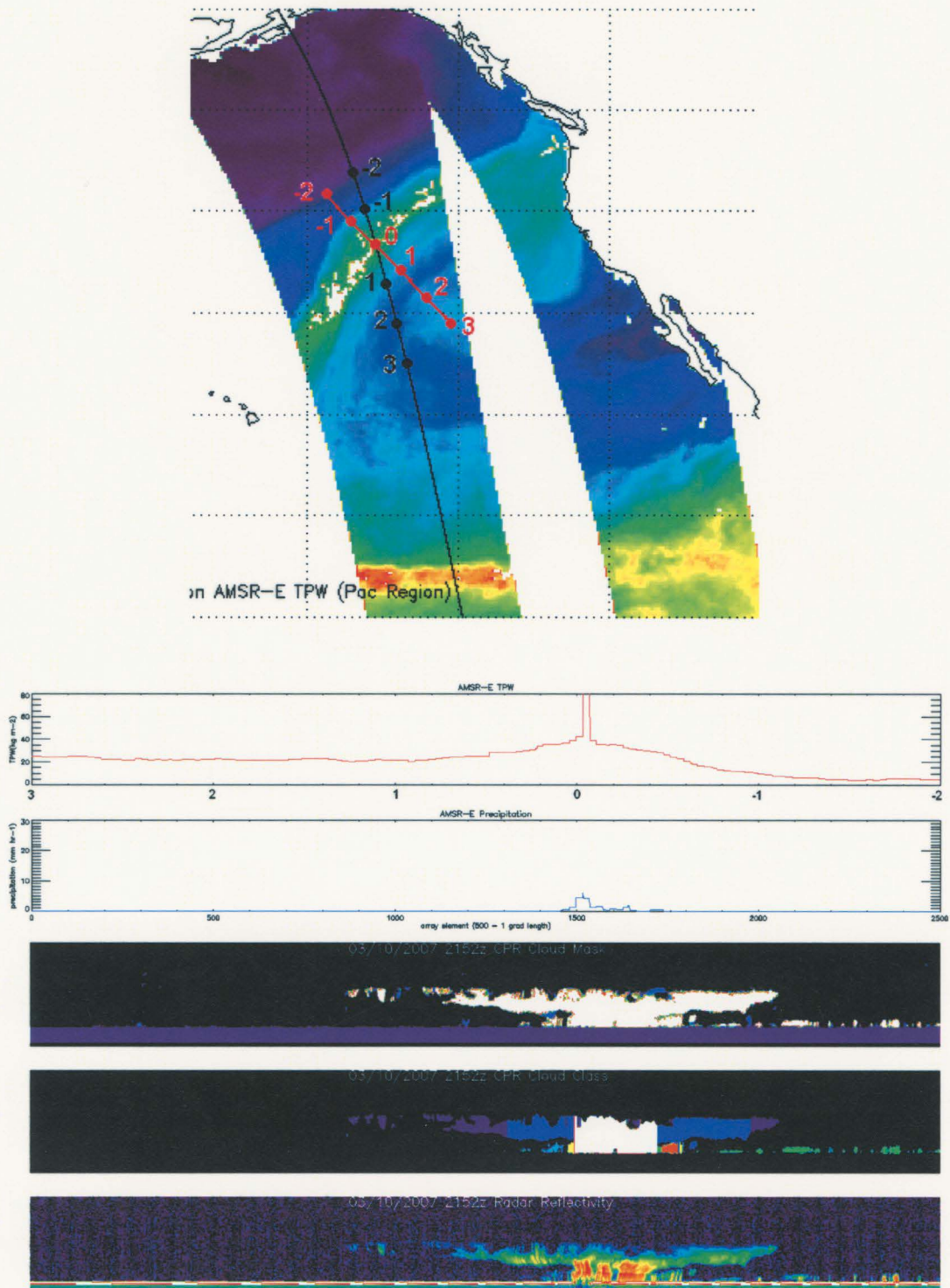
Figure 5.2) River-relative coordinate system based on gradient length. The red line represents a 90° cross-section, and the distance between each dot is the length the river's northern TPW gradient. The corresponding locations on CloudSat's orbit are marked with black dots.
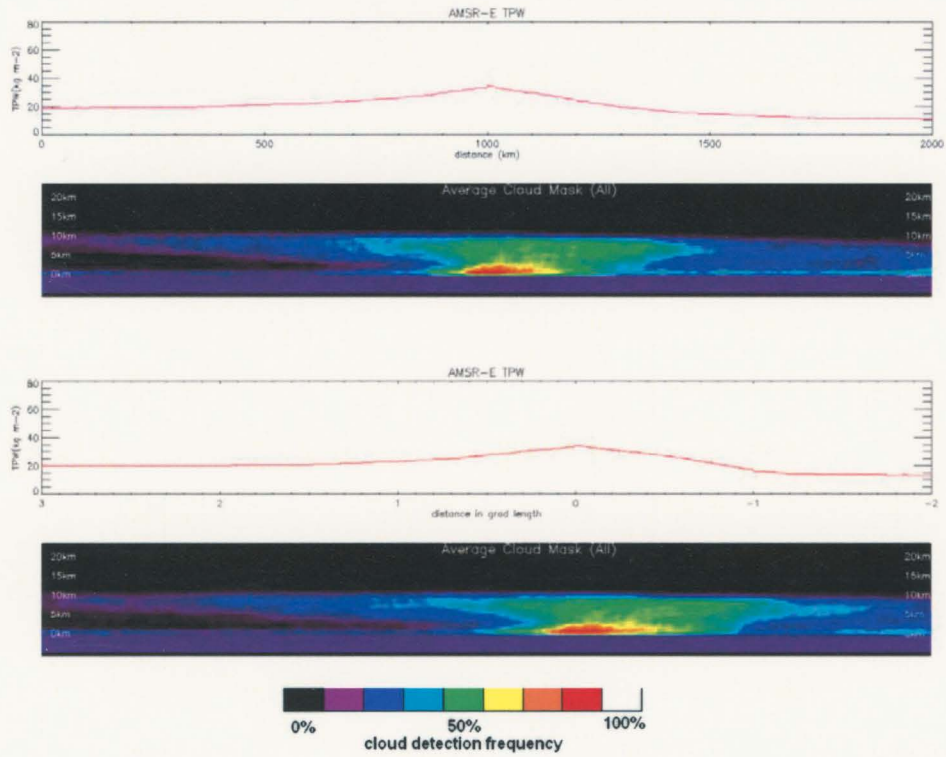
Figure 5.3) The average cloud mask for all 92 river observations.
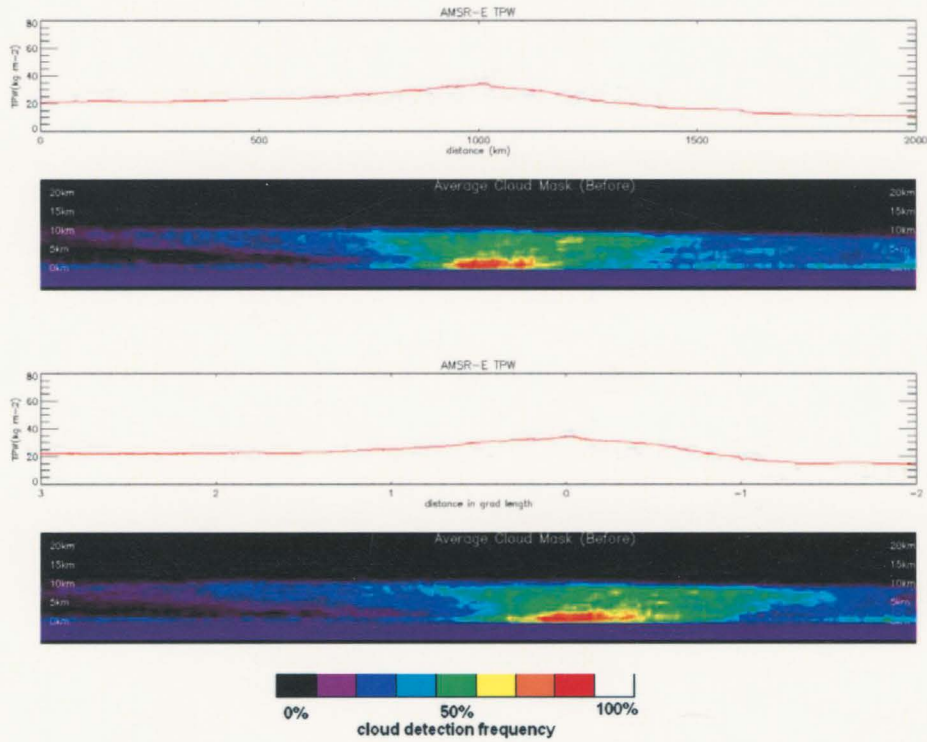
Figure 5.4) The average cloud mask for the 36 "before" observations.
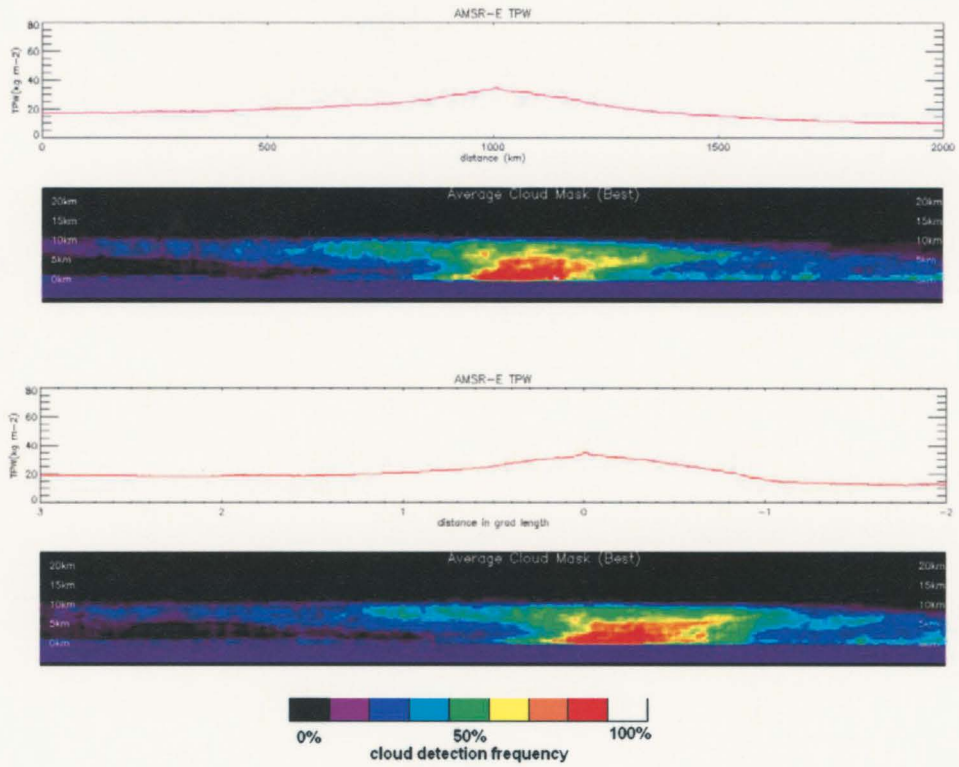
Figure 5.5) The average cloud mask for the 24 "best" observations.
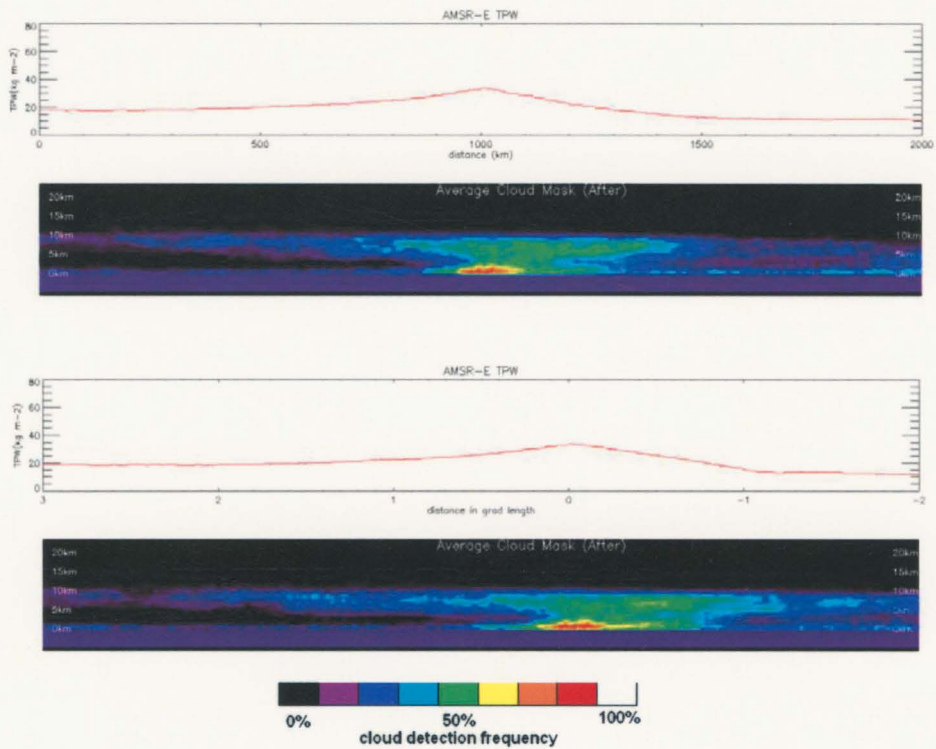
Figure 5.6) The average cloud mask for the 32 "after" observations.
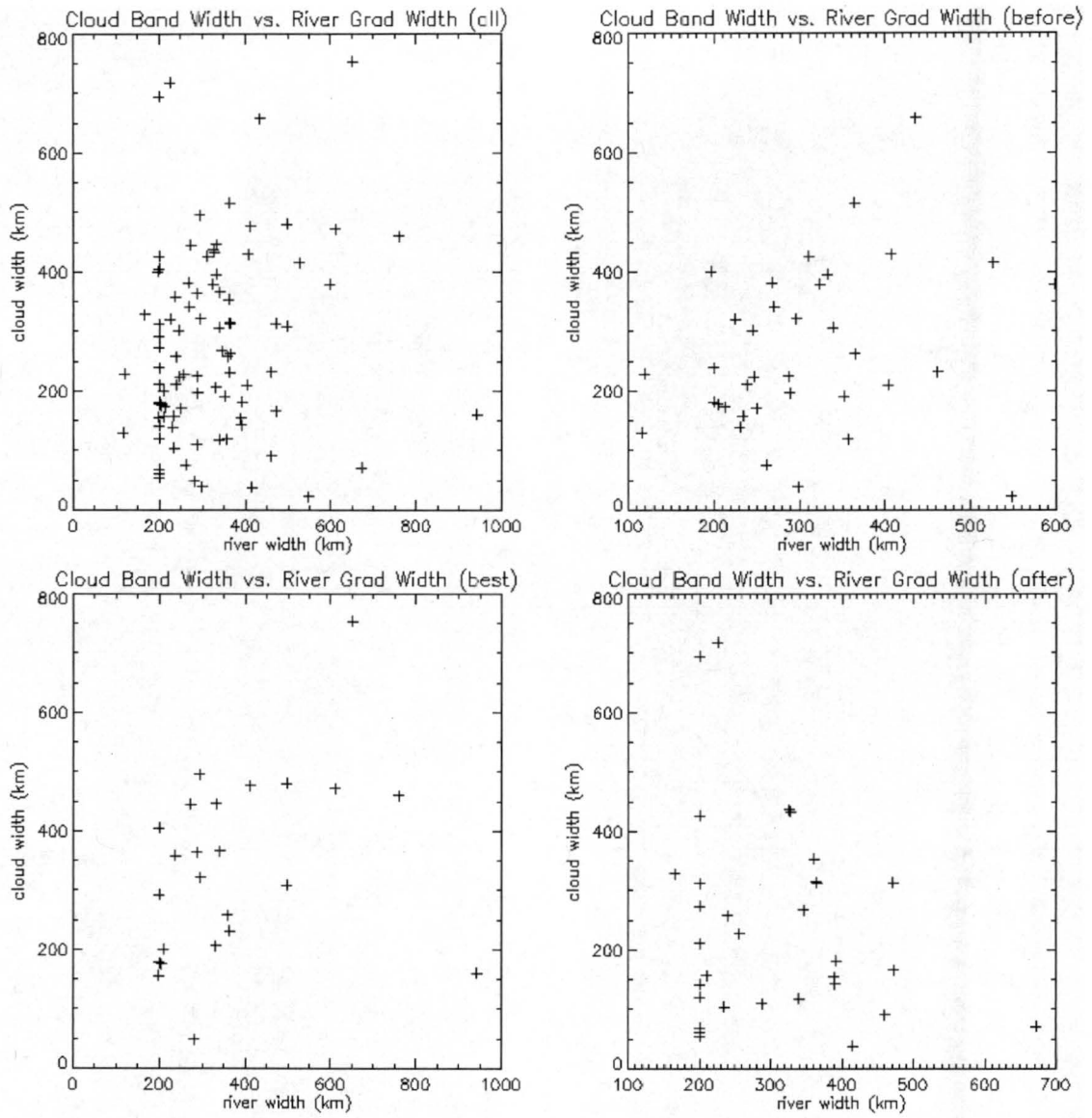
Figure 5.7) Scatter plot of the width of the northern TPW gradient versus the horizontal width of the cloud band.

92
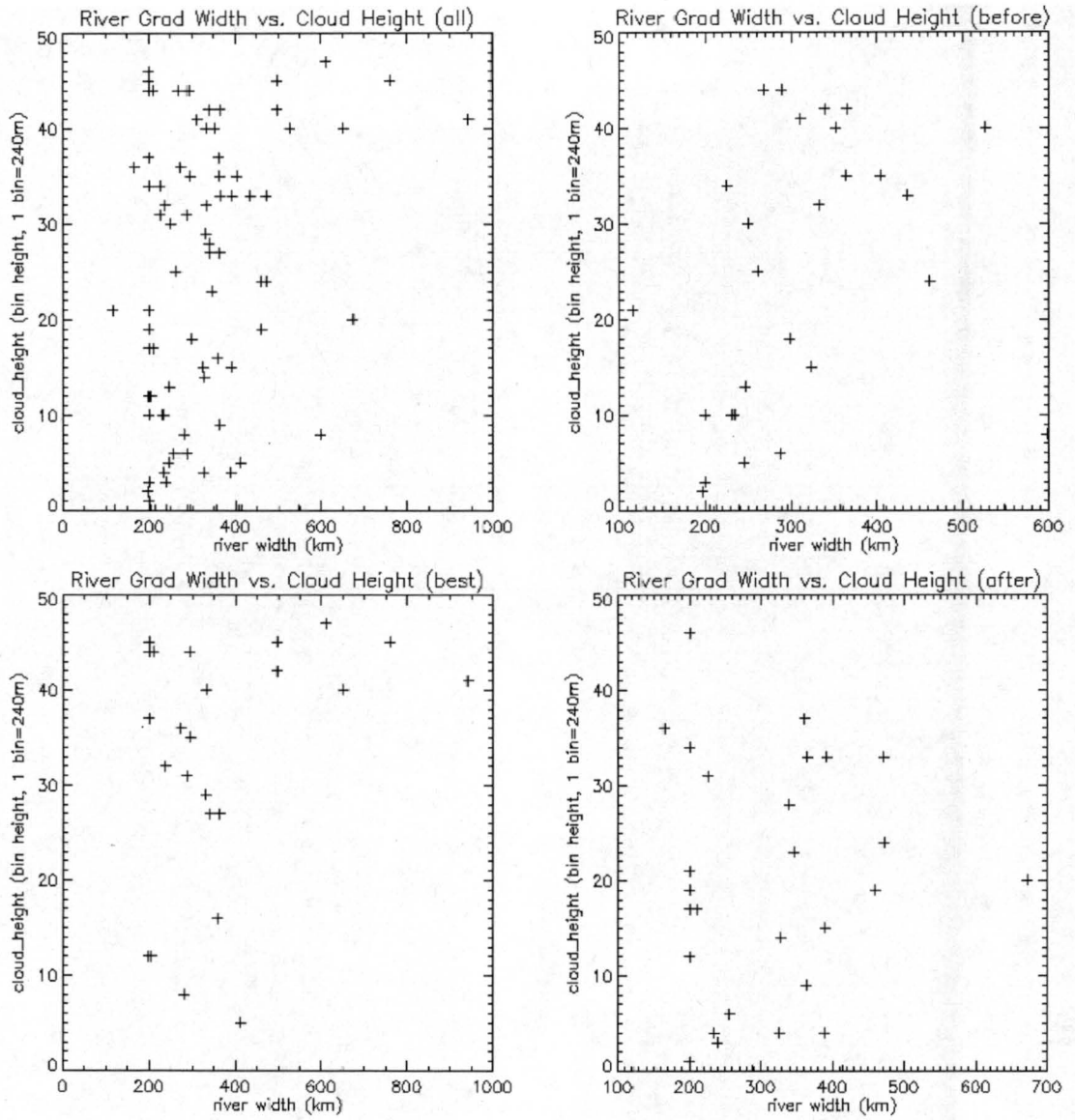
Figure 5.8) Scatter plot of the width of the northern TPW gradient versus the vertical height of the cloud band.
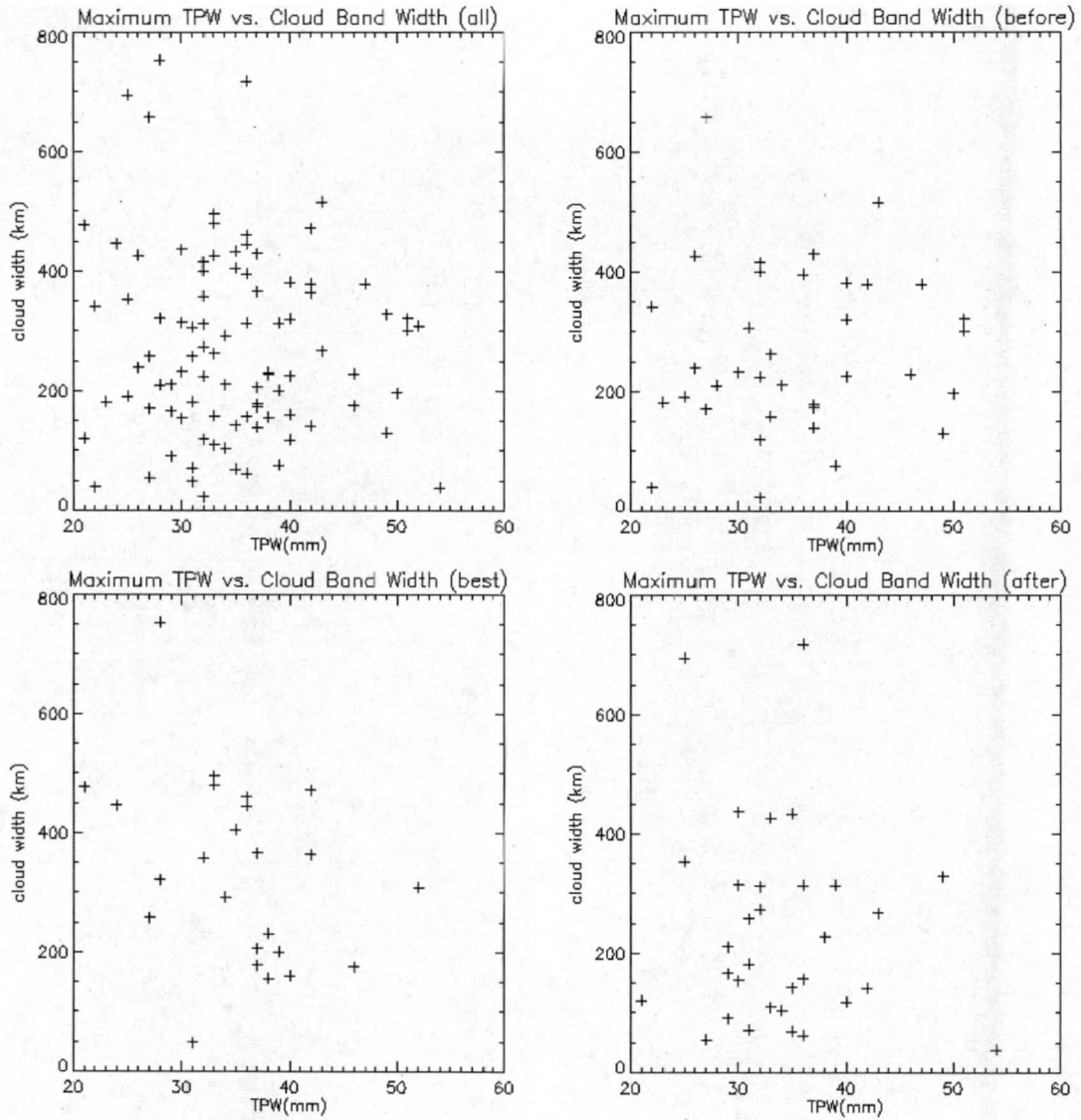
Figure 5.9) Scatter plot of the maximum TPW occurring within the river cross-section versus the horizontal width of the cloud band.
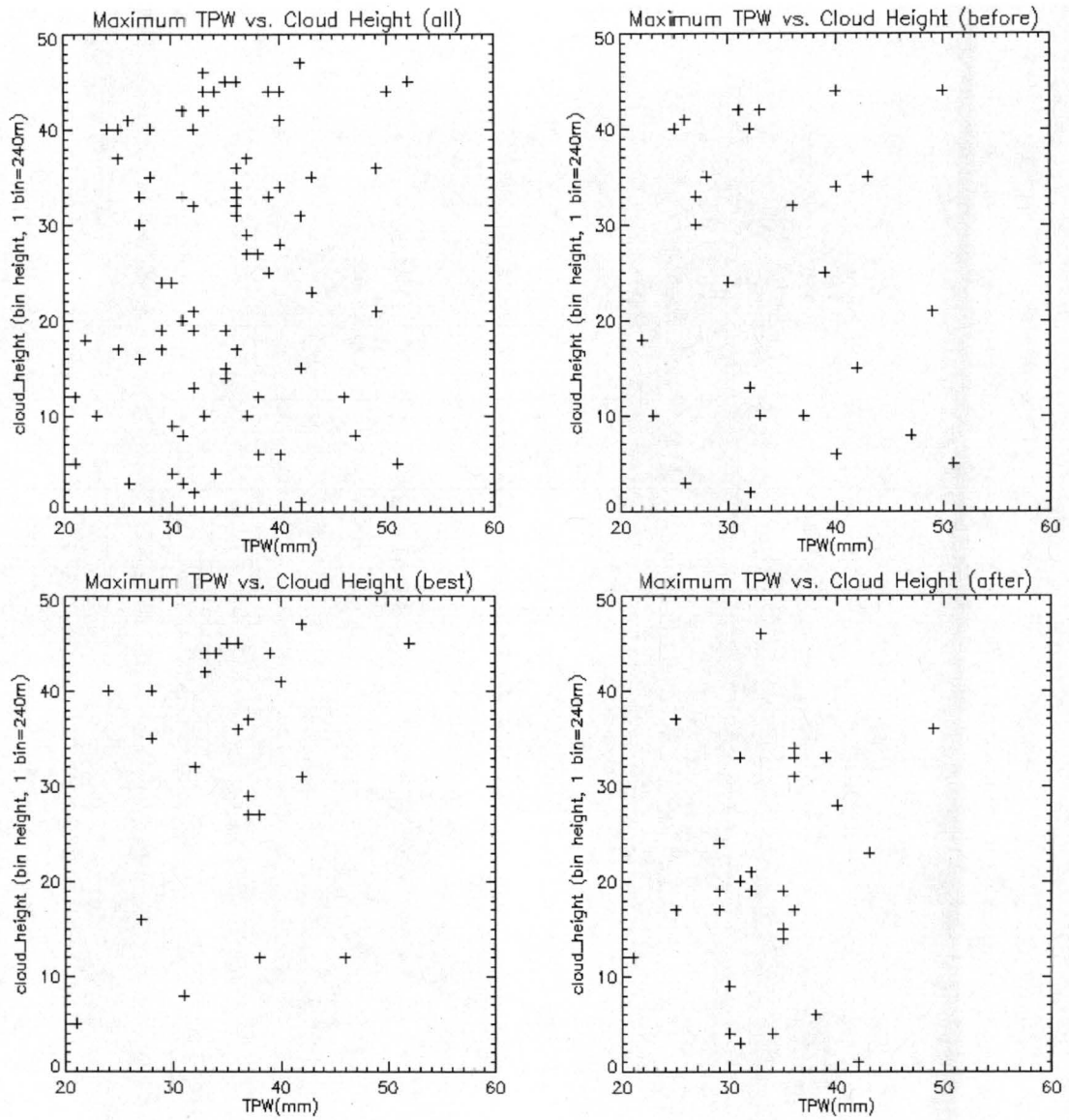
Figure 5.10) Scatter plot of the maximum TPW value within the river cross-section versus the vertical height of the cloud band.

6. CONCLUSIONS AND SUGGESTED FUTURE WORK

6.1 Conclusions

Atmospheric rivers are important meteorological features that affect both local weather and global climate. Though many river characteristics have already been studied extensively, such as wind patterns and moisture transport, cloud structure within rivers is less well understood. The goal of this project was to examine vertical cloud structures within atmospheric rivers and their relationships with other meteorological variables. Knowledge of cloud structure would provide additional sources of verification for researchers and modelers, and may give operational forecasters another tool to distinguish between typical landfalling polar fronts and major record-setting precipitation events.

From CloudSat observations, we find that the typical cloud structure within an atmospheric river is a spatially-enhanced variant of the classic "comma cloud" tail associated with midlatitude cyclones over land. While the high level cloud bands are similar in spatial extent in both rivers and land-based cyclones, the river's low-level cloud band is usually wider than the classic cyclone pre-frontal cloud band. The atmospheric river often contains regions of heavy precipitation and convection more than 100km in horizontal extent. The majority of the convection takes the form of large thunderstorm clusters much wider than typical linear convective systems (typically about

10km in horizontal extent), though linear convection can also occur. Occasionally atmospheric rivers fail to produce deep clouds (greater than 5km in vertical extent) at any point in their life spans. This failure may often be related to the river's moisture content, but there is at least one case of a river with average TPW values failing to produce deep clouds. These cases will still produce at least a band of shallow convective clouds or mid-level nimbostratus during maturity. There were no cases of a river failing to produce clouds above the boundary layer at any time in their life spans.

The cloud structure within atmospheric rivers changes over its lifespan of about three to five days. Unfortunately there may not be enough information in the present study to characterize clouds at the beginning of a river's lifespan, but it is fairly clear that deep cloud formation occurs most frequently when the river is most intense; that is, when the river possesses its highest TPW values (typically above 40mm) and well-defined moisture gradients (about 5mm/100km or greater). Late in the river's lifespan the deep cloud band will erode, usually leaving a low level cloud band and sometimes a layer of high clouds composed of remnant lifted moisture. It should be noted that atmospheric rivers almost always possess some form of cloud features occurring within the river's moisture axis. A completely cloud free river seems to be very rare at most. However, rivers do not always possess high-level cloud bands, even when the river is well-developed and possessing high TPW values.

6.2 Suggested Future Work

The most obvious method of improving the results of this project would be adding more observations to the current dataset. Adding more observations would give a better representation of variability occurring across multiple rivers. As shown in the case studies, rivers do not have a universal cloud structure, and the variability is highly noticeable even with the 22 river events during 2006/2007. There may be multiple different modes of cloud structure that could be identified with more sampling. This would also reduce biases caused by CloudSat's narrow field of view, caused by poor representation of "lumpiness" in the cloud bands. More observations could also aid the time-evolution partitioning of the data. CloudSat sometimes misses rivers that are not oriented to intersect its field of view. This occurs most frequently with developing rivers, which can be little more than 2000km long and easily slip between CloudSat passes. In addition to this, observations of rivers in other ocean basins may help identify similarities or differences between atmospheric rivers occurring in places other than the northern Pacific.

This project used AMSR-E derived precipitation as a complement to cloud measurements, but it is also possible to use the CPR measurements themselves to estimate precipitation occurring within rivers. The AMSR-E precipitation product has a 25km or so spatial resolution, and this may miss very heavy localized precipitation common in convective systems. The CPR has a resolution on the order of a kilometer, so CloudSat would be able to detect heavy localized precipitation occurring along its orbital track. There was no CPR-derived precipitation available at the beginning of the project,

but at present there is such a product in the experimental phase. It should be available operationally in the near future.

It would also be useful to add a wind component to the moisture and cloud observations. Atmospheric rivers are most importantly regions of high water vapor transport, and moisture transport requires both moisture and wind. Unfortunately, wind is a difficult meteorological variable to measure remotely, particularly in areas where thick precipitating clouds frequently occur over the feature of interest. Measuring surface winds near the river might be useful as a proxy for low level convergence along the polar front, but surface winds may not be indicative of the strength of the low level jet. The best way to obtain wind information would be the use of reanalyses and numerical models. There is currently work being done to retrieve wind within rivers, so it should be possible to include reliable wind estimates with moisture in the near future.

The next useful step beyond simple cross-section averages would be expanding the preliminary river-relative coordinate systems presented in this project in order to place CloudSat observations in a better spatial and temporal context. The spatial coordinate system currently only covers the river's cross-section, with little regard for positioning along the length of the moisture axis. However, as seen in the case studies, atmospheric rivers are not symmetric along their lengths. In particular, river cloud structure can be different at the river's southern end, at the junction between the river and the surface low, and near land. A spatial coordinate system along the river's length could help better separate observations so that different cloud-producing processes occurring along the river's length are not crossed. The current temporal system has little regard for a river's lifespan, and so it is probably biased by long-living rivers that receive more CloudSat

observations. A more useful temporal coordinate system would divide a river's lifespan into formation, maturity, and dissipation stages that use the river's features to divide up the data set (similar to how severe weather researchers currently classify tornadoes). This system should remove bias from long-lived rivers by normalizing for lifespan.

This new coordinate system could be used in conjunction with other meteorological instruments to provide coverage of the river's cloud structure between CloudSat's observations. For example, the GOES imagers would be very useful in this respect. CloudSat can help interpret features appearing in the GOES imager data, and in turn GOES can identify cloud features outside of CloudSat's field of view. GOES could be used for identifying thunderstorm clusters which CloudSat might miss because of its narrow field of view and its 12hr temporal coverage (Aqua suffers the timing issue as well). It may also be possible to use GOES to link cloud structure within atmospheric rivers to the extratropical cyclone attached with the river. As stated previously, there is an observed connection between latent heat within atmospheric rivers and the intensity of the cyclone itself, and the river's cloud structure may provide some insight into that. GOES may be able to detect potential river-induced intensification on a time-scale that is operationally useful. In the same way, other instruments can benefit from CloudSat observations and in turn fill the gaps in CloudSat's observations.

REFERENCES

Aumann et al, 2003: AIRS/AMSU/HSB on the Aqua Mission: Design, Science Objectives, Data Products, and Processing Systems. *IEE Trans. On Geosci. And Rem. Sensing*, **41**, 253-264.

Bao, J.-W. et al, 2006: Interpretation of Enhanced Water Vapor Bands Associated with Extratropical Cyclones: Their Formation and Connection to Tropical Moisture. *Monthly Weather Review*, **134**, 1063-1080.

Blackwell, K. G., 2000: Tropical Plumes in a Barotropic Model: A Product of Rossby Wave Generation in the Tropical Upper Troposphere. *Monthly Weather Review*, **128**, 2288-2302.

Browning, K. A. and C. W. Pardoe, 1973: Structure of Low-Level Jet Streams Ahead of Midlatitude Cold Fronts. *Quart. J. Roy. Meteor. Soc.*, **99**, 619-638.

Carlson, T. N., 1991. Midlatitude Weather Systems. HarperCollins Academic, 507pp.

Chahine et al, 2006: AIRS Improving Weather Forecasting and Providing New Data on Greenhouse Gases. *Bull. Amer. Met. Soc.*, **87**, 911-926.

Davey, C. A., 2000: Satellite Moisture Profiling of Eastern Pacific Moisture Plumes. M.S. Thesis, Colorado State University, 113 pp.

Hudak, D. and H. Barker, 2005: The Canadian CloudSat/Calypso Validation Project (C3VP). Found online
[http://c3vp.org/docs/sci_plan/C3VP_Science_Plan_v2005-02-24.pdf]

Iskenderian, H, 1995: A Ten-Year Climatology of Northern Hemisphere Tropical Cloud Plumes and Their Composite Flow Patterns. *Journal of Climate*, **8**, 1630-1637.

Kawanishi, T. et al, 2003: The Advanced Microwave Scanning Radiometer for the Earth Observing System (AMSR-E), NASDA's Contribution to the EOS for the Global Energy and Water Cycle Studies. *IEE Trans. On Geosci. And Rem. Sensing*, **41**, 184-194.

Langland, R. H. et al, 1999: The North Pacific Experiment (NORPEX-98): Targeted Observations for Improved North American Weather Forecasts. *Bull. Amer. Met. Soc.*, **80**, 1363-1384.

McGuirk, J. P., A. H. Thompson and N. R. Smith, 1987: Moisture Bursts over the Tropical Pacific Ocean. *Monthly Weather Review*, **115**, 787-798.

McGuirk, J. P., A. H. Thompson and J. R. Schaefer, 1988: An Eastern Pacific Tropical Plume. *Monthly Weather Review*, **116**, 2505-2521.

Mecikalski, J. R. and G. J. Tripoli, 1998: Inertial Avaiable Kinetic Energy and the Dynamics of Tropical Plume Formation. *Monthly Weather Review*, **126**, 2200-2216.

Newell, R. E. and Y. Zhu, 1992: Tropospheric Rivers? – A Pilot Study. *Geophys. Res. Lett.*, **12**, 2401-2404.

Newell, R. E. and Y. Zhu, 1994: Tropospheric Rivers: A One-Year Record and a Possible Application to Ice Core Data. *Geophys. Res. Lett.*, **21**, 113-116.

Neiman, P. J. et al, 2002: The Statistical Relationship between Upslope Flow and Rainfall in California's Coastal Mountains: Observations during CALJET. *Monthly Weather Review*, **130**, 1468-1492.

Parkinson, C. L., 2003: Aqua: An Earth-Observing Satellite Mission to Examine Water and Other Climate Variables. *IEE Trans. On Geosci. And Rem. Sensing*, **41**, 173-183.

Ralph, F. M., P. J. Neiman, and G. A. Wick, 2004: Satellite and CALJET Aircraft Observations of Atmospheric Rivers over the Eastern North Pacific Ocean during the Winter of 1997/98. *Monthly Weather Review*, **132**, 1721-1745.

Ralph, F. M., P. J. Neiman, and R. Rotunno, 2005: Dropsonde Observations in Low-Level Jets over the Northeastern Pacific Ocean from CALJET-1998 and PACJET-2001: Mean Vertical-Profile and Atmospheric-River Characteristics. *Monthly Weather Review*, **133**, 899-910.

Ralph, F. M. et al, 2006: Flooding on California's Russian River: Role of Atmospheric Rivers. *Geophys. Res. Lett.*, **33**, 5 pp.

Randel et al, 1996: A New Global Water Vapor Dataset. *Bull. Amer. Meteor. Soc.*, **77**, 1233-1246.

Stephens, G. L. et al, 2002: The CloudSat Mission and the A-Train. *Bull. Amer. Meteor. Soc.*, **83**, 1771-1790.

Taylor, G. H., C. Hale and K. Kuykendall, 2006: November 2006 Record-Setting Rainfall and Flooding, *Oregon Climate Service*, found online [http://www.ocs.orst.edu/page_links/whats_new/november_flooding.html]

Wang, Z., personal communication, September, 2007

Wang, Z. and K. Sassen, 2001: Cloud Type and Macrophysical Property Retrieval Using Multiple Remote Sensors. *Journal of App. Met.*, **40**, 1665-1682

Wentz, F. J. and T. Meissner, 2000: ATBD AMSR Ocean Algorithm. *Remote Sensing Systems*, 55 pp.

Wentz, F. J., C. Gentemann and P. Ashcroft: On-Orbit Calibration of AMSR-E and the Retrieval of Ocean Products. found online [http://www.ssmi.com/papers/amsr/on-orbit_calibration_amsre_and_ocean_products.pdf]

White, A. B. et al, 2003: Coastal Orographic Rainfall Processes Observed by Radar during the California Land-Falling Jets Experiment. *Journal of Hydromet.*, **4**, 264-282.

Zhu, Y. and R. E. Newell, 1998: A Proposed Algorithm for Moisture Fluxes. *Monthly Weather Review*, **126**, 725-735.

Zhu, Y. and R. E. Newell, 1994: Atmospheric Rivers and Bombs. *Geophys. Res. Lett.*, **21**, 1999-2002.

CloudSat Standard Data Products Handbook, CIRA, found online [http://www.cloudsat.cira.colostate.edu/cloudsat_documentation/CloudSat_Data_Users_ Handbook.pdf]

CloudSat 2B GEOPROF Quality Statement: May 2007 (Version R04). CIRA, found online [http://www.cloudsat.cira.colostate.edu/ICD/2B-GEOPROF/CloudSat_2B_GEOPROF_Quality_Statement_R04.doc]

Level 2 GEOPROF Product Process Description and Interface Control Document. CIRA, found online [http://www.cloudsat.cira.colostate.edu/ICD/2B-GEOPROF/2B-GEOPROF_PDICD_3.0.pdf]

Level 2 Cloud Scenario Classification Product Process Description and Interface Control Document. CIRA, found online [http://www.cloudsat.cira.colostate.edu/ICD/2B-CLDCLASS/2B-CLDCLASS_PDICD_4.0.pdf]